SIGNIFICANCE OF SLEDGEHAMMER SOURCE PARAMETERS: A HIGH-RESOLUTION SEISMIC REFLECTION STUDY

by

Dean A. Keiswetter

Don W. Steeples

Richard D. Miller

of the

Kansas Geological Survey

The University of Kansas

Lawrence, Kansas 66045

KGS Open-File Report # 92 - 4

February 26, 1992

Kansas Geological Survey
Open-file Report

Disclaimer

The Kansas Geological Survey does not guarantee this document to be free from errors or inaccuracies and disclaims any responsibility or liability for interpretations based on data used in the production of this document or decisions based thereon. This report is intended to make results of research available at the earliest possible date, but is not intended to constitute final or formal publication.

ABSTRACT

Seismic data quality is affected by source parameters. This thesis examines the significance of sledgehammer source parameters on the basis of seismic energy and spectral content. High-resolution, reflection data were acquired with various sledgehammer configurations at three sites in northeastern Kansas. To provide repeatable impact energy, a mechanical impact device was developed to use gravity as the consistent driving force. Source conditions (parameters) were changed by varying the (1) impact mass, (2) impact plate (mass, surface area, and material), (3) impact velocity, and (4) near-surface compaction.

The results indicate a maximum 6 dB variation in seismic energy may occur when practical sledgehammer parameter changes are made. Seismic energy proved to be dependent on the compaction of the surface material, the plate surface area, and the impact mass, while impact velocity and plate mass do not appear to be significant. Site characteristics, such as material type and natural degree of compaction, dictated which parameters are significant and which are not.

While the sledgehammer source provided dominant reflection frequencies of between 90 and 200 Hz, changes in the spectral characteristics associated with parameter variations were minor. This suggests the site-specific response of earth media dictates the waveform regardless of sledgehammer source parameter changes. Among the parameters that moderately increased the signal-to-noise ratio at particular sites are large plate areas, small impact and plate masses, and highly compacted near-surface conditions.

Aluminum plate material proved to be a viable alternative to steel in both spectral characteristics and seismic energy. Aluminum proved to be more durable than steel, and its lightweight enables easier use in the field.

TABLE OF CONTENTS

LIST OF FIGURES

LIST OF TABLES

INTRODUCTION

The primary purpose of this study is to examine the significance of physical parameters (impact mass, impact velocity, plate mass, surficial plate area, and media compaction) for the sledgehammer seismic source. For this research, high-resolution, reflection seismic data were acquired at three sites in northeastern Kansas and analyzed based on spectral properties and seismic energy. Secondary goals were to investigate miscellaneous acquisition methods which enhance data quality or reduce coherent source-generated noise for the sledgehammer source.

Commonly employed seismic sources for shallow reflection studies include sledgehammers (including various mass drops), modified rifles and guns, propane/oxygen gas-guns, various piezoelectric sources, spark packs, and explosives. Development of high-resolution shallow reflection techniques and equipment (Taylor, 1988) has recently been fueled by environmental and engineering applications (Birkelo et al., 1987; Doornenbal and Helbig, 1983; Jongerius and Helbig, 1988; Gochioco and Cotten, 1989; Miller and Steeples, 1991; Singh, 1984; Miller and Steeples, 1990). The source of choice for a particular project is dependent on target depth, desired resolution of primary target(s), available equipment, budget/time constraints, site topography/access, and near-surface geology. Specific site characteristics exist where each source can be optimal (Miller et al., 1986). In some areas, such as hazardous-waste sites, it may be neither possible nor desirable to use some sources because of the need to avoid disturbing the surface.

The desirability of the sledgehammer as a seismic source relates to low cost, portability, ease of use, comparatively non-destructive nature, and safety considerations. Although experiments by Pullan and MacAulay (1985) suggest the sledgehammer is not always the optimum source, it has been shown to provide high quality seismic data at some sites (Miller et al., 1989).

Materials in the immediate vicinity of most energy sources are subjected to non-linear deformation, and do not obey infinitesimal wave theory. Outside the non-linear region near the source, often referred to as the equivalent cavity for explosive sources (Anstey, 1957), conventional

wave theory accurately predicts particle motion. Due to the extreme complexities in the non-linear region, understanding the energy transformation between the source and the seismic waves is not a simple task. A significant number of publications deal with the problem of seismic wave generation for explosive sources (Murphey, 1961; Gaskell, 1956; Sharpe, 1942), while relatively few studies have been conducted for falling mass and/or hammer impacts (Mereu et al., 1963).

This research investigates the ideas and results of past researchers with an aim to specifically evaluate the sledgehammer as a seismic source for shallow (<300 m) reflection surveys. Experiments are grouped into two categories: (1) Miscellaneous tests, and (2) Core experiments. Core experiments address primary goals such as the importance of plate mass, hammer mass, impact velocity, plate surface area, and media compaction. Miscellaneous tests address plausible variations in acquisition techniques for the sledgehammer source. These include the effects of a non-centered impact, multiple bounces, use of "downhole plates", and steel versus a sand-filled dead-blow hammer made of hard rubber. The results of this work will aid seismologists who choose to employ the cheap, environmentally safe, and simplistic sledgehammer source.

Previous Work

Hubert (1925) and Kasahara (1954) were among the first to investigate source parameters for falling masses. They released various masses (2.7 to 117 kg) from various heights (up to 11 meters), and concluded that (1) arrival times and seismogram character were independent of the falling mass and drop-height, and (2) the amplitude of the wave was proportional to the square root of the potential energy of the falling mass. Kasahara (1954) tried placing wood, brass, and rubber materials at the impact point and observed no significant change.

Gough (1952) studied sledgehammer-earth coupling effects during development of a short range seismic instrument and concluded that for hard surfaces a direct hammer blow (no plate) produced the best results, while for unconsolidated sand an iron plate, 0.2 m x 0.2 m x 0.01 m , placed at the impact point produced superior results. It was noted in this work that the seismic energy is greatest when the hammer rebounds the least. Gough (1952) does not indicate which elements of the seismogram (amplitude, frequency, signal-to-noise ratio, etc.) were used to determine the quality of the records.

Mason (1957) tried to control the frequency content by decreasing the duration of impact between the falling mass and the Earth's surface. Frequency content produced by a falling mass has been shown theoretically and experimentally to be a function of the duration of impact (Lamb, 1904). The duration of impact for a perfectly elastic spherical body colliding with an elastic, plane surface of infinite mass has been shown (Hertz, 1896) to be dependent on the elastic properties of the plane surface medium and the mass, velocity and radius of the falling sphere. Assuming the falling mass and the earth to be analogous to the elastic sphere and infinite plane surface respectively, Mason (1957) tried with moderate success to control the frequency content by varying the mass, velocity and radius of the falling mass (22.7 to 136 kg, radii from 0.05 to 0.12 m, falling from heights between 0.9 to 2.7 m). He observed changes of around 7% about the mean period, where theory suggested 40%. The non-elastic behavior (plastic wave deformation) of the material in the vicinity of the source was credited with the discrepancy.

Neitzel (1958) measured the amplitude and wave shape (frequency) generated by various falling masses (109 kg and 2 086 kg) and showed the efficiency of the mass drop to be approximately one thousand times that of dynamite explosions in terms of reflection amplitude. Primary disadvantages of the mass drop included large surface waves and low frequency content compared to dynamite sources. Neitzel (1958) concluded data quality improves through use of (1) large seismometer groups (up to 64 seismometers), (2) many source drops per trace (vertical stacking), and (3) large source-to-receiver offsets (>240 m).

Domenico (1958) conducted a series of experiments in West Texas to evaluate composite drops (source array obtained by adding source gathers after static correction during processing) for the mass drop technique. The energy source was a 2 700 kg steel mass measuring 0.9 m x 1.5 m x 0.2 m, dropped a distance of 2.7 m. Included in this work are reports of field experiments conducted at two sites which test the reciprocity principle for surface impacts. One site strongly supported the principle, while the second showed seismic traces of like raypaths to strongly differ both in amplitude and phase. Later tests showed the results to be repeatable. Domenico (1958) proposed the changes observed in the two sites were due to near-surface material differences. The site exhibiting high reciprocity had a nearly homogenous, 30 m thick, sand cover while the second site was covered by a veneer of soil.

Mereu et al. (1963) theoretically and experimentally modelled factors that influence the efficiency of seismic wave generation by a falling mass. Two media, the first consisting of fine sand and the second a sand-silt-clay mixture similar in composition to sandy till, were housed in a plywood box, 1.1 m x 1.1 m x 0.9 m, for laboratory experiments. Spherical masses (ball bearings) ranging from 0.008 kg to 0.359 kg served as the impact masses as well as the source-media coupler (the coupler represents a counterpart to flat impact plates). A variety of coupler materials (brass, wood, wax, steel, aluminum, lead, and rubber) and shapes (spheres, hemispheres, cylinders, hollow hemispheres) were included. Receivers were buried directly below the couplers, and the seismic pulse was photographed on an oscilloscope. The seismic signal addressed was that of

the first arrival only. Source conditions were changed by altering the (1) falling mass, (2) drop-height, (3) degree of compaction of the medium, and (4) plate mass and surface area. Mereu et al. (1963) established the concept of virtual plate speed (discussed in detail below) in the medium immediately following impact. Among his results for compressional waves are the following:

(1) $A=(p^{0.67})(V_p)$, where A is the amplitude of the seismic pulse, p is the plate mass, and V_p the virtual speed of the plate.
(2) Seismic energy is not directly proportional to source energy, but rather related to the virtual plate speed.
(3) For a given source energy, large falling masses produce seismic energy more efficiently than smaller impact masses.
(4) Multiple source pulses are generated when the mass of the falling weight is greater than that of the plate, complicating the recorded wavelet.
(5) The waveform depends on the degree of surface compaction, the plate mass, and the medium.

Virtual Plate Speed

Elastic wave generation due to a falling mass striking a plate results from interaction between the plate and the medium, not between a falling mass and the plate (Mereu et al., 1963). If impact duration is long compared to the free oscillation periods of colliding rigid bodies, it has been shown that most of the kinetic energy will result in translational energy rather than vibrational energy within the objects (Rayleigh, 1906). In the case of plate-earth interaction, the elastic properties of a steel impact plate and earth materials are sufficiently different that only translational motion of the plate results (Mereu et al., 1963). This assumption implies the plate acquires free motion (although damped due to the medium) just after impact of the mass. Experiments that measured the duration of impact versus duration of seismic pulse showed that most of the recorded source pulse was indeed generated after the impact was over (Mereu et al., 1963). This has two significant implications: (1) no driving force need be considered for falling impact cases, and (2) the elastic waves generated in the medium must originate at the plate-earth interface rather than at the

point of contact between the plate and the falling mass. The momentary speed the plate acquires just after impact will be referred to as the virtual speed (V_p) of the plate hereafter.

To establish how the character of the waveform depends on the elastic properties of the earth, the plate mass, and the impact velocity, consider the problem analogous to a single mass-spring system in which viscous damping is present. If we assume the duration of impact is short compared to the interaction of the plate-earth system, then no driving force need be considered. The second-order differential equation for this system is given by;

$$M\frac{d^2y}{dt^2}+C\frac{dy}{dt}+Dy=0$$

where C and D are constants that depend on the elastic parameters of the medium and the surface area of the plate, y is the plate position, and M is the mass of the plate (Mereu et al., 1963). For our case,

$M\frac{d^2y}{dt^2}$ = *the impact force,*

$C\frac{dy}{dt}$ = *the frictional force, and*

Dy *is the elastic force.*

The initial conditions (t=0) needed to solve this equation for our case are the following;

$$y(0)=0, \quad and \quad \frac{dy(0)}{dt}=V_p,$$

where t=0 is defined as the end of the falling mass-plate interaction. If we further assume the motion is underdamped, the solution is;

$$y(t)=e^{\frac{-C}{2M}t}\left(V_p\right)\left\{\frac{2M}{\sqrt{4DM-C^2}}\right\}\sin\left(\frac{\sqrt{4DM-C^2}}{2M}t\right), \qquad (2)$$

and the quasi-circular period (T) (Boyce and DiPrima, 1986) is,

$$T = \frac{4M\pi}{\sqrt{4DM - C^2}}. \qquad (3)$$

Mereu (1962) originally solved this problem, but an alternative method is given in appendix B.

Equations (2) and (3) provide two important bits of information. First, the form of source pulse depends on plate mass and the elastic properties of the medium, but not on V_p. That is, assuming an underdamped motion ($C^2 << 4DM$), the frequency content of the source pulse is inversely proportionally to the square root of plate mass. Second, the magnitude of the displacement is directly related to the virtual plate speed, and is related to the elastic properties of the medium by a complicated function.

The above analysis is in good agreement with observations of wave motion produced when a pressure pulse of arbitrary form is applied to the interior surface of a spherical cavity in an ideally elastic medium (Sharpe, 1942).

The above discussion indicates seismic waves are initiated at the plate-medium interface, but the question of how the plate interacts with the impact mass has not been addressed. The coefficient of restitution is a measure of the elastic properties between the impact mass and the plate;

$$e = \frac{\left(P_F - U_f\right)}{(u - p)},$$

where U_F = rebound velocity of impact mass, P_F = velocity of plate after impact, u = velocity of impact mass at impact, and p is the initial velocity of the plate. Using collision theory, conservation of momentum, the coefficient of restitution (e) equation, and initial conditions stated earlier (p. 6), the following equations governing plate motion due to impact force were derived by Mereu (1962);

$$V_p = \frac{(1+e)h}{(h+p)}u \qquad (4)$$

and

$$U_f = \frac{(h-ep)}{(h+p)}u,$$

where h=falling impact mass, and p=mass of plate. The expression for U_f shows the impact mass (h) will rebound if h<ep, and rebound height will increase as h gets smaller with respect to the product of the coefficient of restitution and plate mass (ep).

The proportionality constant which relates virtual plate speed and amplitude, A, is termed the coupling constant (K) and is given by

$$A = K V_p.$$

Substituting equation (4) for V_p,

$$A = K\frac{(1+e)h}{(h+p)}u.$$

This equation implies the amplitude of the seismic signal is directly related to the velocity of the falling mass, but is not linearly related to the potential energy of the falling mass (Mereu et al., 1963). Clever laboratory experiments conducted by Mereu (1962) indicate the coupling constant, K, is proportional to plate mass raised to the 0.67 power, for a medium of sand, silt and clay (similar to a sandy till matrix). Therefore the amplitude is given by;

$$A = (p^{0.67})\left(\frac{(1+e)h}{(h+p)}\right)u, \qquad (5)$$

for a media of sand, or sand-silt-clay mixtures.

Source Conditions

The elastic limit of near-surface media constrains how much impact energy can be applied before permanent deformation and/or plastic wave formation occurs. Plastic waves, as referred to here, have strains that are not large enough for the medium to be treated as a Newtonian fluid, but still result in permanent deformation. Plastic waves deplete the available kinetic energy, reduce elastic particle motion and produce a non-minimum phase pulse (Dobrin and Savit, 1988). As plastic waves pass, grains in the medium are compressed (compacted) and work hardening occurs.

During plastic wave propagation, the seismic pulse will change from a minimum phase wavelet to a non-minimum phase wavelet as well as be reduced in amplitude (Dobrin and Savit, 1988). Karman and Durwez (1950) used the Lagrangian coordinate method to show that the velocity of a plastic wave (V_{pl}) is given by

$$V_{pl} = \sqrt{\frac{1}{\rho_0}\frac{d\sigma}{d\varepsilon}}, \qquad (1)$$

where ρ_0 is density, σ is the stress, ε is the strain, and therefore $\frac{d\sigma}{d\varepsilon}$ is the slope of the stress-strain curve. A stress-strain curve (Figure 1), established for unconsolidated materials by Dix (1952) and Dereciewicz (1958), shows steep slopes for small strains. Thus small amplitude displacements will travel at higher velocities than large amplitude displacements, altering the waveshape.

The loss of source energy and waveshape broadening associated with plastic waves can be minimized by using an impact plate or compacting the media before recording. The chosen impact plate should be of sufficient surface area to reduce the stress at impact such that little or no permanent deformation is observed. Conservation of momentum requires that much of the original source energy must remain with the impact mass in the form of rebound energy if the mass of the plate is extremely large compared to the impact mass. Therefore, the mass of the impact plate

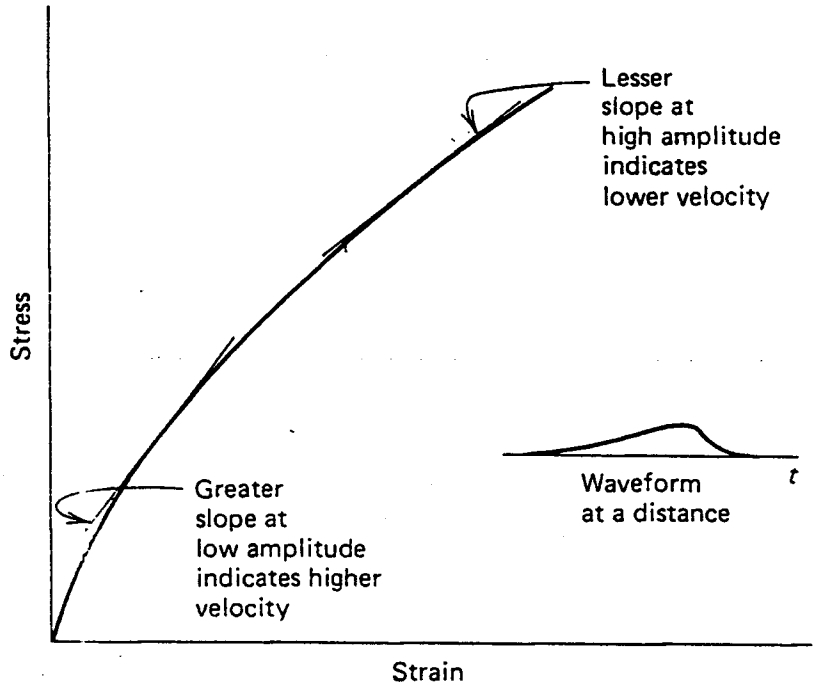

Figure 1. Pulse spreading in soft material with nonlinear stress-strain curve. (Dix, 1952)

should not be greater than the impact mass. Compacting the media will increase the elastic limit, and decrease permanent deformation for a given source energy.

SITE GEOLOGY

Sledgehammer comparison data were collected at three test sites, all located within 1 km of the Lawrence, Kansas, city limits (Figure 2). Although the sites had different material types present in the upper few meters, bedrock at the sites consists of either Lawrence or Stranger Formation limestone, sandstone, or shale (Figure 3). The near-surface materials present at each of the sites were determined by split spoon sampling techniques, and range from weathered shaly, soil profiles to mature sand-dominated alluvial deposits. All three sites are uniformly underlain at depth by an 800 m thick sequence of flat-lying Paleozoic rocks overlying Precambrian basement. Cyclic Pennsylvanian sequences of marine and non-marine shale, sandstone and limestone strata comprise the upper half of the total Paleozoic sequence.

The first test site is located on the University of Kansas campus on a grassy field (herein called the KU Campus site, Figures 2, 4). The Lawrence formation outcrops at the site with near-surface material consisting of a typical black, Kansan soil profile (order Mollisols; Birkeland, 1984) to depths of around 0.8 m, underlain by silty rich soil which grades into shale at around 3.0 m. A strong reflection representing the top of the Stanton limestone is present at approximately 85 ms on seismic data recorded in this area (Knapp and Watney, 1987).

The second test site (herein called Snodgrass Ranch site) is located about 0.5 km south of the city limits of Lawrence on a grassy field immediately south of a small farm pond (Figures 2, 5). The near-surface material at this site consists of compacted, course sand- to pebble-sized gravel, overlying a minimum of 10.5 meters of light brown and yellow clay. The static water level at this site is at 1 m depth, as evidenced by water that accumulated in a fresh drill hole. Bore hole information suggests a strong reflector should be present at the base of the 33 m-deep Tonganoxie sandstone.

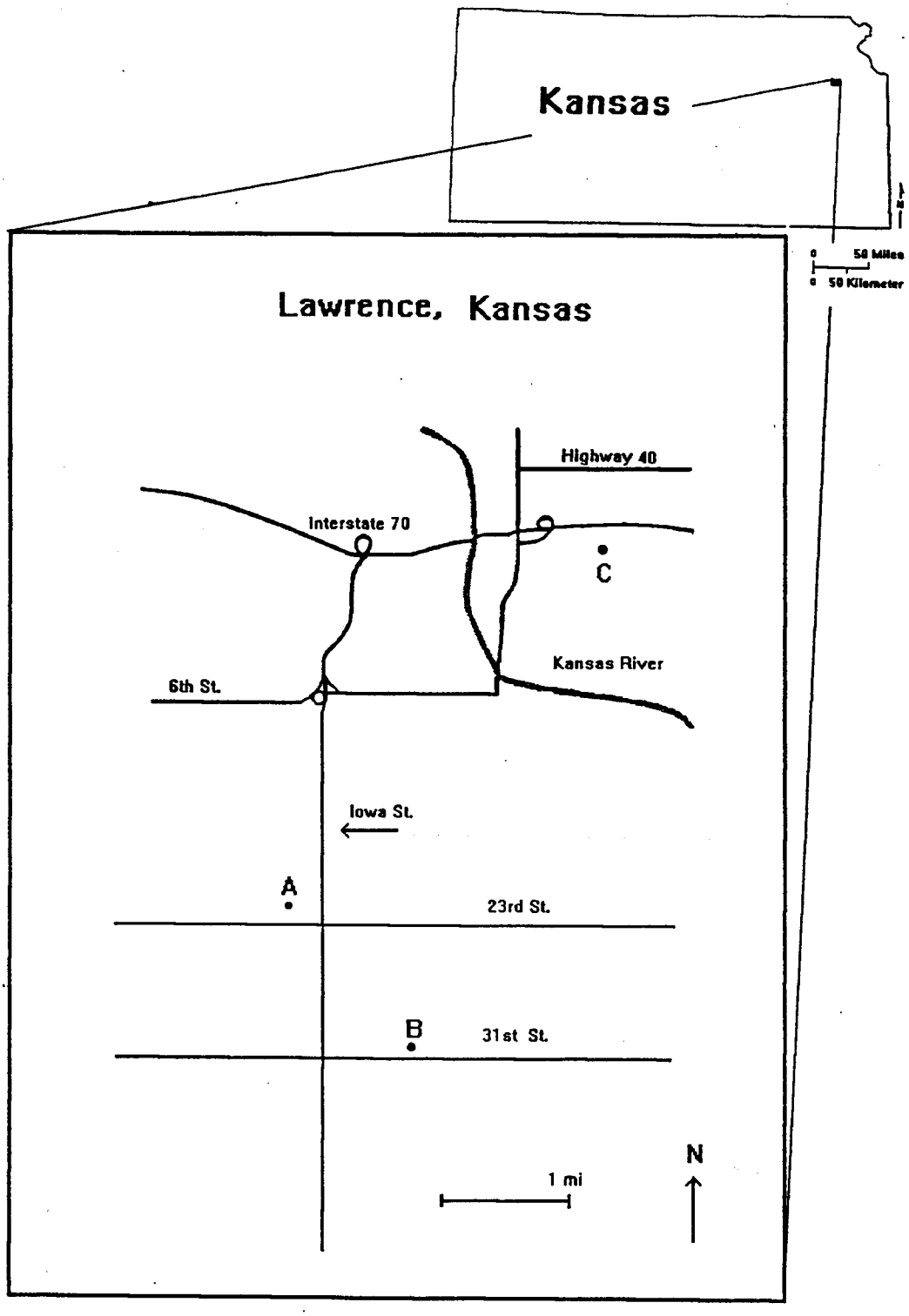

A = KU Campus Site B = Snodgrass Ranch C = Sandpit Site

Figure 2. Location of study area and study sites.

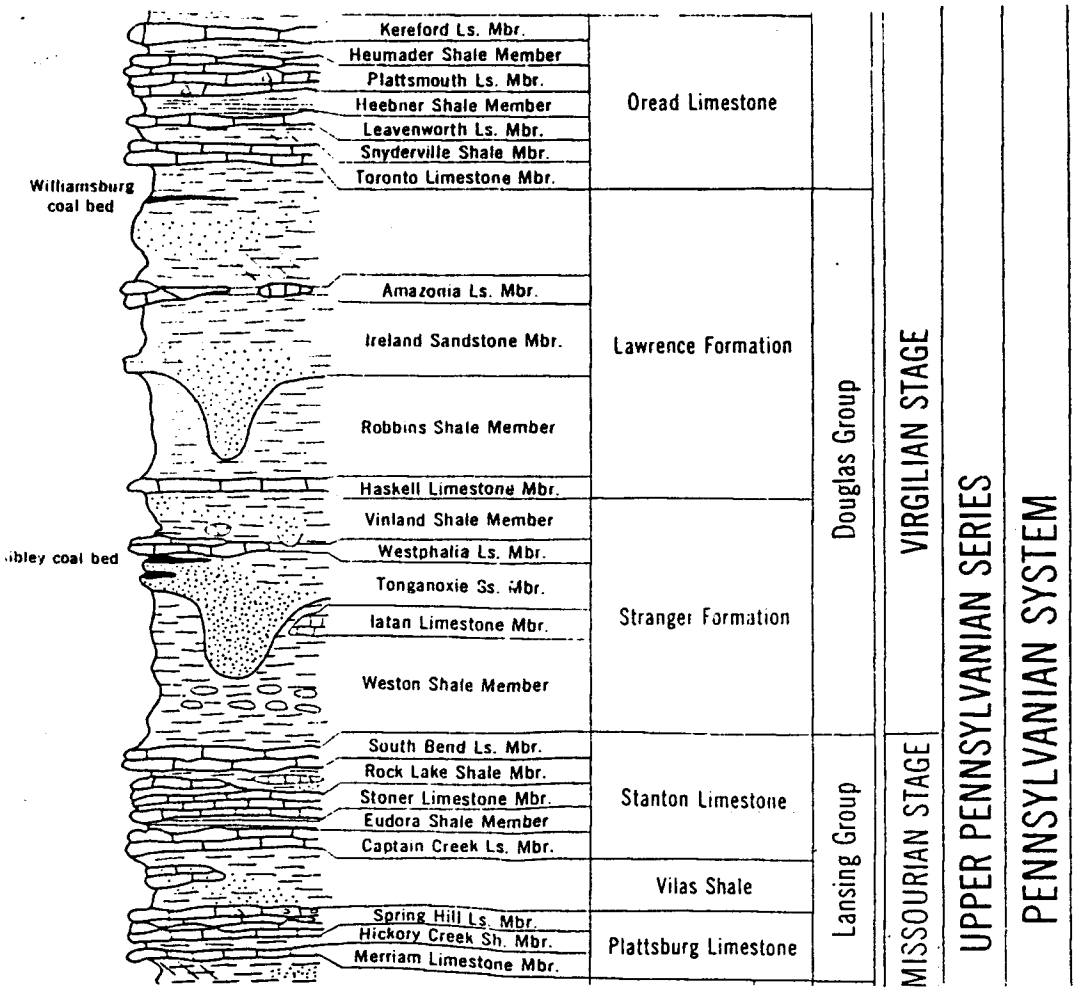

Figure 3. Classification of rocks units in Kansas (Zeller, 1968).

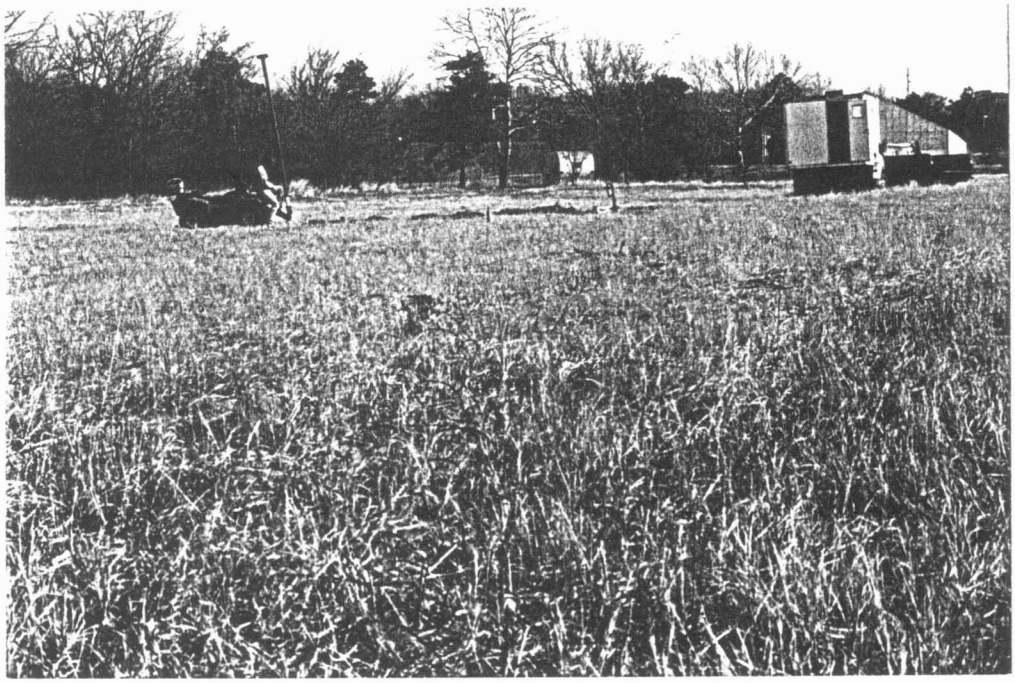

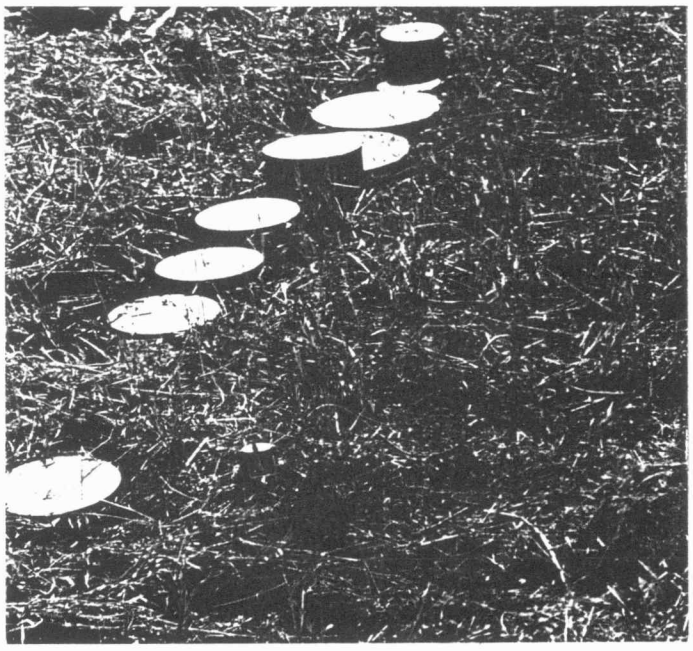

Figure 4. Near-surface condition of the KU Campus site is shown in the bottom photograph, while the mechanical impact device (MID), and the 3 m hammer-handle extension are displayed in the top photo.

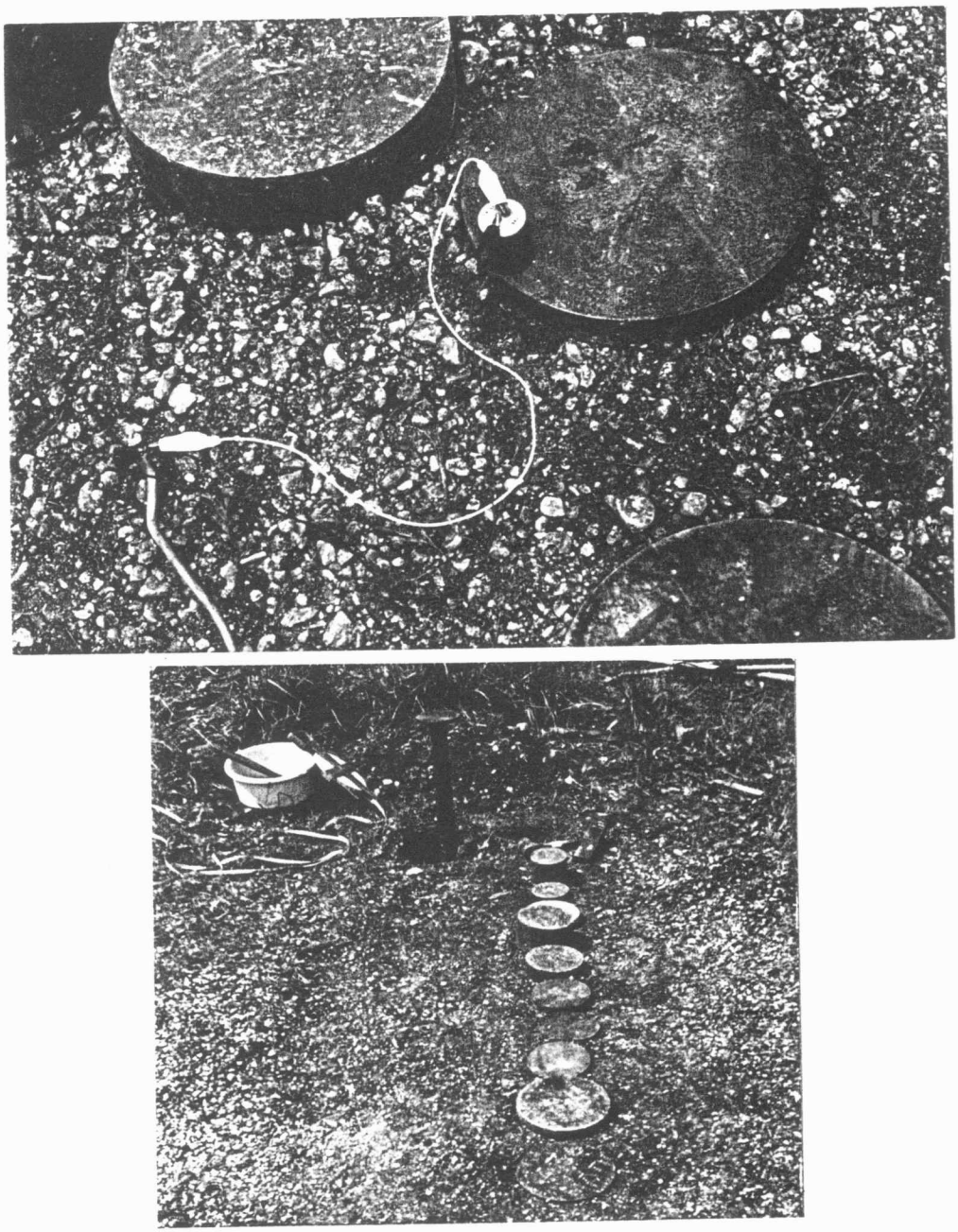

Figure 5. Snodgrass Ranch site, poorly sorted gravel-size rock fragments are present at the surface. A geophone element (top) provided a reliable time break. The plates are displayed (bottom) according to the pre-arranged acquisition procedure.

The third site (herein named the Sandpit site) is located approximately 0.5 km north of the city limits of Lawrence within the Kansas River valley on a heavily travelled sand and gravel roadway within the bounds of an industrial sand dredging operation (Figures 2, 6). Heavy equipment operations have caused extreme compaction of near surface materials. The upper 0.08 m consists of coarse sand-size quartz grains, and is underlain by an extremely compacted (0.04 m) layer which consists of poorly sorted, coarse sand- to pebble-size lithic rock fragments. Underlying the compacted gravel are black soil deposits (order Mollisols) to a minimum depth of 5 m. The edge of the dredge pond is within 50 m of the line location with a static water level less than 2 m below the elevation of the test line. Bedrock reflections at this site occur at approximately 45 ms two-way time (Grantham, 1990).

ACQUISITION METHODS / APPARATUS DESIGN

An Input/Output, Inc. DHR 2400 seismograph was used to amplify, analog filter, analog-to-digital (A/D) convert, and record 24-channel seismic reflection records. Data were digitally recorded on half-inch magnetic tape in a modified SEG-Y format. The 1000 samples recorded at 1/4 ms intervals resulted in a 2000 Hz Nyquist frequency, and a 250 ms record length. The 12 bit A/D converter (11 bits + sign) ideally provides a dynamic range of 72 dB. The fixed-gain levels used during data acquisition were chosen to maintain a minimum word size of 9 bits but less than a full 11 bits for each trace, thereby maximizing the recorded signal without saturating the A/D converter (clipping). A 10 Hz geophone, placed within 0.2 m of the hammer/plate contact provided a reliable time zero.

A series of walkaway-noise tests was performed at each site prior to data acquisition to determine the optimum recording window (table 1) for reflection information (Hunter et al., 1984). All data used in comparisons were recorded with pre-A/D, low-cut filters with 24 dB per octave rolloff and a -3 dB point of 110 Hz. Analog high-cut filters with 24 dB per octave rolloff above a corner frequency of 1000 Hz were used to reduce the amplitude of unwanted high-frequency noise and prevent aliasing of high

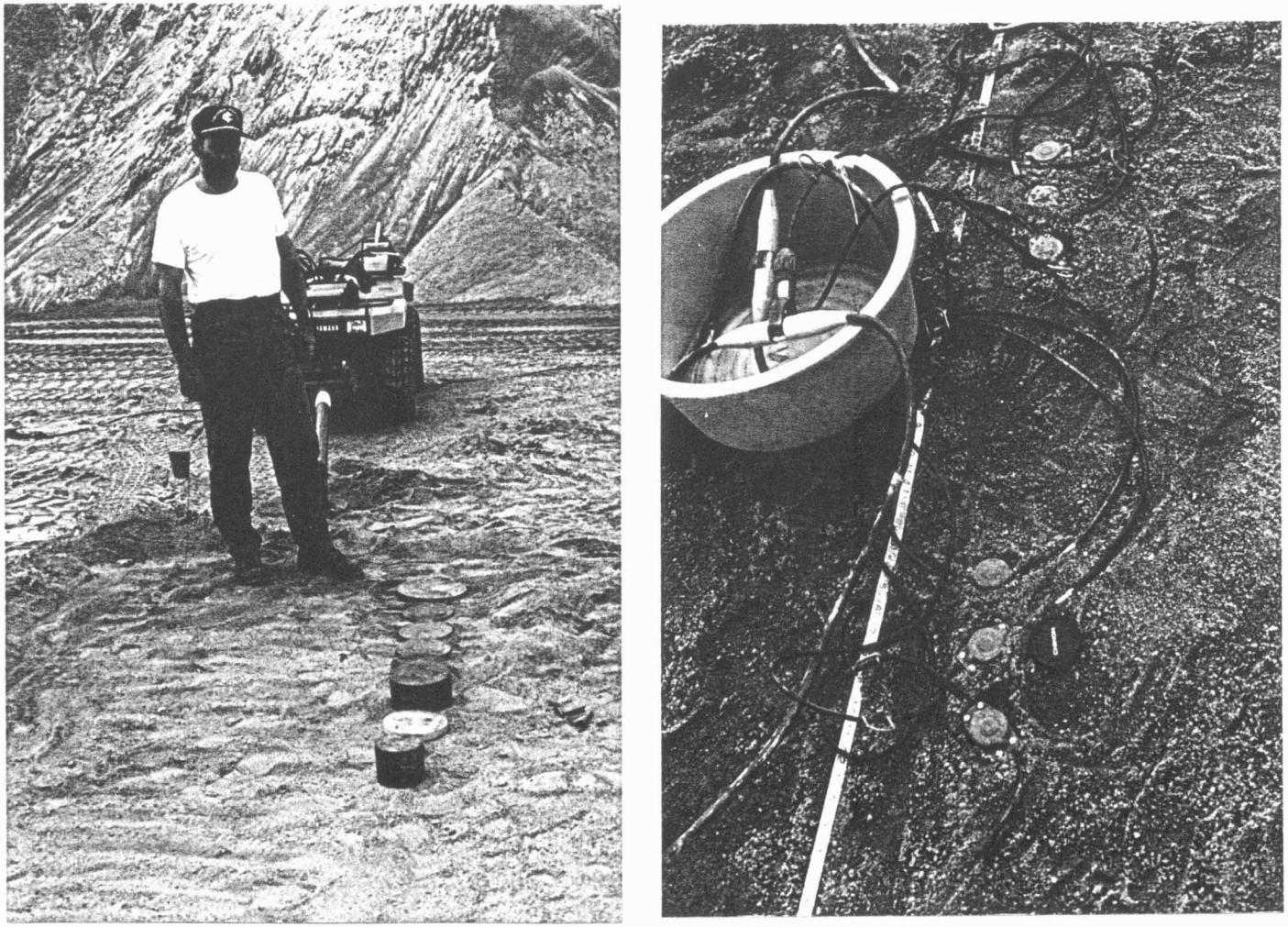

Figure 6. The Sandpit site is located within the Kansas River valley. At this site, mature sand deposits have been compacted by heavy, industrial equipment travel during sand dredging operations.

frequencies. The high-cut filters attenuate the 2000 Hz alias frequency by 24 dB prior to A/D conversion. Identical analog filters were used at all three sites to allow comparison of site-specific spectral properties.

The receivers were three 40 Hz L28E Mark Products geophones damped to 0.67 of critical, on 0.14 cm spikes, wired in series, and spaced 0.25 m apart parallel to the lines. The geophones were securely planted and left in place for the duration of testing at each site. All data used for comparison purposes were acquired at each site within a 6-hour time period, during which no major change in environmental conditions (such as rain, temperature changes, and/or wind variations) occurred.

End-on shooting geometries were used at all sites, with line locations chosen to minimize topographic changes. Source locations were chosen to be sufficiently far from surface obstacles to avoid potential recording of reflected air coupled waves (Hunter and Steeples, 1986).

A sequence of consistent pre-shooting steps was followed at each site prior to recording data. First, a source area of four square meters was cleared of debris and vegetation to reduce inconsistent plate seats. The source area was small enough that for the closest source-receiver offset (Snodgrass Ranch site) the distance between the source and the nearest receiver varied no more than 8% which is within the allowable rule of thumb for comparison tests (Hunter and Steeples, 1986). Second, plates were seated within the manicured source area on previously undisturbed surface material by a single hammer blow. The progression of the impacts within the source area during testing was toward the receivers to avoid previously agitated near-surface media. This technique minimized the chance of observed variations being the result of inconsistent experimental procedure.

Consistency and repeatability in the amount of source energy imparted to the ground is paramount to the detection of subtle signal variations involved here. A mechanical impact device (MID) was designed and constructed to use gravity as the consistent driving mechanism. Ball bearings were implemented in a pivot device designed to be attached to an All Terrain Vehicle (ATV) (Figure 7a,b).

KU Campus Site	
source-to-nearest-receiver	30 m
receiver station spacing	1.22 m
target reflector depth	100 m
Snodgrass Ranch Site	
source-to-nearest-receiver	13.4 m
receiver station spacing	0.6 m
target reflector depth	30 m
Sandpit Site	
source-to-nearest-receiver	16.5 m
receiver station spacing	0.6 m
target reflector depth	35 m

Table 1

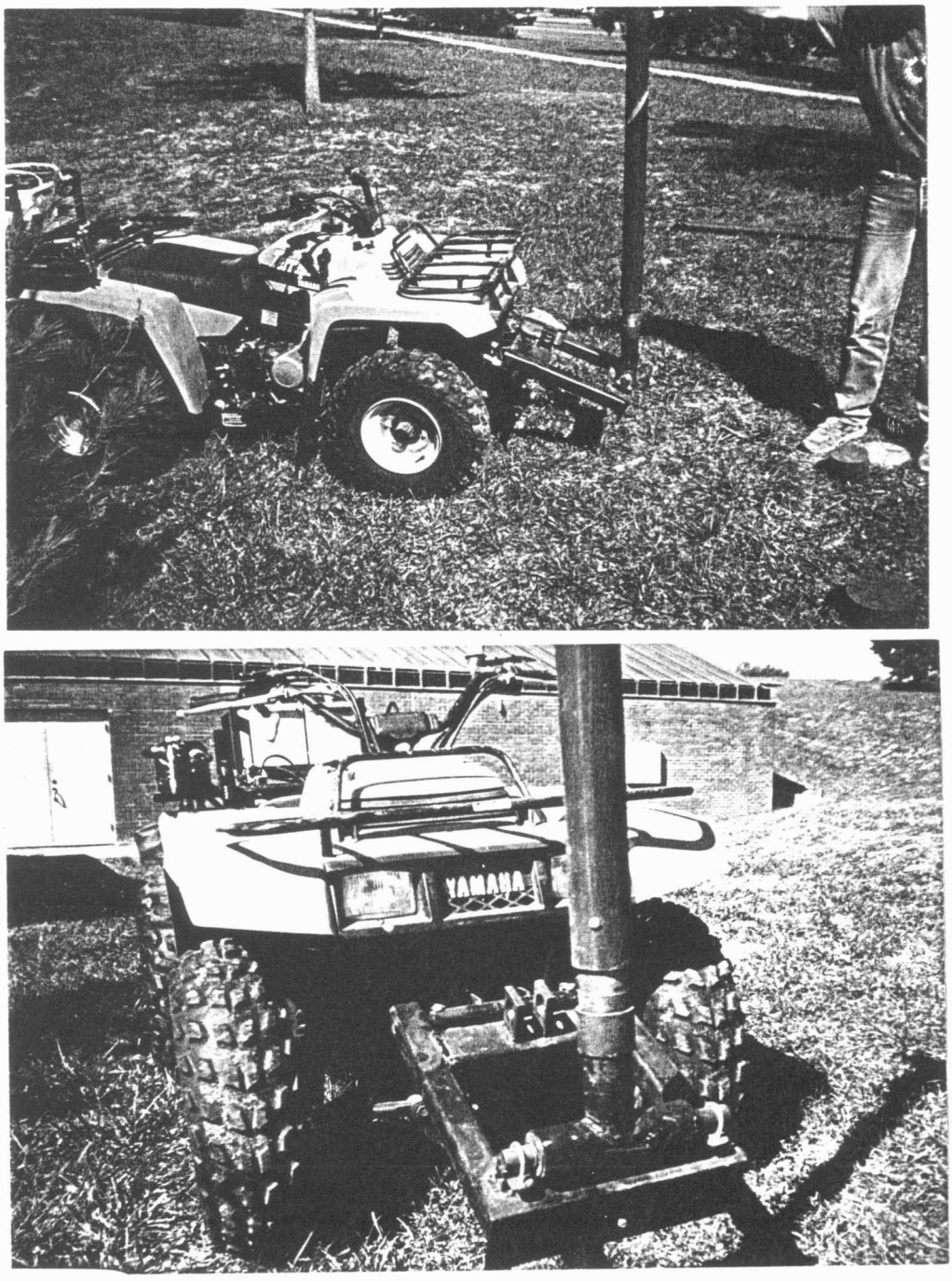

Figure 7a. Photographs of the All Terrain Vehicle (ATV) and the mechanical impact device (MID).

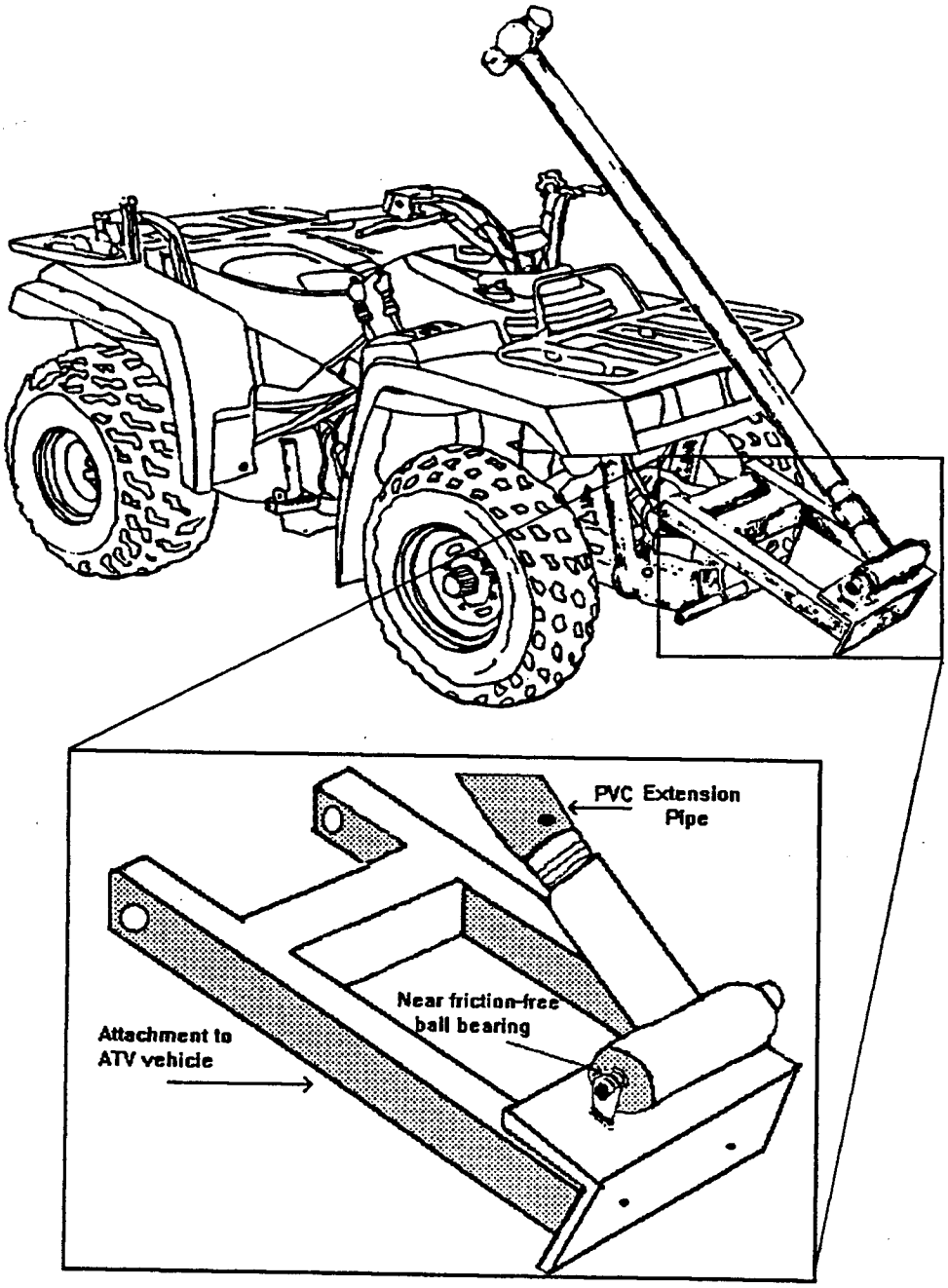

Figure 7b. Line drawing of ATV and the mechanic impact device (MID).

The MID proved (Appendix A) to be more repeatable than human operated swings (rms errors of 6% versus 30% respectively). Thus, energy variations less than 0.5 dB and 6 dB for the MID and human-operated impacts, respectively, can be explained by experimental error. During later discussions seismic energy variations less than 1.0 dB are, for practical purposes, considered insignificant.

The human operators, which included five people of different physical stature, provided unpredictable impact energies (Appendix A). To avoid potential misinterpretations due to variable source energy, a single sledgehammer operator should used for an entire project.

The MID can deliver blows from various sledgehammer masses with impact velocity dependent on the selected swing arm length (1 or 3 m). The impact mass listed in table 3, is measured at the impact point, and includes the mass of the sledgehammer plus the PVC hammer handle extension. Thick walled PVC pipe was used to retard the motion of the extension arm upon impact (this motion is considered negligible in relation to the impact mass during later discussions). Three common off-the-shelf sledgehammer masses (Table 3) combined with the two impact velocities (Table 2) provide a range of source kinetic energy from 78 to 448 J (Table 4). In perspective, one grain (0.06 gm or 0.002 ounce) of dynamite releases 230 J of energy, and one grain of black powder load releases 210 J of energy.

Extreme care was taken during data acquisition to eliminate inconsistent experimental procedures; efforts were made to employ a uniform release of the impact mass, vertically position the extension arm above the pivot center, and maintain a constant height above ground surface of the pivot center. Sledgehammer impacts were caught by hand on rebound after the initial impact to avoid multiple source pulses.

Ten different plates (Table 5) and three different hammer masses (Table 3), each with either different total mass, surface area, or material were included in the tests. The cylindrical plates were constructed of either mild steel alloy or aluminum. The hammers were all standard, off-the-shelf sculptured cylindrical steel masses on the end of oak handles. Repeated impacts did not destroy the steel alloy or aluminum plates, and

Impact Velocity (m/s) of Sledgehammer at Impact

	3.6 kg Hammer	5.4 kg Hammer	9.1 kg Hammer
1 meter Ext.	5.5	5.5	5.5
3 meter Ext.	8.5	8.5	8.5
Manual Swing	11.1	11.6	9.6

Table 2

Impact Mass of Source Combinations

Hammer	1 m Extension*	3 m Extension*
3.6	5.0	7.7
5.4	7.7	10.4
9.1	10.4	12.7

*Mass of hammer (kg) plus extension apparatus at impact

Table 3

Kinetic Energy at Impact - KE = (0.5)(m)(v^2)

*Impact Mass (kg)	1 m Extension (J)	3 m Extension (J)	Human Operated
3.6	----	----	221 (39)**
5.4	----	----	363 (47)
9.1	----	----	419 (121)
5.0	78 (2)	----	----
7.7	116 (2)	278 (18)	----
10.4	157 (4)	376 (3)	----
12.7	----	448 (8)	----

* Impact Mass = Sledgehammer Mass + Extension Arm **( ) = rms error

Table 4

Impact Plate Specifications

Surface Area (cm^2)	Diameter (cm)	Thickness (cm)	Mass (kg)
137	13.2	2.5	2.7
137	13.2	10.2	10.9
274	18.7	0.6	1.4
274	18.7	2.5	1.8*
274	18.7	1.3	2.7
274	18.7	2.5	5.4
274	18.7	5.1	10.9
274	18.7	10.2	21.8
548	26.4	0.6	2.7
548	26.4	2.5	10.9

~38 Common sledgehammer (all weights)

* Aluminum Plate

Table 5

the same set of ten plates and three hammers was used at each of the three sites.

To assess the merits of avoiding the highly attenuative near-surface materials by placing the source energy one meter below the surface, additional tests included 'downhole plates'. The 'downhole plates' consisted of either slightly modified auger flights (Figure 8), or a plate attached to an extension (extension-plate) which was then lowered into a previously drilled hole. The length of the auger flights (0.48 and 0.74 m) was adjusted such that their mass was 5.4 and 10.9 kg respectively in order to correlate to surface plates of equal mass. The modified auger flights (5 cm in diameter) were manually screwed into the ground with a pipe wrench such that the top of the flight was about 2 cm above the surface prior to impact.

The extension-plate consisted of two circular plates separated by steel cylindrical tubing. During acquisition, the extension-plate (21.8 kg) was placed in a fresh 0.18 m diameter hole, 0.9 m deep. Prior to recording an impact, the bottom of the hole was cleared of loose debris which fell into the hole during drilling.

DATA PROCESSING/SEISMIC ENERGY

Data processing was done on an Intel 80386-based microcomputer using a proprietary seismic processing package (Eavesdropper) developed by the Kansas Geological Survey (Somanas et al., 1987). All data were analyzed in field file format and as amplitude spectra.

Relative amplifier gain is critical to amplitude evaluations between field files. Care was taken during data acquisition to faithfully write down the amplification applied to each of the 24 channels, for each impact. A corrective gain, dependent on the original pre-A/D gain, was then applied digitally to each individual channel to bring the total gain (sum of both the field and display amplification) to a constant for the study site. All records within subsequent comparisons possess equivalent gain. Based on a visual data inspection, the combined gain setting was chosen as the proper amount required to produce a distinct, clear seismogram.

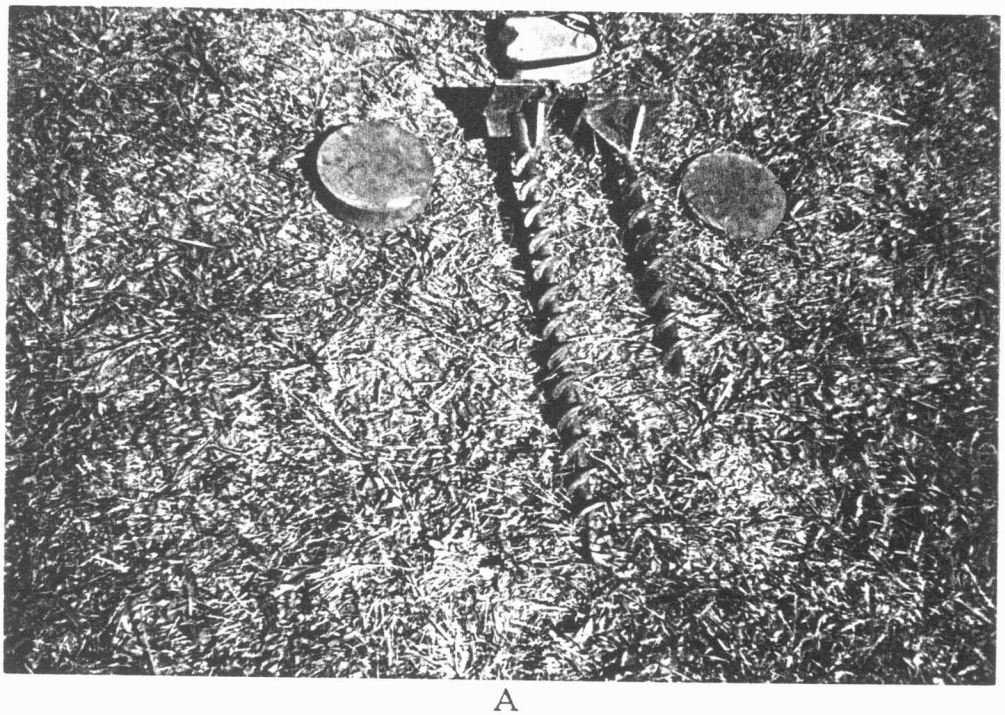

A

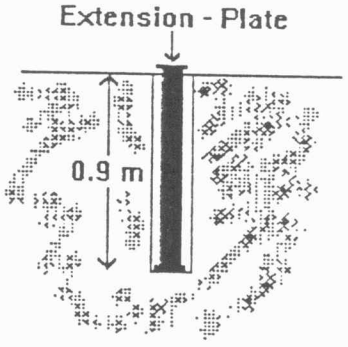

B

Figure 8. Photograph of the auger flights (A), and line drawing of the extension-plate apparatus (B) tested. The camera case in the photo is 10 cm x 15 cm.

To describe energy fluctuations, the square of the trace signal (individual samples) were summed for each drop gather. This sum will be referred to as the seismic energy herein. All data from a given site possessed equivalent gain prior to calculating the seismic energy (Table 6).

RESULTS

MISCELLANEOUS TESTS

Various source configurations were used to examine non-centered impact effects. The MID allowed the sledgehammer impact to be positioned directly on the plate's edge. Non-centered impacts showed as much as a 2.6 dB decrease in seismic energy as well as a lower signal-to-noise ratio (Figure 9) than centered impacts.

When the sledgehammer was allowed to bounce unrestricted on the impact plate, the air-coupled wave increased by as much as 5 dB relative to like impacts that were manually caught during the initial rebound (Figure 10). As a result, during subsequent testing all impacts were restricted from repeatedly impacting (bouncing on) the plate.

Acquisition techniques have been developed for projectile sources which decrease air-coupled wave interference and increase the energy content of seismic signals (Pullan and MacAulay, 1985). The main advancement in projectile sources centered on the idea of firing the source downhole, such that the bullet impacts more consolidated materials, thus avoiding enhanced attenuation by the near-surface materials (Steeples, 1984). Adopting this idea, tests which included striking 'downhole plates' were conducted to determine the merits of placing the impact energy beneath the surface material.

The downhole auger flights proved to not produce the same data quality as surface plates. As much as a 6 dB decrease in seismic energy was observed for the auger flights compared to a surface plates of like mass. In addition, spectra for the data show a 50 Hz decrease in peak frequency from the surface plate to the auger flight (Figure 11).

Data quality was enhanced, however, by the use of the downhole extension-plate. Subsurface emplacement of the plate produced 5 dB more seismic energy than the surface configuration as well as increased the

Composite Fixed Gain Settings

KU Campus Site.....	Channels 1-19=94 dB
	Channels 20-24=102 dB
Snodgrass Ranch Site.....	Channels 1-7=74 dB
	Channels 8-24=78 dB
Sandpit Site.....	Channels 1-13=94 dB
	Channels 14-24=98 dB.

Table 6

Snodgrass Ranch Site

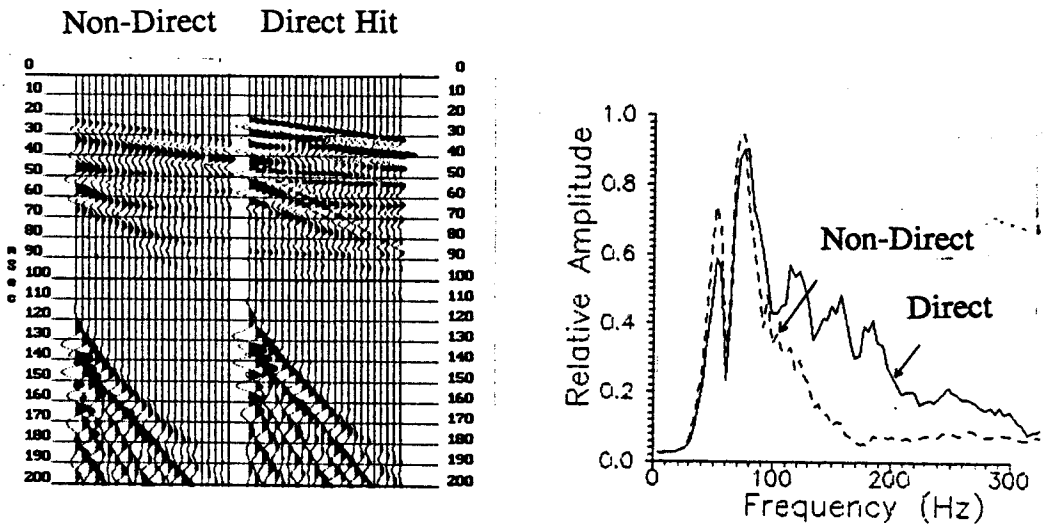

True Amplitudes

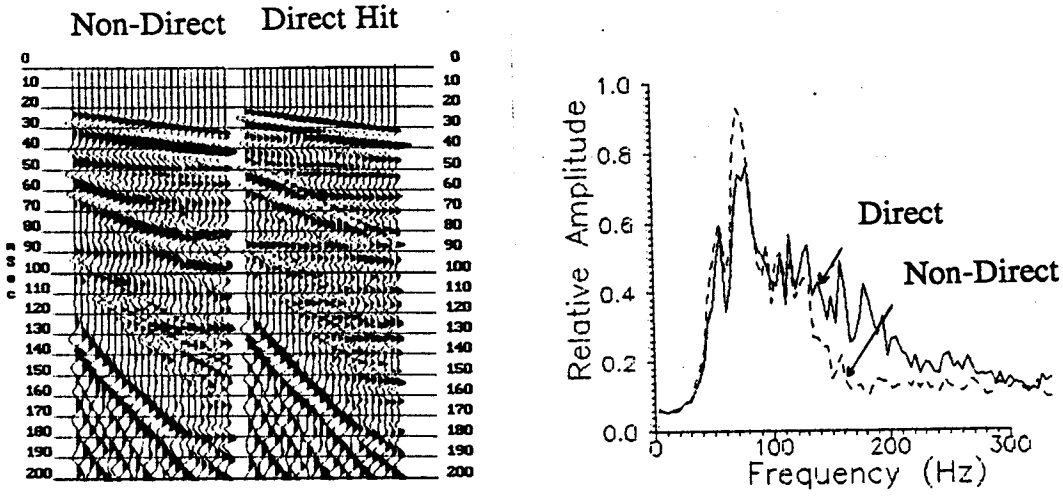

Amplitude Adjusted (AGC)

Figure 9. Data comparison generated by a non-direct (non-centered) versus a direct (centered) impact. Sledgehammer source included the 10.4 kg impact mass, 10.9 kg impact plate (548 cm^2) and an impact velocity of 5.5 m/s. In these, and all following spectra, the amplitude values have been normalized and consequently are relative comparisons only.

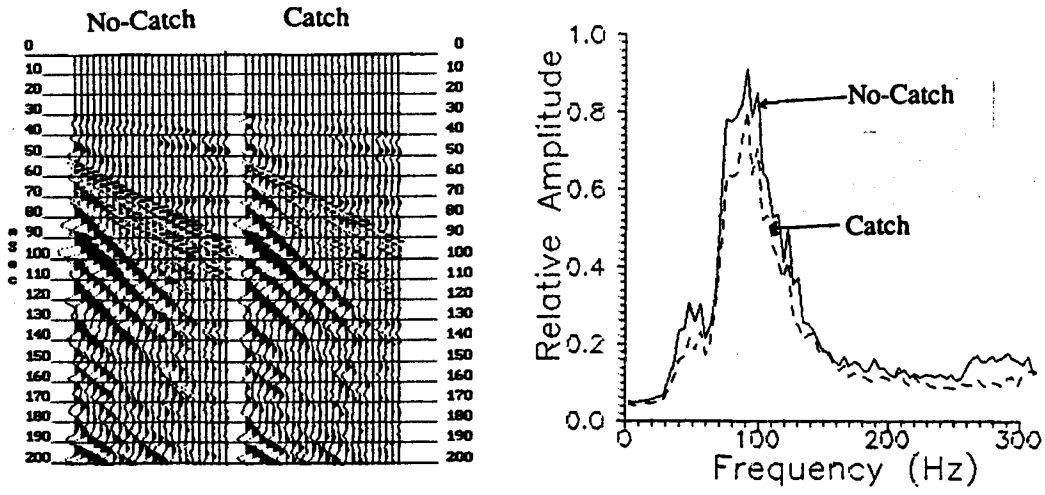

A

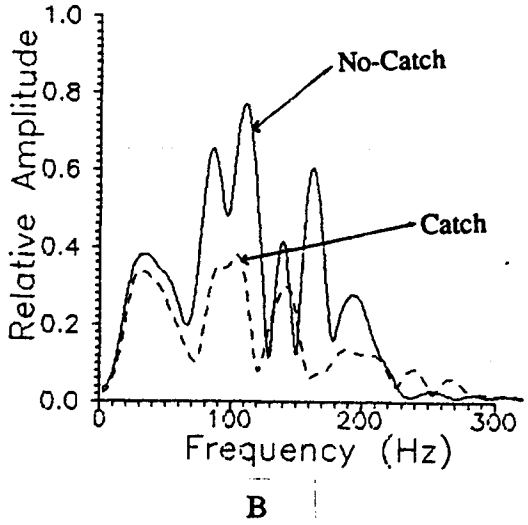

B

Figure 10. Data acquired at the Sandpit site exhibit the effects a multiple-impact blow (bounce) may have relative to a single blow (no bounce)(A). Shown also are spectra of the air-coupled wave from each of the records (B). For the multiple-impact blow, the sledgehammer (7.7 kg) was allowed to bounce on the plate (1.4 kg, 137 cm^2) unrestricted. Impact velocity was 5.5 m/s for both cases.

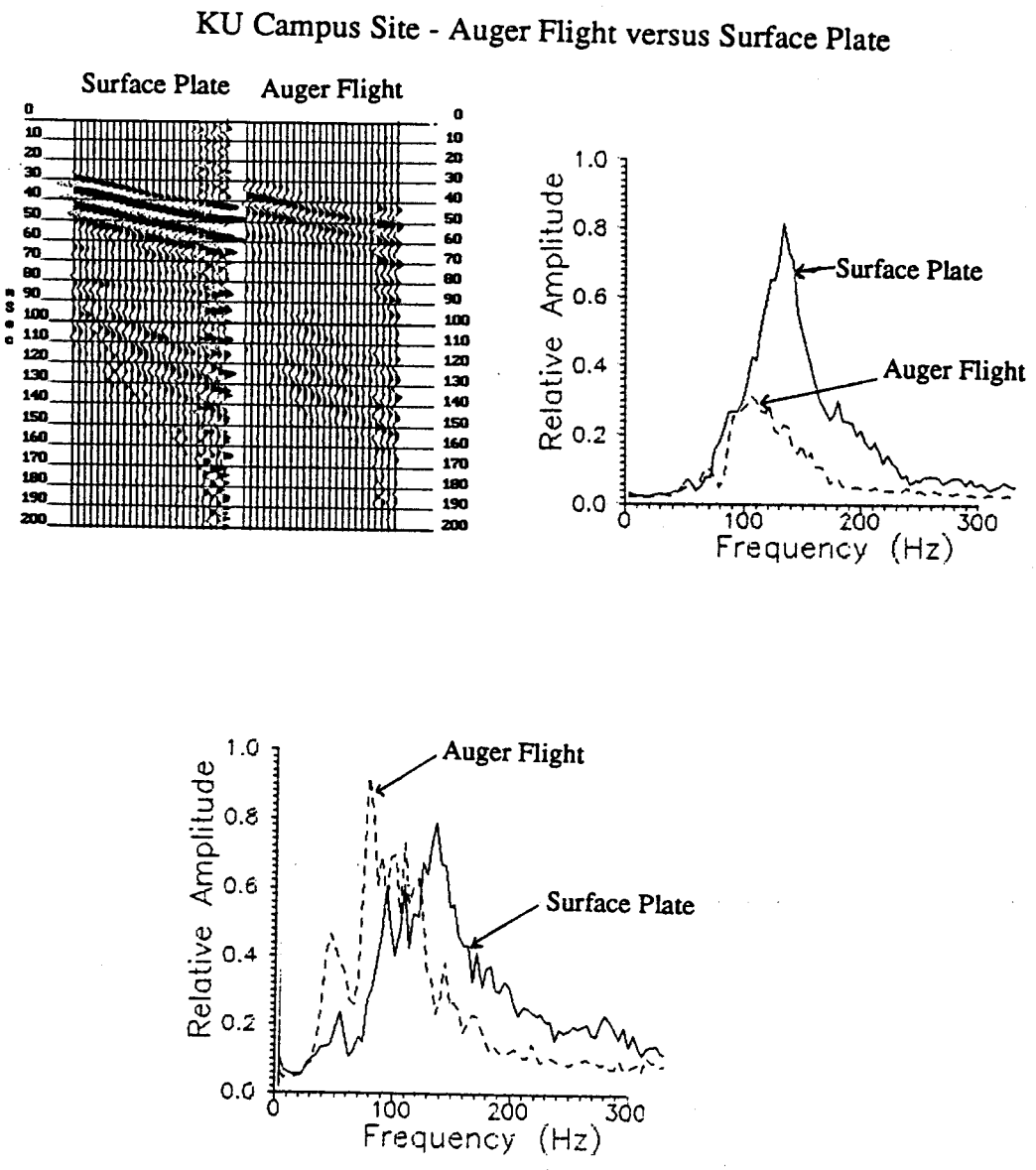

Figure 11. Comparison of auger flight and surface plate seismic data. A decrease in seismic energy and peak frequency is observed for the auger flight relative to the surface plate configuration. Sledgehammer source includes the 5.4 kg surface and auger plates, 7.7 kg impact mass, and an impact velocity of 5.5 m/s.

signal-to-noise ratio (Figure 12). Drilling a hole for the extension-plate complicates the sledgehammer source a great deal. Thus, although seismic data quality is increased the acquisition efforts involved may severely limit the technique's usefulness.

Source-generated air-coupled wave interference is a problem (Pullan and MacAulay, 1985) not unique to hammer sources (Steeples, 1984). Acquisition techniques developed to reduce this unwanted energy for projectile sources have been relatively successful in some cases (Pullan and MacAulay, 1985; Steeples and Miller, 1990). With the exception of an unsuccessful attempt to reduce the air-coupled waves by striking a plastic plate on the surface (Pullan and MacAulay, 1985), acquisition techniques to reduce the amplitude of air-coupled waves are conspicuously absent in the literature.

Two experiments were conducted to reduce the air blast; the first addressed the plate and the second the hammer. Initial experiments which involved impact plate covers of various rubber and foam materials resulted in a uniform decrease in amplitude throughout the seismogram.

Impacts from the steel hammer to a steel plate produced more air-coupled wave energy than an impact involving the dead-blow hammer (hard rubber molding filled with sand) and the same plate (Figure 13). Data collected at two of the study sites show that while the seismic energy increased 2.0 dB from the dead-blow hammer to the steel hammer, the air-coupled wave energy increased 5 dB. These data may indicate dead-blow hammers should be used in lieu of steel hammers, and at the very least deserve further testing. Frequency content does not appear to be a function of hammer material.

CORE EXPERIMENTS

Variations in the air-coupled wave were analyzed using surgical mute procedures and shown to be insignificant (<1 % of the total seismic energy). For our purposes, the air-coupled wave will be considered constant in all records, and signal deviances addressed are considered an effect of the particular parameter that was changed.

KU Campus Site - Extension Plate versus Surface Plate

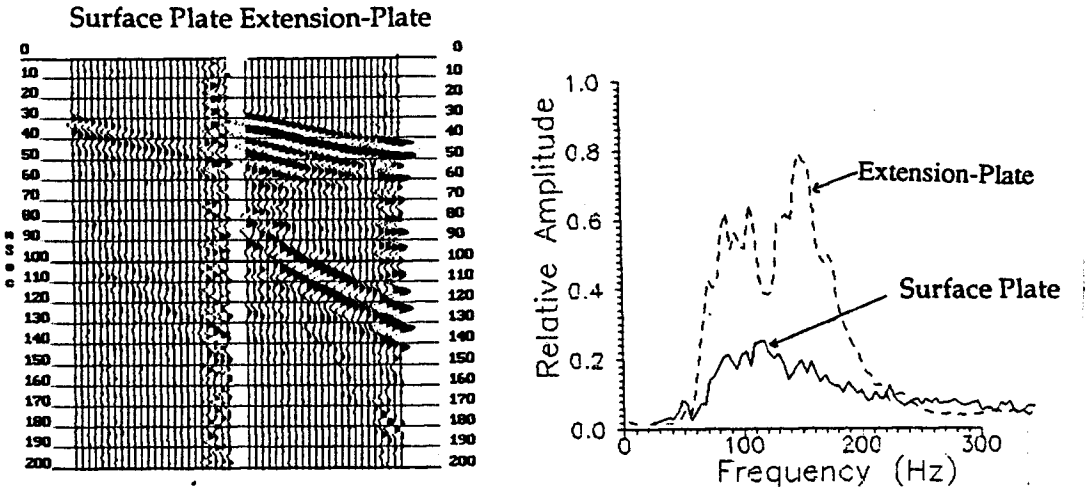

True Amplitudes

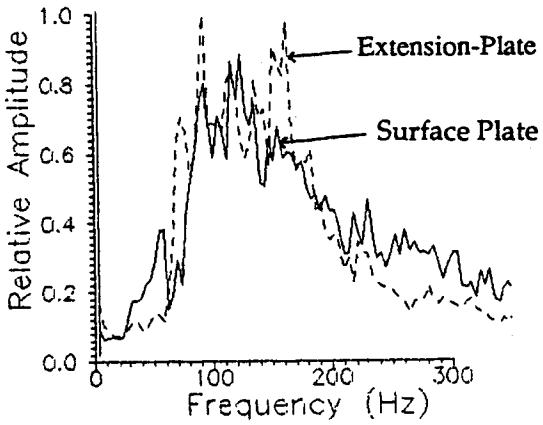

Amplitude Adjusted

Figure 12. Seismic effects of a surface plate versus a downhole extension plate (both 21.8 kg); constant sledgehammer source (7.7 kg impact mass, 5.5 m/s).

Sandpit Site

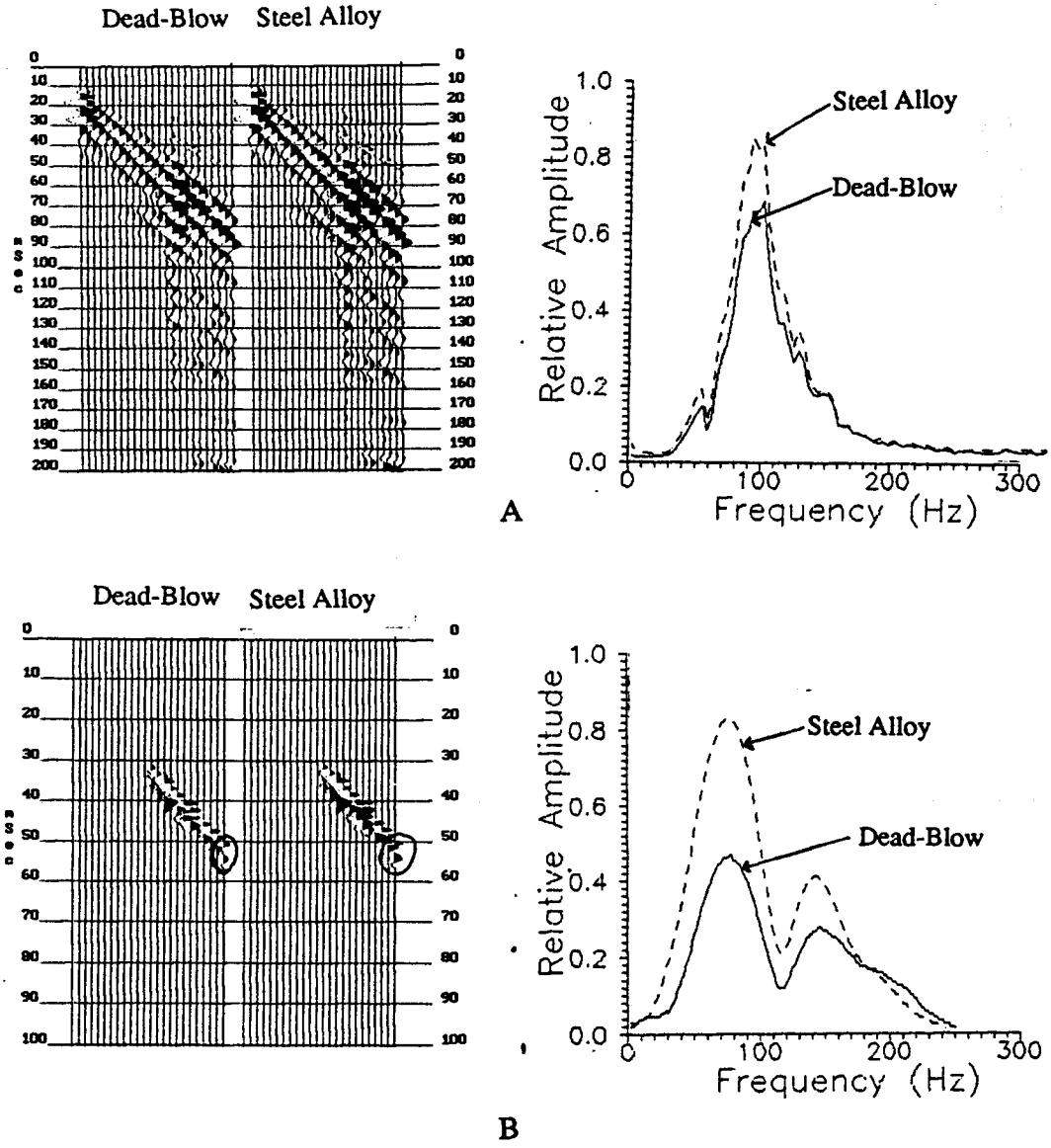

Figure 13. (A) Data comparison from a steel hammer and a rubberized dead-blow hammer (both 0.9 kg) at the Sandpit site. Although the steel hammer produced 2.0 dB more seismic energy than the dead-blow hammer, the air-wave energy increased 5.0 dB. (B) Air-blast only. The wavelet used in calculating the spectra is circled. Nearest source-receiver offset is 3.0 m, and receiver group spacing is 0.6 m.

A. Effects of Compaction

To determine the significance of seating an impact plate, 20 consecutive impacts to a static plate position were recorded at each of the study sites.

Seismic energy increases associated with surface material compaction proved to be dependent on the near-surface media. Increases in seismic energy from the initial impact to that of the 20th impact were greatest for soil, slightly less for gravels, and negligible for compacted sands (Figure 14).

Plate surface area plays a crucial role in determining the rate of increase with successive impacts; increases in seismic amplitudes are inversely proportional to the surface area of the plate (Figure 15). Two things of importance are seen in these data. First, a plate of large surface area requires fewer impacts before permanent deformation is reduced compared to a plates of smaller surface areas for a given source energy. Secondly, after 20 impacts, the smaller (136 cm^2) plate levelled off at almost the same amplitude sum as the larger (529 cm^2) plate. Apparently, site characteristics constrained signal energy levels.

The signal-to-noise ratio increased as the near-surface became compacted (Figure 16) at some sites. This phenomenon may be associated with a decrease in plastic waves (and associated waveshaping) as the media strength increases.

B. Plate Surface Area Variations

The question of plate surface area is important if there is an observable change in the recorded signal when an impact plate is used. From a rudimentary consideration it is clear that an impact plate will distribute the impact energy over a greater area, lowering the stress and reducing permanent deformation. Previous experiments showed seismic energy levels to increase when plates were used relative to impacts without plates.

The effects of plate surface area are site dependent. Within the range of surface areas tested, the average seismic energy increase is approximately 3.4 dB for a doubling of plate surface area at the KU

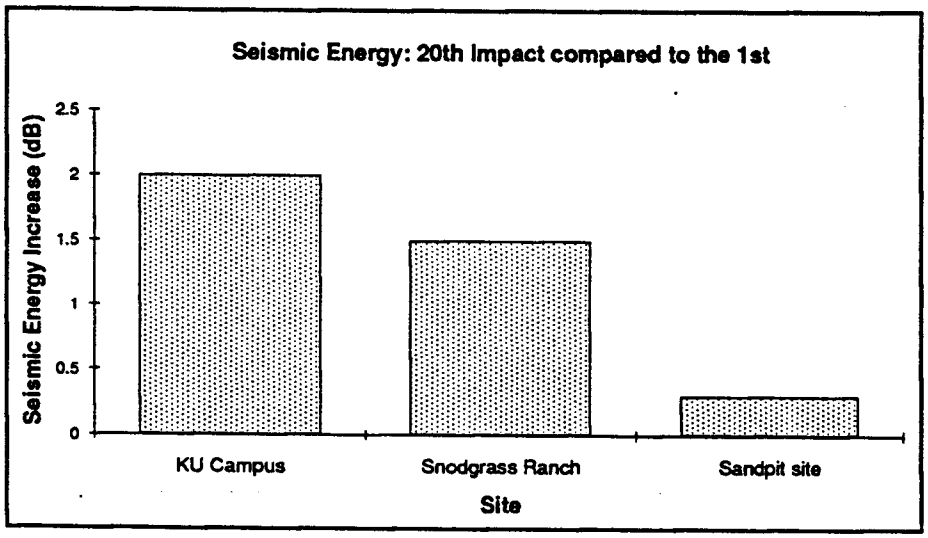

Figure 14. Increases in seismic energy for successive impacts are inversely proportional to near-surface material strength. Sledgehammer configuration included a 10.9 kg (274 cm^2) impact plate, 10.4 kg impact mass, and 5.5 m/s impact velocity.

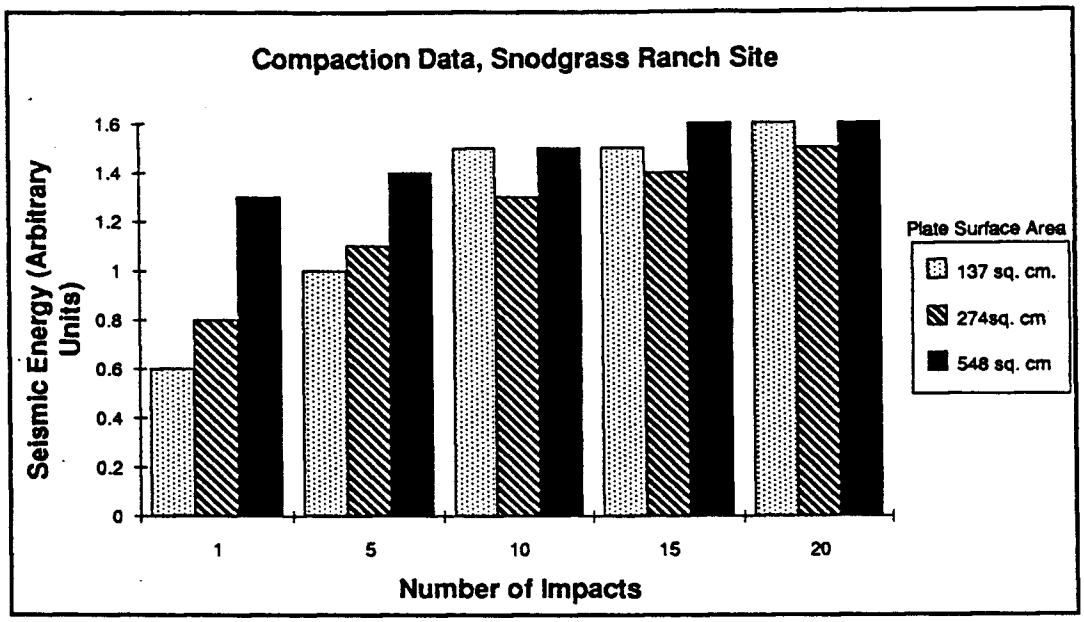

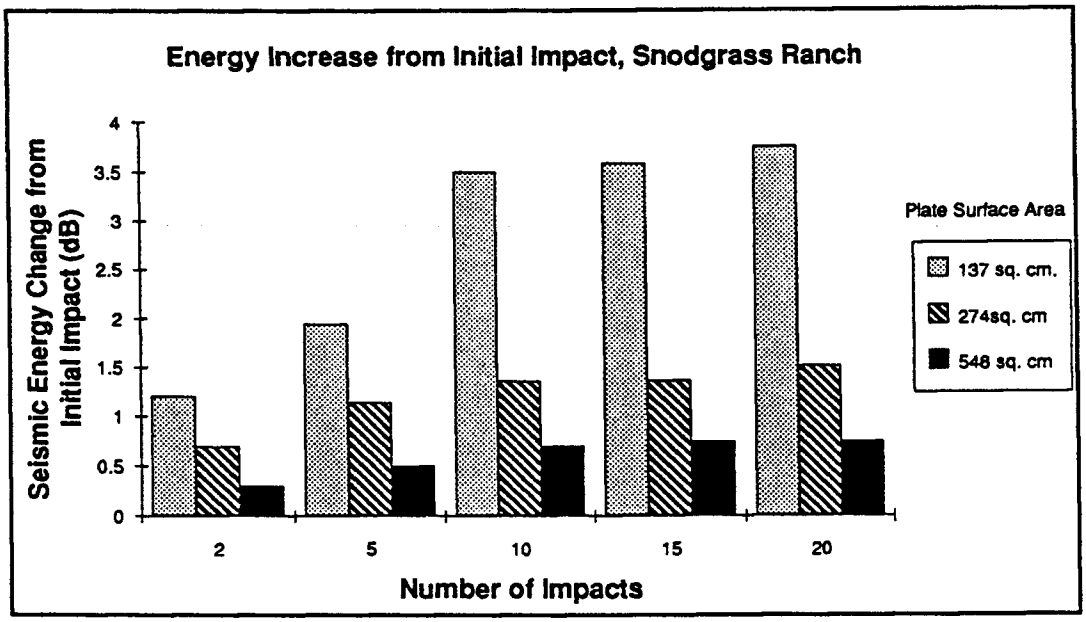

Figure 15. Seismic energy variation as a function of repeated impacts. Characteristics of this site apparently determined maximum signal amplitudes. Source conditions (10.9 kg plate mass, 10.4 kg impact mass, 5.5 m/s impact velocity) were held constant during the test.

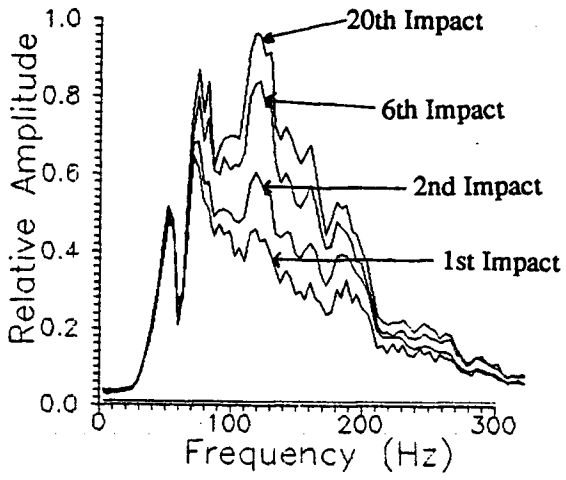

Figure 16. The ratio of 120 Hz to 70 Hz information increased as surface media is compacted by repeated sledgehammer impacts at this site. The sledgehammer source included the 10.4 kg impact mass, 10.9 kg (137 cm^2) impact plate, and 5.5 m/s impact velocity.

Campus site, 1.1 dB at the Snodgrass Ranch site, and 0.4 dB at the Sandpit site. A sample of the seismograms collected at the study sites is shown in figure 17.

To further analyze the role plate surface area has in seismic wave generation, surgical mute procedures allowed the rate of increase for windows dominated by particular wavetypes (i.e. body waves and surface waves) to be compared.The results showed that both wave types increased at about the same rate. For the plates involved, surface waves were not preferentially increased as the surface area increased.

Choosing the proper plate can increase frequency content as well as maximize seismic efficiency for some sites. In addition to a 5.1 dB increase in seismic energy, the 548 cm^2 plate produced peak frequencies that are 40 Hz higher than the 137 cm^2 plate at the KU Campus site (Figure 18). Higher frequency content is believed to be associated with the amount of wavelet distortion linked to plastic waves, which is inversely proportional to plate area for a given impact energy level. No significant change in frequency content could be seen for data acquired at the Snodgrass Ranch or Sandpit sites. At these later sites, it is believed that the attenuation of the earth reduces high frequency components regardless of whether they are present in the source pulse or not.

Generalities ascertained from the these data appear to be consistent for both plate masses (2.7 and 10.9 kg) included in the tests.

C. Impact Energy/Seismic Energy Relationship

Source energy can be altered by changing the impact velocity or the impact mass. The question addressed here is whether the seismic efficiency (defined as the ratio of seismic energy to source energy) is altered by increasing the impact mass while maintaining constant velocity or vice versa.

Figures 19 and 20 graphically display seismic energy versus source energy for a single plate at the study sites. These plots are representative of the relationships between source energy and seismic energy for all plate masses. Two interesting observations can be made from these data. First, the seismic energy increases faster when the impact mass is increased while

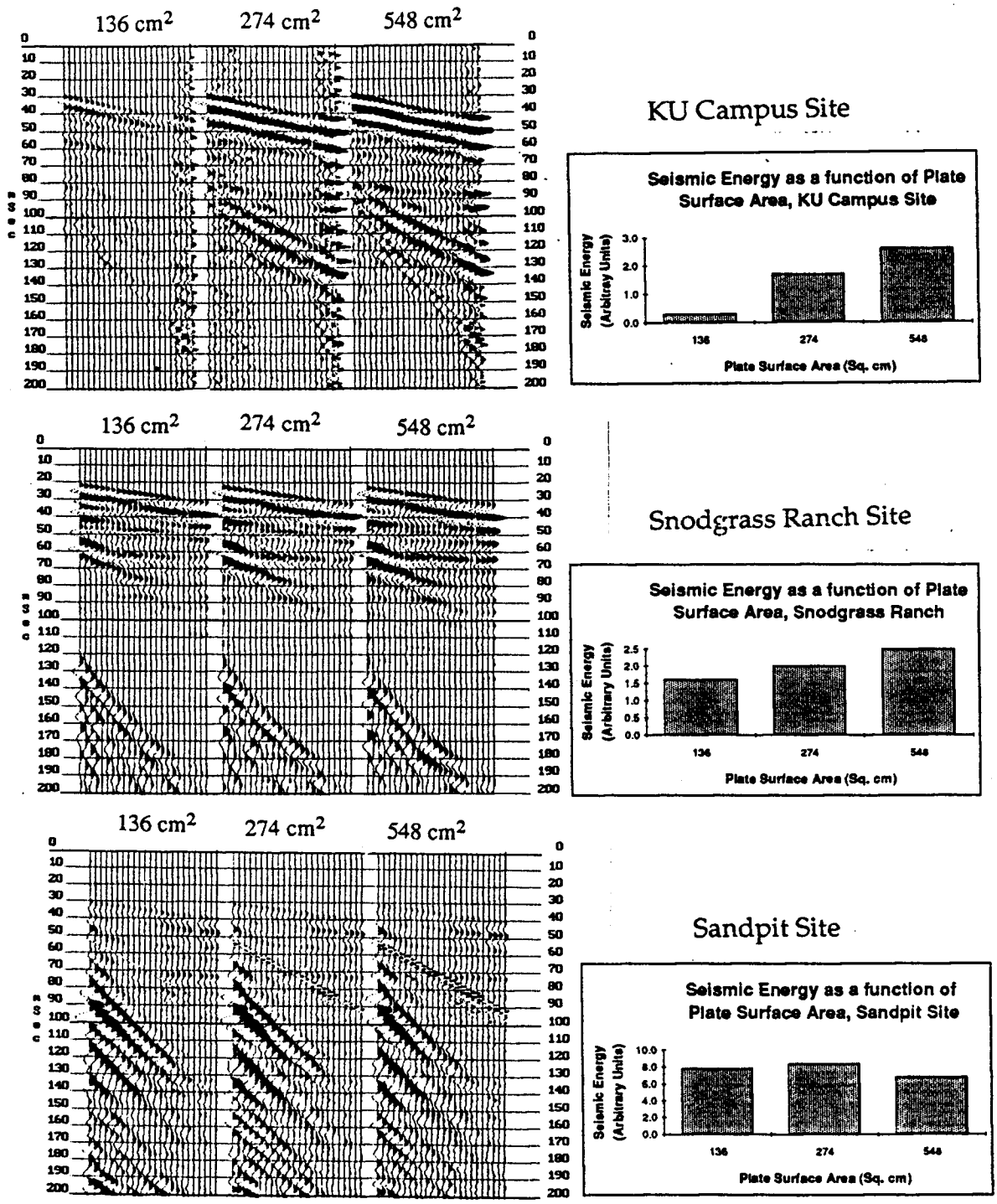

Figure 17. Seismic signal as a function of plate surface area. Sledgehammer source included the 10.4 kg impact mass, 2.7 kg impact plate, and 8.5 m/s impact velocity at all sites.

KU Campus Site

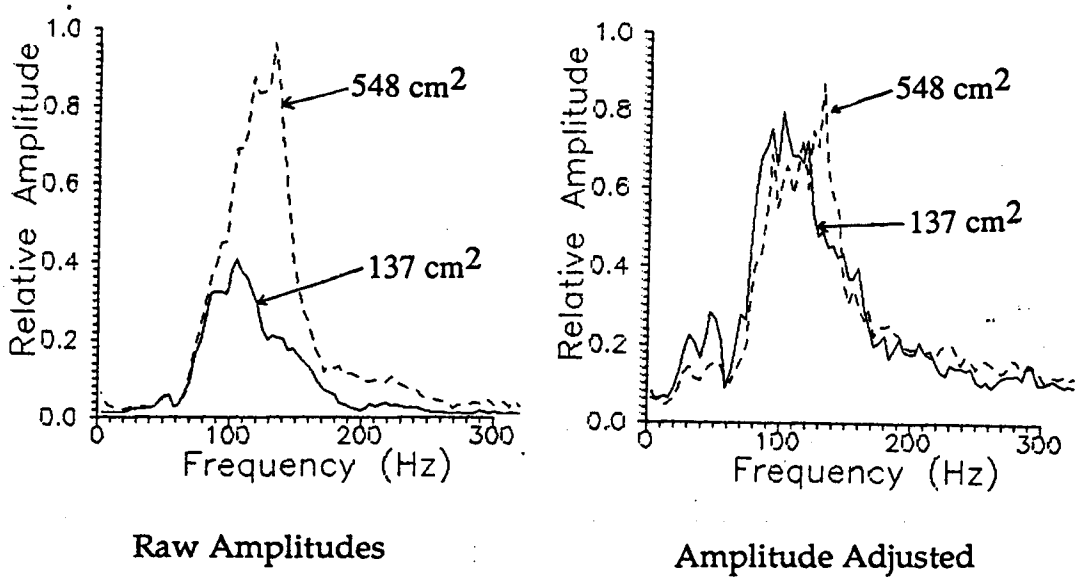

Figure 18. Spectra showing a 30 Hz higher peak frequency for the 548 cm^2 (dashed) plate compared to the 137 cm^2 plate (solid). The impact mass (10.4 kg), impact plate (10.9 kg), and impact velocity (5.5 m/s) are constant.

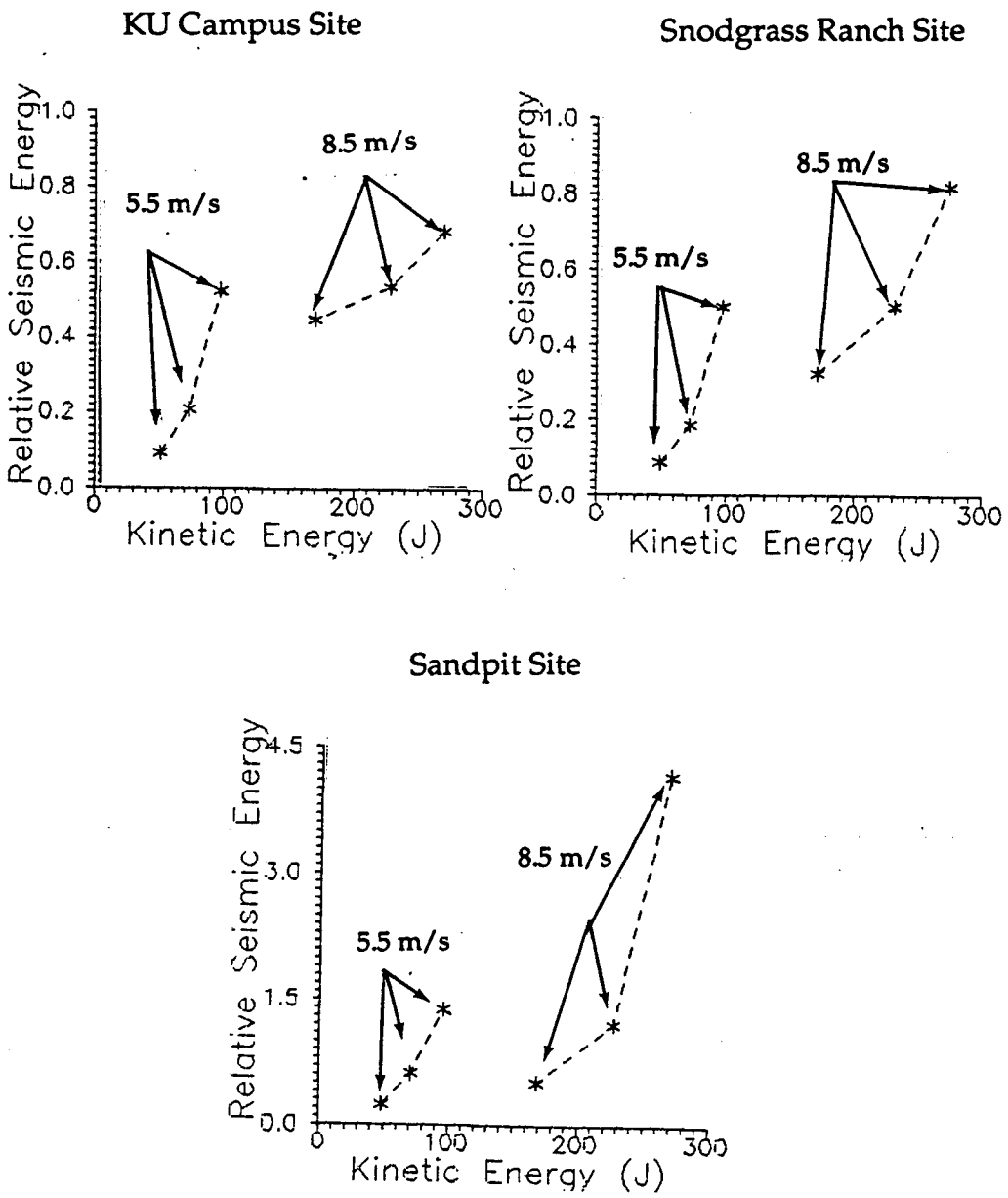

Figure 19. Seismic energy versus impact energy. Different slope patterns are seen for the 5.5 m/s impact velocity versus 8.5 m/s. All data have been normalized and show relative seismic energy. All sites have been scaled identically, thus the y-axis scale for the Sandpit site represents changes in seismic energy that are 4.5 times that observed at either the KU Campus or Snodgrass Ranch site. Data are for a single plate (1.4 kg, 549 cm^2).

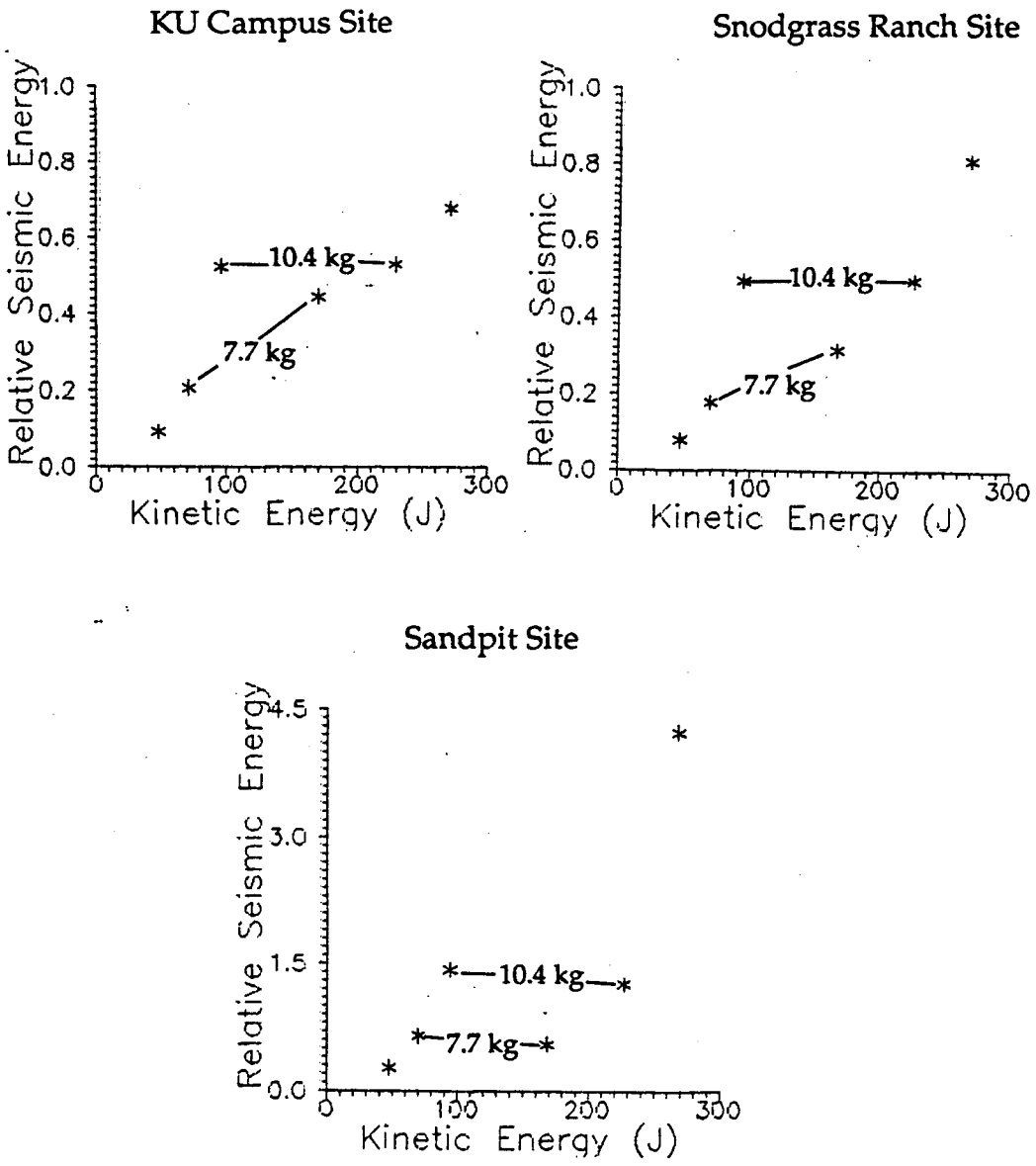

Figure 20. Same data as shown in figure 24 except attention is directed to impacts of equal mass, but different impact velocity. Increasing the impact velocity does little to increase seismic energy at these sites. Data are for a single plate (1.4 kg, 549 cm^2).

the impact velocity remains constant (Figure 19) relative to when the impact velocity increases and the impact mass is fixed (Figure 20). In other words, within the range of these experiments, seismic efficiency is greater for a large impact mass travelling at a slow impact velocity than for a small impact mass travelling at a higher velocity. This result supports Mereu et al. (1963).

Second, the near-surface medium determines the rate of seismic energy increase with increasing impact energy. This is seen by comparing the change in seismic energy for a given source energy change (compare the slopes) for different sites (Figure 19). For a given change in source energy, compacted sands (Sandpit site) showed greater increases in seismic energy than the soil environments (KU Campus site).

D. Impact Velocity Variations

For constant impact mass and plate mass, seismic energy changes are theoretically directly proportional to the impact velocity change. That is,

$$\frac{A_1}{A_0} = \left[\frac{\frac{p^{0.67}(h)}{(h+p)} V_1}{\frac{p^{0.67}(h)}{(h+p)} V_2} \right] = \frac{V_1}{V_2} ,$$

where impact mass (h) and plate conditions (p) are constant. For our case, the predicted (Mereu et al., 1963) seismic energy increase associated with the 54% increase in impact velocities (5.5 to 8.5 m/s) is 3.8 dB.

Although theory predicts impact velocity to substantially influence seismic energy, these experimental results indicate impact velocity does not greatly affect data quality at these sites. The average seismic energy increase for all three sites due to the impact velocity increase is approximately 1.3 dB, or around 1/3 that predicted. The standard deviation of the data is substantial (Table 7), and the shown schematically in figure 21. At the test sites, these irregular effects on seismic energy apply for both impact masses and all plate masses included.

* = Aluminum Plate					Recorded Seismic Energy (units) Study Sites				Signal Change (dB)			
Plate Mass (kg)	Hammer Mass	Impact Mass	Impact Velocity		KU	Snodgrass Site	Sandpit Site		KU Campus Site	Snodgrass Site	Sandpit Site	
1.4	5.4	7.7	5.5		2.413	2.970	5.942					
1.4	3.6	7.7	8.5		3.406	3.090	5.923		*3.0*	*0.3*	*0.0*	
1.8*	5.4	7.7	5.5		ND	2.228	4.59					
1.8*	3.6	7.7	8.5		ND	2.561	5.987		*No Data*	*1.2*	*2.3*	
2.8	5.4	7.7	5.5		1.884	2.291	5.466					
2.8	3.6	7.7	8.5		2.704	2.625	5.497		*3.1*	*1.2*	*0.0*	
5.4	5.4	7.7	5.5		3.168	2.306	4.473					
5.4	3.6	7.7	8.5		2.246	2.250	5.269		*-3.0*	*-0.2*	*1.4*	
10.9	5.4	7.7	5.5		2.446	1.848	4.634					
10.9	3.6	7.7	8.5		3.063	2.776	5.560		*2.0*	*3.5*	*1.6*	
21.8	5.4	7.7	5.5		1.619	2.294	5.214					
21.8	3.6	7.7	8.5		1.633	2.984	7.501		*0.1*	*2.3*	*3.2*	
	Mean Ratio of : (8.5m/s) / (5.5 m/s) >				1.2	1.2	1.2		1.3	1.5	1.5	Mean
			Standard Deviation>		0.3	0.2	0.2					
1.4	9.1	10.4	5.5		3.067	4.018	9.035					
1.4	5.4	10.4	8.5		3.060	4.390	8.439		*0.0*	*0.8*	*-0.6*	
1.8*	9.1	10.4	5.5		ND	3.179	7.418					
1.8*	5.4	10.4	8.5		ND	3.616	8.281		*No Data*	*1.1*	*1.0*	
2.8	9.1	10.4	5.5		2.458	3.639	8.302					
2.8	5.4	10.4	8.5		3.887	3.978	8.833		*4.0*	*0.8*	*0.5*	
5.4	9.1	10.4	5.5		1.916	3.293	7.523					
5.4	5.4	10.4	8.5		2.845	3.201	8.343		*3.4*	*-0.2*	*0.9*	
10.9	9.1	10.4	5.5		2.982	3.225	6.807					
10.9	5.4	10.4	8.5		3.382	3.241	8.031		*1.1*	*0.0*	*1.4*	
21.8	9.1	10.4	5.5		1.757	3.474	5.807					
21.8	5.4	10.4	8.5		1.450	3.808	9.471		*-1.7*	*0.8*	*4.2*	
	Mean Ratio of : (8.5m/s) / (5.5 m/s) >				1.2	1.1	1.2		1.7	0.6	1.4	Mean
			Standard Deviation>		0.3	0.1	0.2					

Table 7. Data grouped according to constant impact mass but varying impact velocity. The change in seismic energy (dB) is shown on the right.

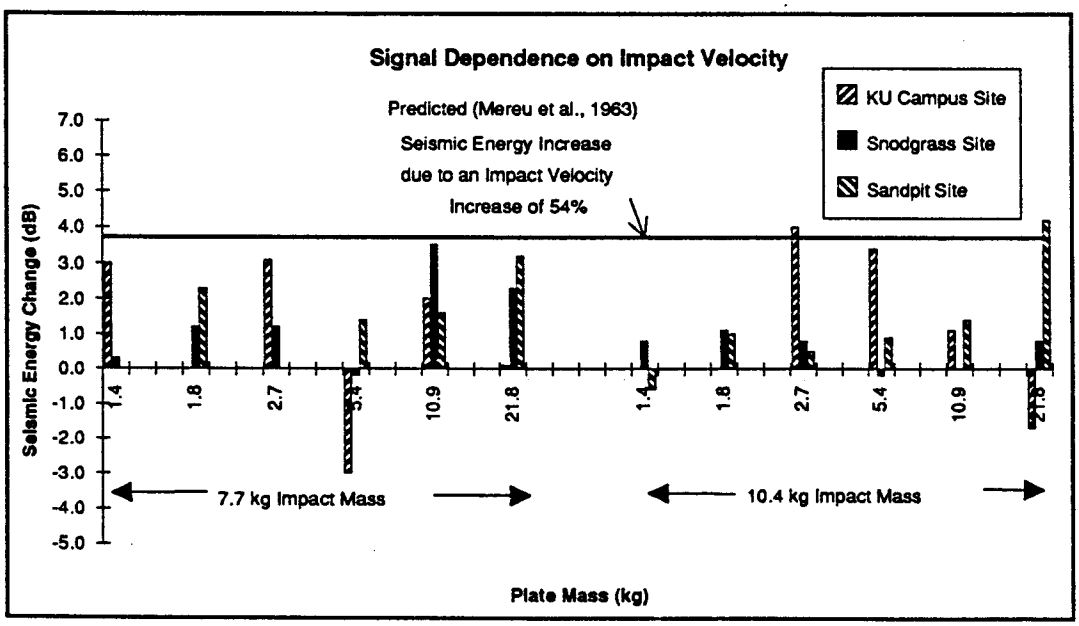

Figure 21. The variability in seismic energy due impact velocity increases (54%), while the impact mass and plate remain constant, is schematically shown in this plot. No data were collected for the 1.8 kg (aluminum) plate at the KU Campus site, the other apparent gaps in the figure are where no change (0 dB) in signal amplitudes was observed.

Spectral characteristics show no dependence upon impact velocity variations (5.5 m/s versus 8.5 m/s). This indicates that hammer impact velocity may not be a critical factor in maintaining consistent source wavelets for CDP surveys.

E. Impact Mass Variations

This section examines the effect impact mass has on the recorded energy and spectral properties of seismic data.

Theoretical work by Mereu et al. (1963) appears to be site specific, and limited to environments of soft, deformable near-surface materials. The predicted (Mereu et al., 1963) increase in seismic energy due to increasing impact mass agrees with results from the KU Campus site, but differs by as much as 4 dB from data acquired at the Snodgrass Ranch and Sandpit sites (Figure 22). The discrepancy between predicted and observed changes can possibly be explained by the strength of the near-surface materials present at the sites. The relationship between impact mass and seismic energy derived by Mereu (1962) was based on a matrix similar to sandy till. Extending the results of Mereu (1962) to sites with near-surface materials of gravel or compacted sand does not appear to be valid.

An increase in impact mass will increase the recorded seismic energy, but the amount of increase is site dependent. Within the limits of these experiments, seismic energy increases at sites with compacted near surfaces (Sandpit site) were roughly 3 times that observed for soil material (KU Campus site) for the same impact mass increase (Figures 19 and 23).

These data suggest that when acquiring CDP seismic data at a site with naturally firm and compacted near-surface materials, an average 5 dB increase in seismic energy can be obtained by doubling the sledgehammer mass. If the surface is soft and ductile, such as soil, doubling the impact mass may produce less substantial (<2 dB) increases in seismic energy.

Analysis of spectral characteristics for all data at the study sites indicates low frequency (100 Hz and lower) components were generally bolstered more than high frequency (>100 Hz) components as impact mass increased (Figure 24). This suggests that if the desired resolution requires

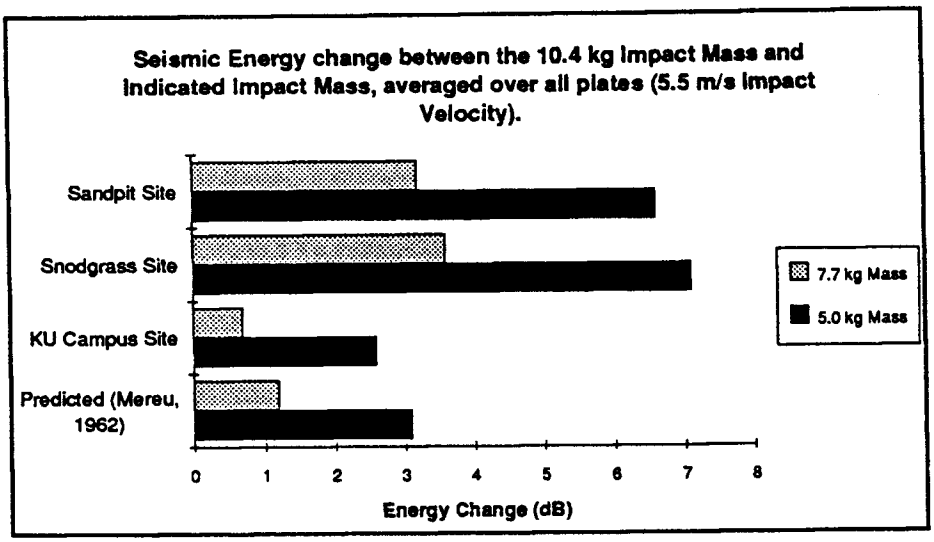

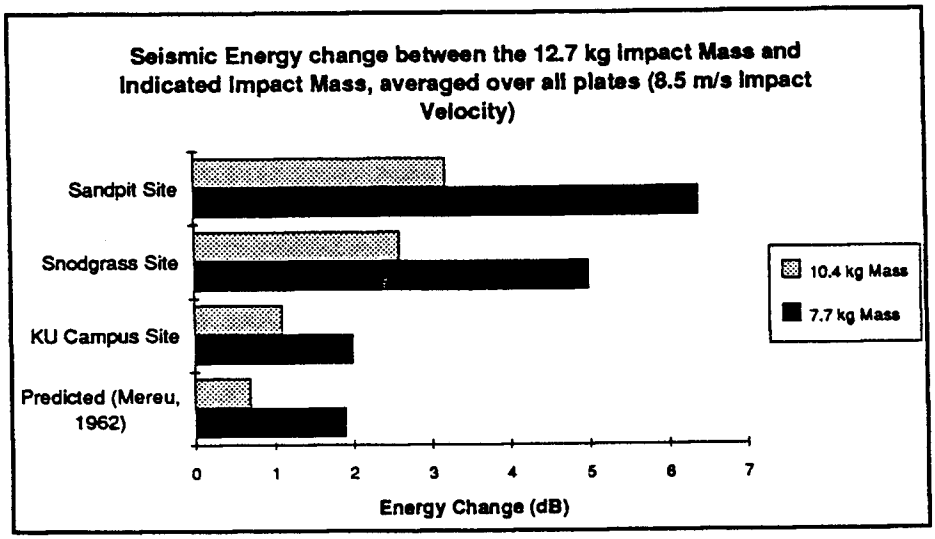

Figure 22. Seismic energy associated with an impact mass increase, are shown in this graph. Predicted increases (Mereu et al., 1963) correspond well with KU Campus data, but differ from the Snodgrass Ranch and Sandpit sites.

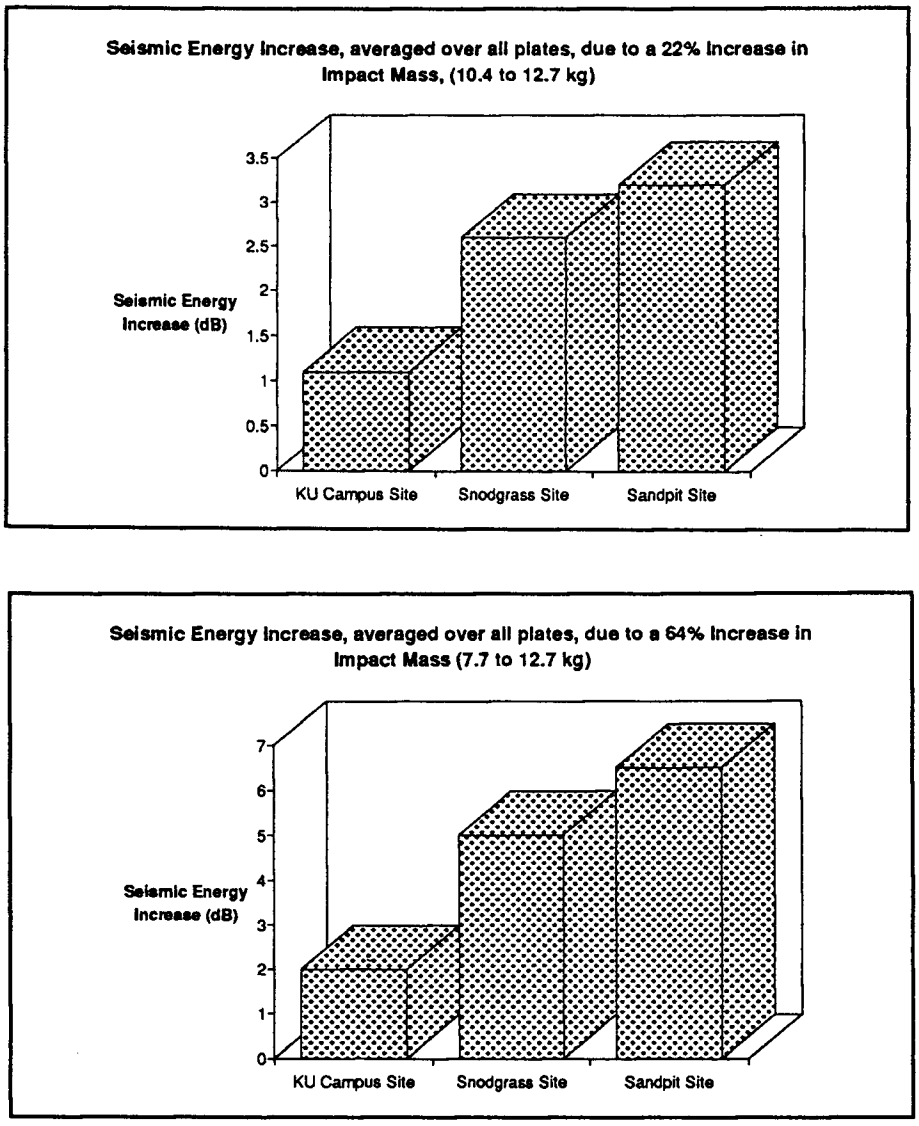

Figure 23. Seismic energy associated impact mass increases. Impact velocity for these data was 8.5 m/s.

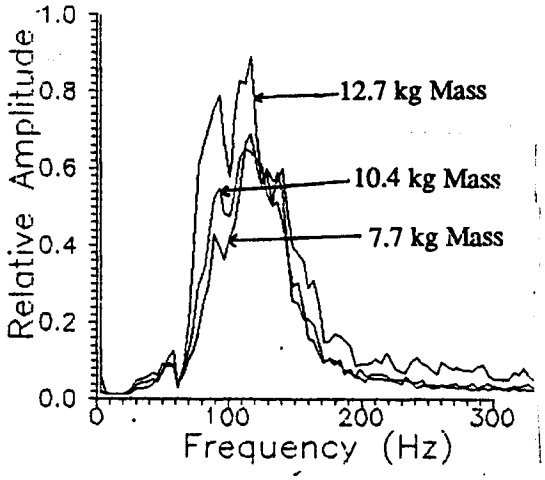

KU Campus Site
Parameters: 2.7 kg plate, 8.5 m/s impact velocity

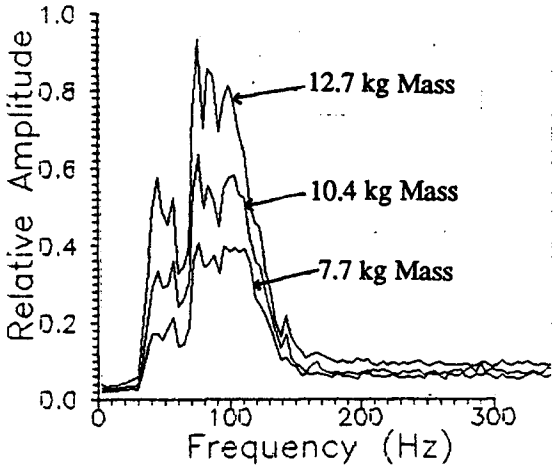

Sandpit Site
Source: 2.7 kg plate, 8.5 m/s impact velocity

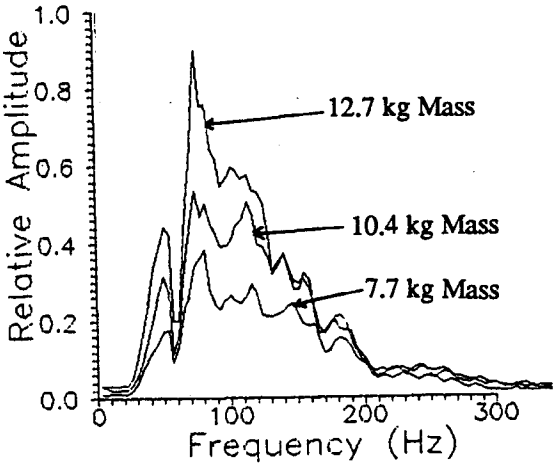

Snodgrass Ranch Site
Source: 2.7 kg plate, 8.5 m/s impact velocity

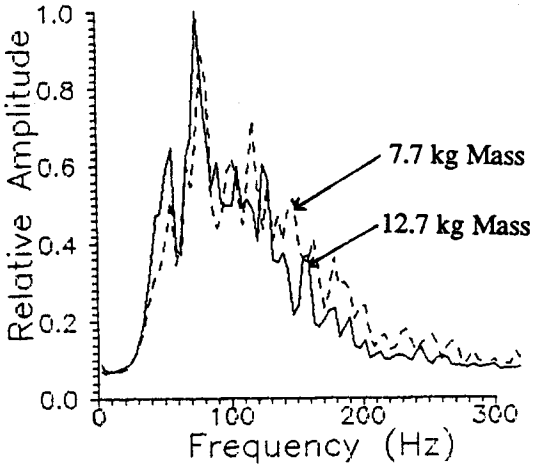

Snodgrass Ranch Site,
Amplitude adjusted to show frequency content
Source: 2.7 kg plate, 8.5 m/s impact velocity

Figure 24. Amplitude-versus-frequency spectra showing the effect of variable impact mass. A tendency towards preferentially boosting low frequency amplitudes (<100 Hz) was observed throughout the data sets.

dominant reflection frequencies above 110 Hz, small impact mass (within the changes involved here) may provide higher signal-to-noise data.

F. Plate Mass Variations

This section of the study is to determine if some combination of plate mass and corresponding plate-earth couple produce superior seismic data. In addition to the array of plates tested (Table 5), data from a sledgehammer impact directly onto the surface (no plate) were acquired. The result of no-plate configurations was a decrease in seismic energy; soil materials show larger decreases than compacted sands relative to plate configurations. Impact plates may not be needed if the near-surface material is of sufficient strength for the source energy. Although the difference between no-plate versus plate impacts was not constant, all sites exhibited seismic energy increases when an impact plate was used.

No significant energy or frequency change was observed between plates constructed of aluminum and steel. The durability of the aluminum plate compared to steel alloy plates makes it superior for repeated impacts during data acquisition. Throughout the tests, aluminum proved to be a viable alternative to steel impact plates.

Although plate mass theoretically plays a substantial role in energy transfer (Table 8, Mereu et al., 1963; also Virtual Plate Speed section), data acquired for this study show no significant correlation between plate mass and seismic energy (Figure 25).

Converse to predicted results (Mereu et al., 1963), the smallest plate mass (1.4 kg) produced the highest seismic energy (average of 1.5 dB more energy) at the Snodgrass Ranch site. Assuming plate-earth couple is equivalent for all plates at this site, this suggests virtual plate speed is directly related to seismic amplitudes. If virtual plate speed is the dominant factor at this site, however, seismic energy should uniformly decrease with enlarging plate mass since virtual plate speed decreases with enlarging plate mass. This is not observed in the data, but rather small (0.5 dB) unpredictable fluctuations are present. The data associated with this plate (1.4 kg), therefore, do not indicate a predictable dependence on plate mass but rather the best possible give-and-take combination between

Impact Mass (h)	Plate Mass (p)	Impact Velocity (v)	Virtual Plate Speed*	Predicted Signal**	Signal Change (dB) from previous impact
5.0	1.4	5.5	8.3	10.1	
5.0	1.8	5.5	7.7	11.5	1.1
5.0	2.7	5.5	6.8	13.3	1.3
5.0	5.4	5.5	5.0	15.7	1.4
5.0	10.9	5.5	3.3	16.4	0.4
5.0	21.8	5.5	2.0	15.5	-0.5
7.7	1.4	5.5	8.9	11.0	
7.7	1.8	5.5	8.5	12.7	1.2
7.7	2.7	5.5	7.8	15.2	1.6
7.7	5.4	5.5	6.2	19.1	2.0
7.7	10.9	5.5	4.4	21.5	1.0
7.7	21.8	5.5	2.7	21.6	0.0
10.4	1.4	5.5	9.3	11.4	
10.4	1.8	5.5	8.9	13.3	1.3
10.4	2.7	5.5	8.3	16.3	1.7
10.4	5.4	5.5	6.9	21.5	2.4
10.4	10.9	5.5	5.1	25.4	1.5
10.4	21.8	5.5	3.4	26.8	0.4
7.7	1.4	8.5	13.8	17.0	
7.7	1.8	8.5	13.1	19.6	1.2
7.7	2.7	8.5	12.0	23.5	1.6
7.7	5.4	8.5	9.5	29.6	2.0
7.7	10.9	8.5	6.7	33.3	1.0
7.7	21.8	8.5	4.2	33.4	0.0
10.4	1.4	8.5	14.4	17.6	
10.4	1.8	8.5	13.8	20.6	1.3
10.4	2.7	8.5	12.9	25.2	1.7
10.4	5.4	8.5	10.7	33.2	2.4
10.4	10.9	8.5	7.9	39.3	1.5
10.4	21.8	8.5	5.2	41.3	0.4
12.7	1.4	8.5	14.7	18.0	
12.7	1.8	8.5	14.2	21.1	1.4
12.7	2.7	8.5	13.4	26.1	1.8
12.7	5.4	8.5	11.4	35.4	2.6
12.7	10.9	8.5	8.7	43.3	1.8
12.7	21.8	8.5	6.0	47.1	0.7
*Virtual Plate Speed = (1+e)(h/(h+p))(v), where e = 0.91(Mereu et al., 1963)					
**Predicted Signal = Virtual Plate Speed * Plate Mass^0.67 (Mereu et al., 1963)					

Table 8. Predicted signal (Mereu et al., 1963) variation associated with plate mass variations.

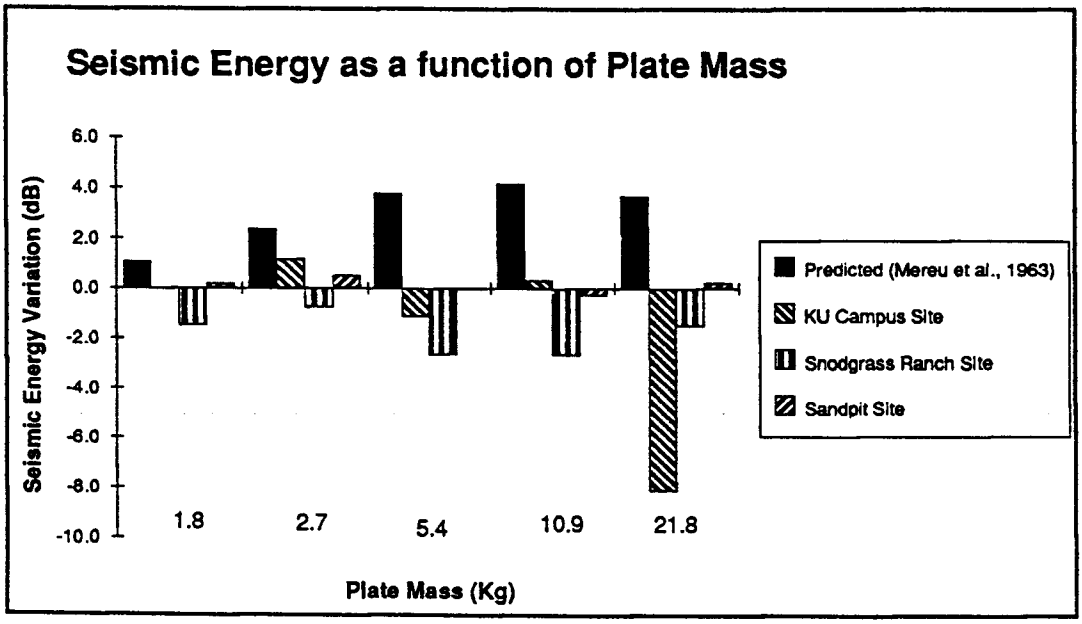

Figure 25. Seismic energy change from the 1.4 kg plate to the indicated plate. This plot illustrates plate mass (within the variations of this experiment) does not constrain seismic energy. Source parameters other than plate mass are constant (8.5 m/s impact velocity, 7.7 kg impact mass, 274 cm^2 plate area).

virtual plate speed and plate-earth couple at this site. Evidently, small plate masses are superior at sites where minimum plastic deformation takes place.

Plate mass can influence frequency content at some sites. At the Snodgrass Ranch site, impacts to smaller plates produced higher signal-to-noise ratios than larger mass plates (Figure 26).

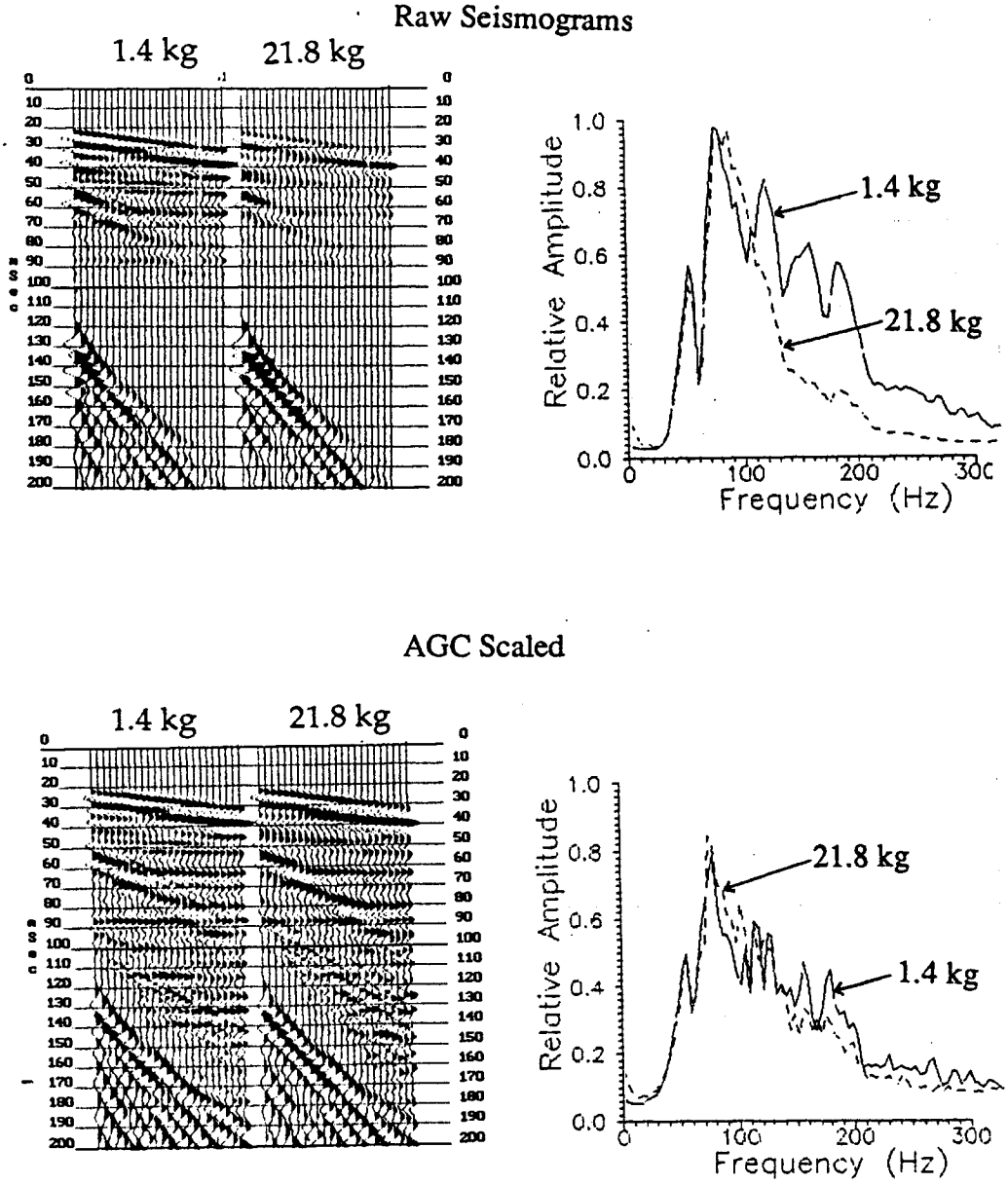

Figure 26. Raw seismograms and spectra from the Snodgrass Ranch site. Although bandwidth is approximately equal (amplitude adjusted), the percentage of high (>120 Hz) to low (<120 Hz) frequency information is clearly greater for the 1.4 kg impact plate versus the 21.8 kg plate. Sledgehammer source included a 7.7 kg hammer and an impact velocity of 5.5 m/s for both plates.

Discussion/Conclusion

From this study, it does not appear that seismic energy increases of greater than 6 dB can be obtained by changing the source parameters within the amount involved here. Changing source parameters for the sledgehammer source, with the exception of compaction, plate surface area, and impact mass, may not produce any signal difference that can be readily assessed in the field. Therefore, if the sledgehammer source does not provide enough energy for the desired target, or provide high enough frequencies for the desired resolution I suggest another source should be used instead of manipulating the source configuration.

Throughout the tests, aluminum plate material produced comparable seismic data quality to steel. Although the cost of obtaining an aluminum plate is higher than steel, aluminum proved to hold up to the impacts (without breaking or being deformed) better than steel. Aluminum plates are also more convenient to use than steel during field operations due to their low density.

The relationship between sledgehammer source parameters and data quality appear to be extremely dependent on near-surface materials. Relations between sledgehammer parameters suggested by Mereu et al., (1963) appear valid only at sites with surface materials comparable to sandy non-indurated deposits.

The sledgehammer source, may provide repeatable source pulses when the near-surface media consists of homogenous compacted sands. The variability in signal will increase as near-surface material strength decreases (e.g. soil). When soil environments are present, these experiments suggest either a practical method of employing the extension-plate, or other sources should be tried. This result agrees with conclusions from Domenico (1958).

A collision between a rubberized, sand-filled dead-blow hammer and a steel plate may produce less air-coupled wave interference than an impact between a steel hammer and the same plate. Data collected for this comparison showed the air-coupled wave to be 3 dB higher for the steel hammer than the dead-blow hammer. Interference from the air wave is a

problem for shallow reflection work and consequentially the application of dead-blow hammers is warranted.

At least one or two impacts to **seat the plate (compact the media)** should occur before recording at all sites. The merits of this effort are dependent on the near-surface material. Experience shows that seismic energy and signal-to-noise may increase as surface media becomes compacted, as well as produce a more consistent pulse. This suggests that when acquiring data along a country road, the impact plate should be on the shoulder of the road, not in the ditch.

Choosing the optimum **surficial plate area** is dependent on the strength of the near-surface material. The plate surface area of choice for a particular site is one with the smallest area (and assuming constant thickness, least mass) that creates little or no plate subsidence when struck by the impact mass. Experience indicates that when using a human operated sledgehammer of standard mass, at a site with a well developed soil profile, a minimum plate surface area of around 600 cm^2 should be employed. A plate of this size may increase the seismic energy 3.5 dB, and increase the signal-to-noise ratio relative to a plate of area 300 cm^2. At sites with higher elastic limits (such as compacted sands and gravels), a surficial plate area of around 250 cm^2 may be used. Ground roll was not preferentially enhanced relative to reflection information as plate surface area increased during these tests.

As the **impact velocity** of the sledgehammer increased approximately 50%, the average increase in seismic energy was 1.3 dB for the sites visited. Within the limits of this study, impact velocity does not significantly alter frequency content.

Sledgehammer mass variations produce effects that are site dependent. Increases in seimic energy at the Sandpit site were rougly 3 times that observed at the KU Campu site. Although low frequency components may be preferentially increased with increasing impact mass at some sites, for a given impact energy the seismic efficiency is greater for large masses (traveling at a slow impact velocity) than small masses (travelling at a high velocity).

Plate mass should be minimized if at all possible for frequency considerations. The signal-to-noise ratio may be higher for small plate masses relative to larger plates at some sites. Seismic energy is not noticeably effected by plate mass; plate masses that ranged from 15% to 100% the impact mass produced comparable results. Plate masses larger than the impact mass decrease the seismic energy, however, and should be avoided.

References

Anstey, N. A., 1957, Modern techniques in seismic reflection recording: Geophysical Prospecting, v. 5, No. 1, p. 45 - 67.

Birkeland, P. W., 1984, Soils and geomorphology: Oxford University Press, 372 p.

Birkelo, B. A., Steeples, D. W., Miller, R. D., and Sophocleous, M., 1987, Seismic reflection study of a shallow aquifer during a pumping test: Ground Water, November-December issue, v. 25, No. 6, p. 703-709.

Boyce, W. E., and DiPrima, R. C., 1986, Elementary differential equations and boundary value problems: Wiley and Sons, Fourth Ed., 645 p.

Dereciewicz, H., 1958, The mechanics of granular matter: Advances in Applied Mechanics, v. 5.

Dix, C. H., 1952, Seismic prospecting for oil: Harper, New York.

Dobrin, M. B., and Savit, C. H., 1988, Introduction to geophysical prospecting: McGraw-Hill Inc., 147 p.

Domenico, S. N., 1958, Generation of seismic waves by weight drops: Geophysics, v. 23, No. 4, p. 665 - 684.

Doornenbal, J. C., and Helbig, K., 1983, High-resolution seismics on a tidal flat in the Dutch Delta-Acquisition, processing, and interpretation: First Break, May, p. 9-20.

Gaskell, T. F., 1956, The relation between size of charge and amplitude of refracted wave: Geophysical Prospecting, v. 4, p. 185 - 193.

Gochioco, L. M., and Cotten, S. A., 1989, Locating faults in underground coal mines using high-resolution seismic-reflection techniques: Geophysics, v. 54, p. 1521 -1527.

Gough, D. I., 1952, A new instrument for seismic exploration at very short ranges: Geophysics, v. 17, No. 2, p. 311 - 333.

Grantham, R. L., 1990, Feasibility of using seismic reflection to detect gas trapped in alluvial materials: Unpublished Master's Thesis, University of Kansas.

Hertz, H., 1896, On the contact of elastic solids: Miscellaneous Papers, Macmilland and Co. Ltd.

Hubert, F., 1925, Earth tremors by falling weights: Zeit Geophysik, v. 1, p. 197.

Hunter, J. A., Pullan, S. E., Burns, R. A., Gagne, R. M., and Good, R. L., 1984, Shallow seismic -reflection mapping of the overburden-bedrock interface with the engineering seismograph-Some simple techniques: Geophysics, v. 49, No. 8, p. 1381 - 1385.

Hunter, J. A., and Steeples, D. W., 1986, Conducting a shallow seismic source comparison (Exp. Abs.): SEG 56th Ann. Mtg., p. 120 - 123.

Jongerius, P., and Helbig, K., 1988, On-shore high-resolution seismic profiling applied to sedimentology: Geophysics, v. 53, p. 1276 - 1283.

Karmen, V., and Durwez, P., 1950, On the propagation of plastic deformation in solids: Journal of Applied Physics, v. 21, p. 987.

Kasahara, K., 1953, Experimental studies on the mechanism of generation of elastic waves IV: Bulletin Earthquake Res. Inst. Tokyo, v. 32, p. 67 - 77.

Knapp, R. W., and Watney, W. L., 1987, Seismic identification of Pennsylvanian cyclothems (Exp. Abs.): SEG 57th Ann. Inter. Meeting, New Orleans, p. 338-341.

Lamb, H., 1904, On the propagation of tremors over the surface of an elastic solid: Philosophical Transactions of the Royal Society London, v. 203, p. 1 - 42.

Mason, R. G., 1957, A small scale field investigation on motion near the source: Geophysical Prospecting, v. 5, No. 2, p. 121 - 134.

Mereu, R., 1962, Methods of converting the kinetic energy of a falling weight into seismic energy: Ph.D. Dissertation, University of Western Ontario, 226 p.

Mereu, R. F., Uffen, R. J., Beck, A. E., 1963, The use of a coupler in the conversion of impact energy into seismic energy: Geophysics, v. 28, No. 4, p. 531 - 546.

Miller, R. D., Pullan, S. E., Steeples, D. W., and Hunter, J. A., 1989, Field comparison of shallow seismic sources near Chino, California (Exp. Abs.): SEG 59th Ann. Mtg., v. 1, p. 262 - 265.

Miller, R. D., Pullan, S. E., Waldner, J. S., and Haeni, F. P., 1986, Field comparison of shallow seismic sources: Geophysics, v. 51, p. 2067 - 2092.

Miller, R.D., and Steeples, D. W., 1990, A shallow seismic reflection survey in basalts of the Snake River Plain, Idaho: Geophysics, v. 55, p. 761 - 768.

Miller, R. D., and Steeples, D. W., 1991, Detecting voids in a 0.6 m coal seam, 7 m deep, using seismic reflection: *Geoexploration*, v. 28, p. 109 - 119.

Murphey, B. F., 1961, Particle motions near explosions in halite: Journal of Geophysical Research, v. 66, No. 3, p. 947 - 958.

Neitzel, E. B., 1958, Seismic reflection records obtained by dropping a weight: Geophysics, v. 23, p. 58 - 80.

Pullan, S. E., and MacAulay, H. A., 1985, A new source for engineering seismic surveys: Presented at the 55th Ann. Mtg., SEG, Washington D. C., p. 168 - 170.

Rayleigh, L., 1906, On the production of vibrations by forces of relatively long duration: Phil. Mag. v. 11, 283 - 291.

Sharpe, J. A., 1942, The production of elastic waves by explosion pressures, theory and empirical field observations: Geophysics, v. 7, No. 2, p. 144 - 154.

Singh, S., 1984, High-frequency shallow seismic reflection mapping in tin mining: Geophysical Prospecting, v. 32, p. 1033 - 1044.

Snedecor, G. W., and Cochran, W. G., 1989, Statistical Methods: Iowa State University Press/Ames, 503 p.

Somanas, C. D., Bennett, B. C., and Chung, Y., 1987, In-field seismic CDP processing with a microcomputer: The Leading Edge, p. 24 - 48.

Steeples, D. W., 1984, High-resolution seismic reflection at 200 Hz: Oil and Gas Journal-Annual Geophysics Report, Dec. 3, p. 86 - 92.

Steeples, D. W., and Miller, R. D., 1990, Seismic reflection methods applied to engineering, environmental, and groundwater problems: *in* Geotechnical and Environmental Geophysics: Ed. by S. H. Ward, p. 1 - 30.

Taylor, S., 1988, Shallow seismic investigations: a source comparison in West Virginia (Abs.): Proceedings of the West Virginia Academy of Science, v. 60, No. 1, p. 22.

Zeller, D. E., 1968, The stratigraphic succession in Kansas, Kansas Geological Bulletin 189, 81 p.

Appendix A - Impact Velocity Data and Error Analysis

Experiments were conducted prior to data acquisition to measure impact velocities and repeatability of the designed mechanical, gravity-driven sources and human-driven swings. The gravity-driven impacts were more repeatable (maximum standard deviation of 0.29 m/s) than the human driven impacts (maximum standard deviation of 1.39 m/s), and of lower impact velocity. The average impact velocity of the 3 m extension configurations was approximately 1.5 times that of the 1 m extension combinations (8.5 m/s versus 5.5 m/s), and approximately 4/5 that of the human driven impacts (8.5 m/s versus 10.8 m/s).

The method used to measure impact velocity involved setting the impact plate and a thin wire a short distance above the plate at a different electric potential than the hammer head and recording the time between contacts (peaks) on an oscilloscope (Figure A-1). Critical to consistent velocity measurements is the release of the impact mass and the height of the pivot center above ground surface. For all recorded impacts, the extension arm was positioned vertically above the pivot center and uniformly released with no initial downward motion. The height of the pivot center was recorded during acquisition of data, and varied no more than 3 cm. Time measurements were resolved to the nearest 0.5 ms (limited by the width of the line on the oscilloscope), and distances were measured to the nearest 0.16 cm (1\16 inch). Using standard statistical techniques (Snedecor and Cochran, 1989, p. 287), the experimental error associated with the velocity values due to inaccuracies of time and distance measurements was less than 1% for both the gravity driven impacts and the human-driven swings (Table A-1 thru A-3).

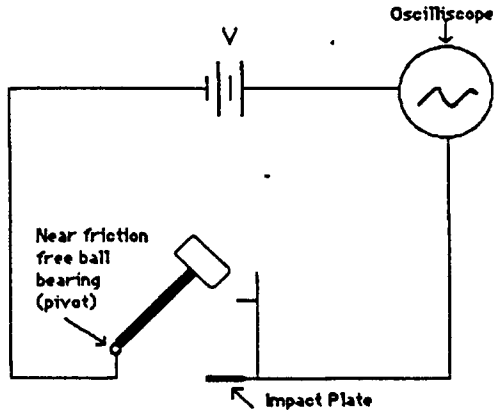

Figure A-1. Cartoon diagram of apparatus designed to measure impact velocities. Two hammer handle extensions (1 and 3 m), and three hammer head masses (3.6, 5.0, and 9.1 kg) where included in the testing.

A

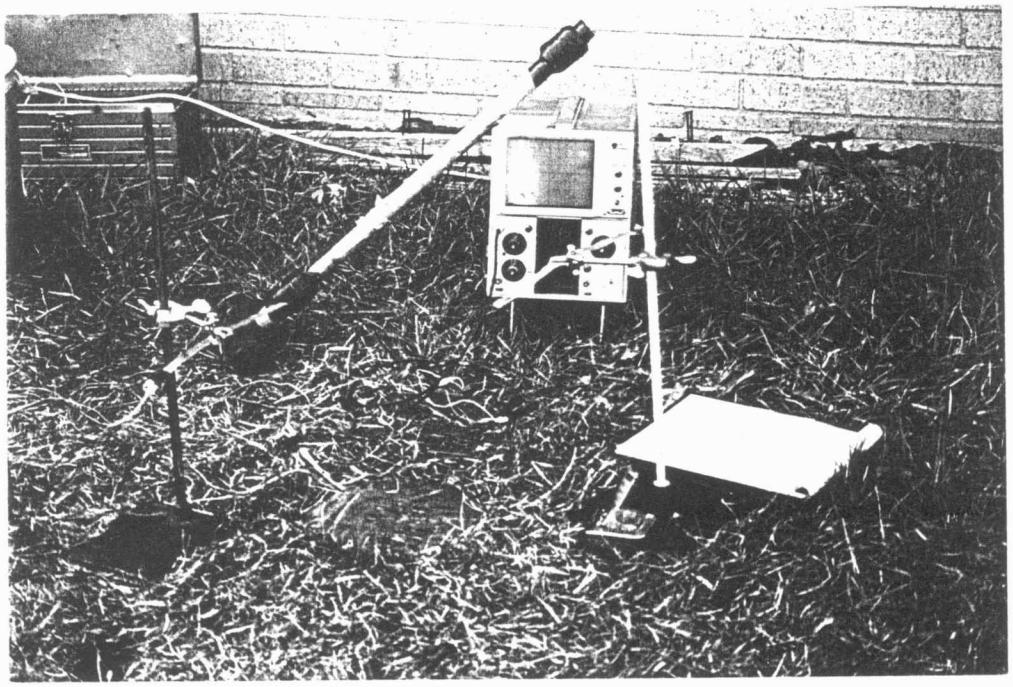

B

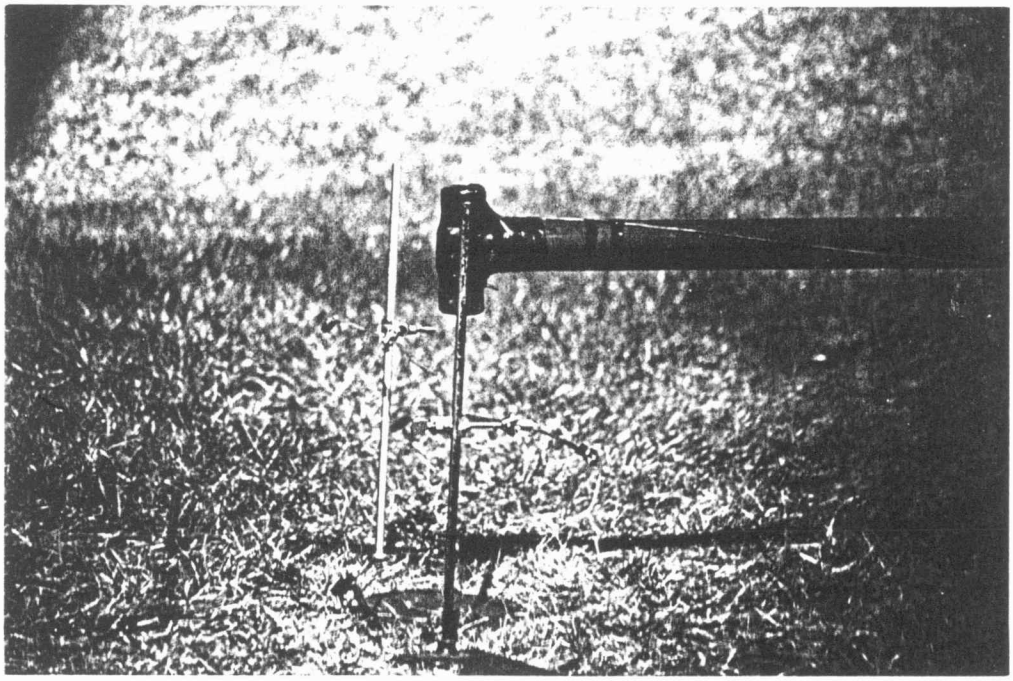

Appendix A-2. Photographs of the repeatability tests showing the method (B) and the equipment used (A).

Method used to calculate the variance of velocity (v) due to measurements of distance (x) and time (t).

Velocity is given by;

$$v = f(x,t) = \frac{x}{t}.$$

The derivative of velocity as a function of x and t is;

$$dv = f_x' dx + f_t' dt$$

where

$$f_x' = \frac{1}{t}, \text{ and } f_t' = -\frac{x}{t^2}$$

$$(dv)^2 = \left[\left(f_x' dx\right) + \left(f_t' dt\right)\right]^2 = \left(f_x' dx\right)^2 + \left(f_t' dt\right)^2 + 2\left(f_x' dx\right)\left(f_t' dt\right).$$

Based on the gausian random error distribution theory,

$$2\left(f_x' dx\right)\left(f_t' dt\right) = 0.$$

Finally,

$$\sigma_v^2 = \left(f_x'\right)^2 \sigma_x^2 + \left(f_t'\right)^2 \sigma_t^2 = \left(\frac{1}{t}\right)^2 \sigma_x^2 + \left(\frac{x}{t^2}\right)^2 \sigma_t^2$$

where

σ_x = deviation of distance measurement

σ_t = deviation of time measurement

σ_v = standard deviation of velocity.

I used an average value of x and t from a single subgroup (e.g. 3.6 kg hammer, 1 m extension) to determine the value of f_x' and f_t'. The standard deviation of velocity associated with measurements of x and t can then be computed.

Velocity Measurements of Impact Configurations

	3.6 kg Hammer, 1 m Extension			5.4 kg Hammer, 1 m Extension			9.1 kg Hammer, 1 m Extension		
	Height (cm)	Time (ms)	Velocity (m/s)	Height (cm)	Time (ms)	Velocity (m/s)	Height (cm)	Time (ms)	Velocity (m/s)
1	25.4	47.5	5.3	24.3	45.0	5.4	27.0	50.0	5.4
2	25.4	46.0	5.5	25.1	45.5	5.5	24.6	45.0	5.5
3	25.4	45.5	5.6	25.3	46.0	5.5	24.8	45.5	5.4
4	25.4	45.5	5.6	25.3	46.0	5.5	24.9	45.5	5.5
5	25.4	45.5	5.6	25.4	46.5	5.5	24.8	45.5	5.4
6	25.1	44.5	5.6	25.6	46.5	5.5	25.3	47.5	5.3
7	26.5	48.0	5.5	25.6	46.5	5.5	24.8	46.0	5.4
8	26.7	48.0	5.6	24.6	45.0	5.5	25.6	47.5	5.4
9	26.7	48.0	5.6	24.8	44.0	5.6	25.9	47.0	5.5
10	26.7	48.0	5.6	25.3	46.0	5.5	26.0	47.5	5.5
11	26.0	47.5	5.5	25.3	46.0	5.5	22.2	40.5	5.5
12	26.0	47.5	5.5	24.9	45.5	5.5	24.6	45.0	5.5
13	27.8	50.0	5.6	25.4	46.0	5.5	24.8	45.5	5.4
14	27.2	48.5	5.6	23.8	43.0	5.5	22.6	41.0	5.5
15	25.6	46.5	5.5	24.9	45.0	5.5	23.1	41.5	5.6
		Average Velocity	5.5		Average Velocity	5.5		Average Velocity	5.5
Calculated Standard Deviation due to errors associated with distance and time measurements (plus or minus)			0.03			0.03			0.03

Table A-1

3.6 kg Hammer, 3 m Extension			
	Height (cm)	Time (ms)	Velocity (m/s)
1	31.0	37.5	8.3
2	31.1	38.0	8.2
3	31.5	38.5	8.2
4	31.6	38.0	8.3
5	31.6	38.0	8.3
6	31.6	39.0	8.1
7	31.8	38.5	8.2
8	31.8	38.5	8.2
9	31.9	38.5	8.3
10	34.8	39.0	8.9
11	29.2	33.0	8.9
12	29.1	33.0	8.8
13	31.0	36.0	8.6
14	31.0	35.5	8.7
15	34.8	39.0	8.9
		Average Velocity	8.5
Calculated Standard Deviation due to errors associated with distance and time measurements (plus or minus)			0.06

5.4 kg Hammer, 3 m Extension			
	Height (cm)	Time (ms)	Velocity (m/s)
1	35.9	42.0	8.5
2	36.0	42.5	8.5
3	36.0	42.5	8.5
4	36.0	42.5	8.5
5	36.4	43.0	8.5
6	36.2	43.0	8.4
7	36.4	43.0	8.5
8	36.5	43.5	8.4
9	37.5	44.5	8.4
10	38.1	45.0	8.5
11	38.1	45.0	8.5
12	38.1	45.0	8.5
13	38.1	45.5	8.4
14	38.6	45.5	8.5
15	38.6	45.5	8.5
		Average Velocity	8.5
Calculated Standard Deviation due to errors associated with distance and time measurements (plus or minus)			0.05

9.1 kg Hammer, 3 m Extension			
	Height (cm)	Time (ms)	Velocity (m/s)
1	42.5	50.0	8.5
2	38.9	47.0	8.3
3	38.9	46.0	8.5
4	34.4	41.0	8.4
5	34.8	42.0	8.3
6	36.1	43.0	8.4
7	35.4	41.5	8.5
8	36.1	43.0	8.4
9	35.7	42.0	8.5
10	35.7	42.0	8.5
11	29.5	34.5	8.6
12	29.9	35.5	8.4
13	31.1	37.0	8.4
14	32.0	37.5	8.5
15	31.5	37.0	8.5
		Average Velocity	8.5
Calculated Standard Deviation due to errors associated with distance and time measurements (plus or minus)			0.05

Table A-2

3.6 kg Hammer, Human driven Swing			
	Height (cm)	Time (ms)	Velocity (m/s)
1	31.8	29.0	10.9
2	31.8	28.0	11.3
3	31.6	29.0	10.9
4	31.8	24.0	13.2
5	31.5	29.0	10.8
6	31.3	27.0	11.6
7	31.1	28.0	11.1
8	31.5	27.0	11.6
9	31.3	31.0	10.1
10	31.3	29.0	10.8
11	31.6	36.0	8.8
12	31.3	27.0	11.6
		Average Velocity	11.1
Calculated Standard Deviation due to errors associated with distance and time measurements (plus or minus)			0.1

5.4 kg Hammer, Human driven Swing			
	Height (cm)	Time (ms)	Velocity (m/s)
1	31.8	28.0	11.3
2	32.1	29.0	11.1
3	32.1	26.0	12.3
4	32.1	27.0	11.9
5	30.0	25.0	12.0
6	30.2	25.0	12.1
7	30.8	26.5	11.6
8	32.0	32.0	10.0
9	31.3	26.0	12.0
10	31.3	28.0	11.2
11	32.4	26.0	12.5
12	30.0	28.0	10.7
		Average Velocity	11.6
Calculated Standard Deviation due to errors associated with distance and time measurements (plus or minus)			0.11

9.1 kg Hammer, Human driven Swing			
	Height (cm)	Time (ms)	Velocity (m/s)
1	31.9	29.0	11.0
2	32.4	33.0	9.8
3	31.3	30.0	10.4
4	32.4	28.0	11.6
5	29.4	29.0	10.1
6	29.9	32.0	9.3
7	30.5	33.0	9.2
8	31.0	30.0	10.3
9	31.1	45.0	6.9
10	30.8	39.0	7.9
11	31.5	40.0	7.9
12	32.4	29.0	11.2
		Average Velocity	9.6
Calculated Standard Deviation due to errors associated with distance and time measurements (plus or minus)			0.07

Table A-3

Appendix B - The Motion of Impact Plate

Consider the plate-earth system to be analogous to a simple mass-spring system in which viscous damping is present. If we assume the duration of impact is short compared to the interaction between the plate and the earth as shown by Mereu (1962), then a well-known second-order differential equation describes the situation. The differential equation is given by;

$$M\frac{d^2y}{dt^2}+C\frac{dy}{dt}+Dy=0$$

where C and D are constants that depend on the elastic parameters of the medium and the surface area of the plate, y is the plate position, and M is the mass of the plate. For our case,

$M\frac{d^2y}{dt^2}$ = *the impact force,*

$C\frac{dy}{dt}$ = *the frictional force, and*

Dy *is the elastic force.*

The initial conditions (t=0) needed to solve this equation are the following;

$$y(0)=0, \quad and \quad \frac{dy(0)}{dt}=V_p,$$

where t=0 is defined to be at the end of the falling mass-plate interaction, and V_p is the virtual plate speed. The characteristic equation is

$$Mr^2+Cr+D=0$$

where

$$r_1, r_2 = -\frac{C}{2M} \pm \frac{\sqrt{C^2-4DM}}{2M}.$$

For the underdamped case:

$$\sqrt{C^2-4DM} < 0,$$

and the solution takes the form,

$$y(t) = e^{\frac{-C}{2M}t}(A\cos\mu t + B\sin\mu t),$$

where

$$\mu = \frac{\sqrt{4DM-C^2}}{2M}.$$

Using the first initial condition, y(0)= 0, we find A = 0.

Taking the first time derivative,

$$\frac{dy(t)}{dt} = -\frac{C}{2M}e^{\frac{-C}{2M}t}(A\cos\mu t + B\sin\mu t) + e^{\frac{-C}{2M}t}(-\mu A\sin\mu t + \mu B\cos\mu t),$$

and the second initial condition we obtain,

$$B = \frac{V_p}{\mu} = \frac{V_p\, 2M}{\sqrt{4DM-C^2}}.$$

The particular solution is:

$$y(t) = e^{\frac{-C}{2M}t}(V_p)\left\{\frac{2M}{\sqrt{4DM-C^2}}\right\}\sin\left(\frac{\sqrt{4DM-C^2}}{2M}\right),$$

and the quasi-circular period (T) (Boyce and DiPrima, 1986) is,

$$T = \frac{4M\ \pi}{\sqrt{4DM-C^2}}.$$

Appendix C KU Campus Seismic Data

Field files from the KU Campus site, as they were collected. Data is roughly organized according to source energy. The data are shown in amplitude adjusted form; no trace normalization or AGC scaling has been performed. The gains for these data are: channels 1-19=94 dB, and channels 20-24 = 102 dB. A general feel for signal changes associated with the parameters can be obtained from these plots.

Key for plate mass:

A=2.7 kg, 548 cm^2
B=10.9 kg, 548 cm^2
C=1.4 kg, 274 cm^2
D=2.7 kg, 274 cm^2
E=5.4 kg, 274 cm^2
F=10.9 kg, 274 cm^2
G=21.8 kg, 274 cm^2
H*=1.8 kg, 274 cm^2
I=2.7 kg, 137 cm^2
J=10.9 kg, 137 cm^2
K=5.4 kg, 0.48 m length, Auger Flight
L=10.9 kg, 0.78 m length, Auger Flight
M=10.9 kg, 0.9 m length, Downhole Plate

Key for Impact Mass (Combined hammer mass and extension mass, measured at impact with a scale):

N=5.0 kg
O=7.7 kg
P=10.4 kg
Q=12.7 kg
R= 30.06 Downhole Rifle
S=Manual Swing (Human)

Key for Impact Velocity:

T=5.5 m/s
U=8.5 m/s

Format for description:
File #, Plate Parameters, Impact Mass, Impact Velocity (Comments if needed)

File 1, C, P, Y.
File 2, D, P, T.
File 3, E, P, T.
File 4, F, P, T.
File 5, G, P, T.
File 6, A, P, T.
File 7, B, P, T.
File 8, I, P, T.
File 9, J, P, T.
File 10, NP, P, T.
File 11, C, N, T.
File 12, D, N, T.
File 13, E, N, T.
File 14, F, N, T.
File 15, G, N, T.
File 16, A, N, T.
File 17, B, N, T.
File 18, I, N, T.
File 19, J, N, T.
File 20, NP, K, T.

File 21, C, O, T.
File 22, D, O, T.
File 23, E, O, T.
File 24, F, O, T.
File 25, G, O, T.
File 26, A, O, T.
File 27, B, O, T.
File 28, I, O, T.
File 29, J, O, T.
File 30, NP, L. T.

File 31, Noise Survey (No Source)
File 32, L, O, T.
File 33, K, O, T.
File 34, M, O, T.
File 35, C, Q, U.
File 36, D, Q, U, (Glancing blow)
File 37, D, Q, U.
File 38, E, Q, U.
File 39, E, Q, U.
File 40, F, Q, U.

File 41, NP, Q, U.
File 42, G, Q, U.
File 43, A, Q, U.
File 44, B, Q, U.
File 45, R. (New Hole)
File 46, Noise Survey (No Source)
File 47, I, Q, U.
File 48, J, Q, U.
File 49, C, P, U.
File 50, D, P, U.

File 51, E, P, U.
File 52, F, P, U.
File 53, G, P, U.
File 54, A, P, U.
File 55, B, P, U.
File 56, NP, P, U.
File 57, I, P, U.
File 58, J, P, U.
File 59, C, O, U.
File 60, D, O, U.

File 61, E, O, U.
File 62, F, O, U.
File 63, G, O, U.
File 64, A, O, U.
File 65, B, O, U.
File 66, I, O, U.
File 67, J, O, U.
File 68, E, M.
File 69, F, M.
File 70, A, M

File 71, B, M.
File 72, E, O, T. (Compaction)
File 73, E, O, T.
File 74, E, O, T.
File 75, E, O, T.
File 76, E, O, T.
File 77, E, O, T.
File 78, E, O, T.
File 79, E, O, T.
File 80, E, O, T.

File 81, E, O, T.
File 82, E, O, T.
File 83, E, O, T.
File 84, E, O, T.
File 85, E, O, T.
File 86, E, O, T.
File 87, E, O, T.
File 88, E, O, T.
File 89, E, O, T.
File 90, E, O, T.

File 98, Rubber Dead Blow Hammer (0.9 kg)
File 99, Steel Alloy Hammer (0.9 kg)
File 100, Rubber Dead Blow Hammer (0.9 kg)

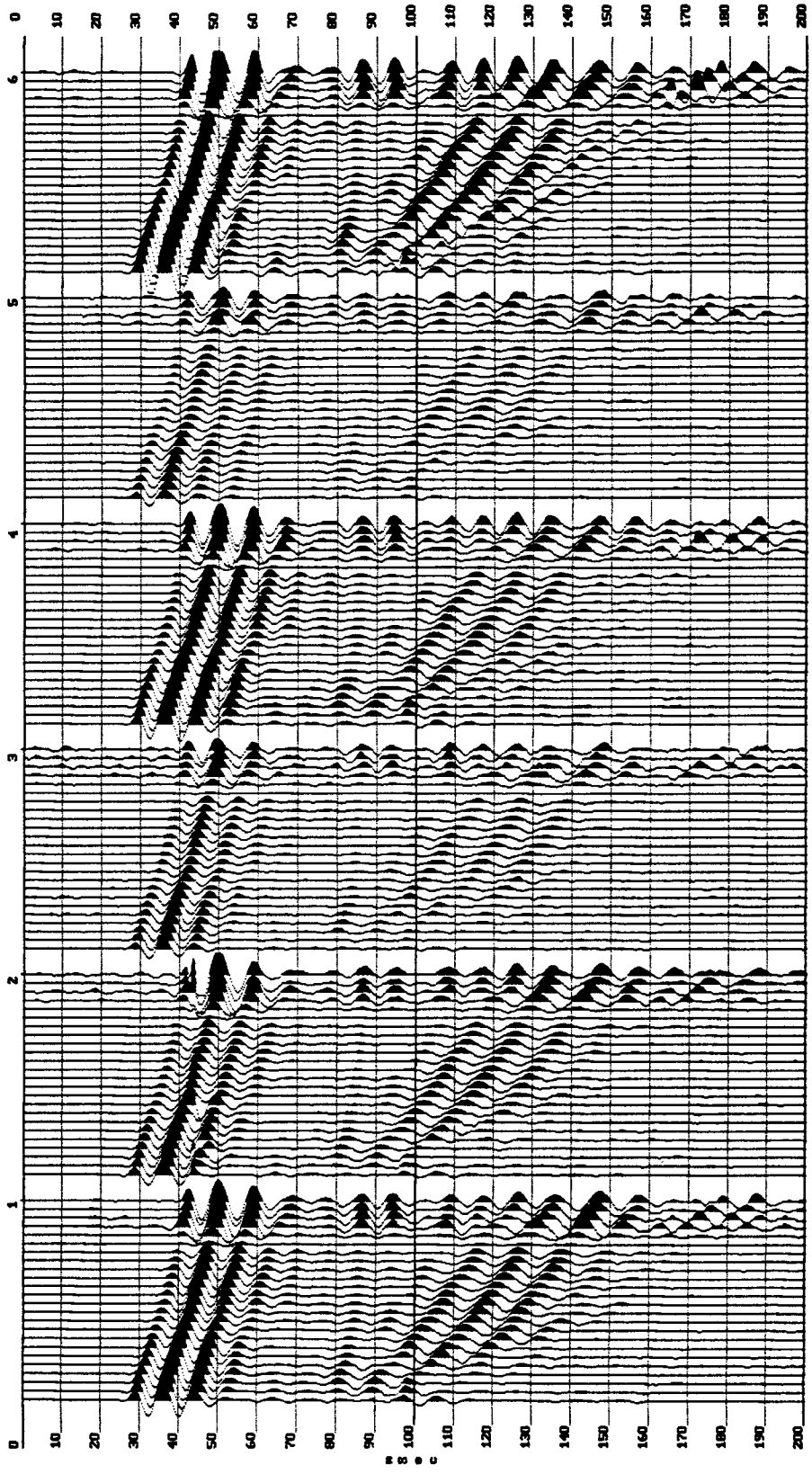
0
10
20
30
40
50
60
70
80
90
100
110
120
130
140
150
160
170
180
190
200
msec

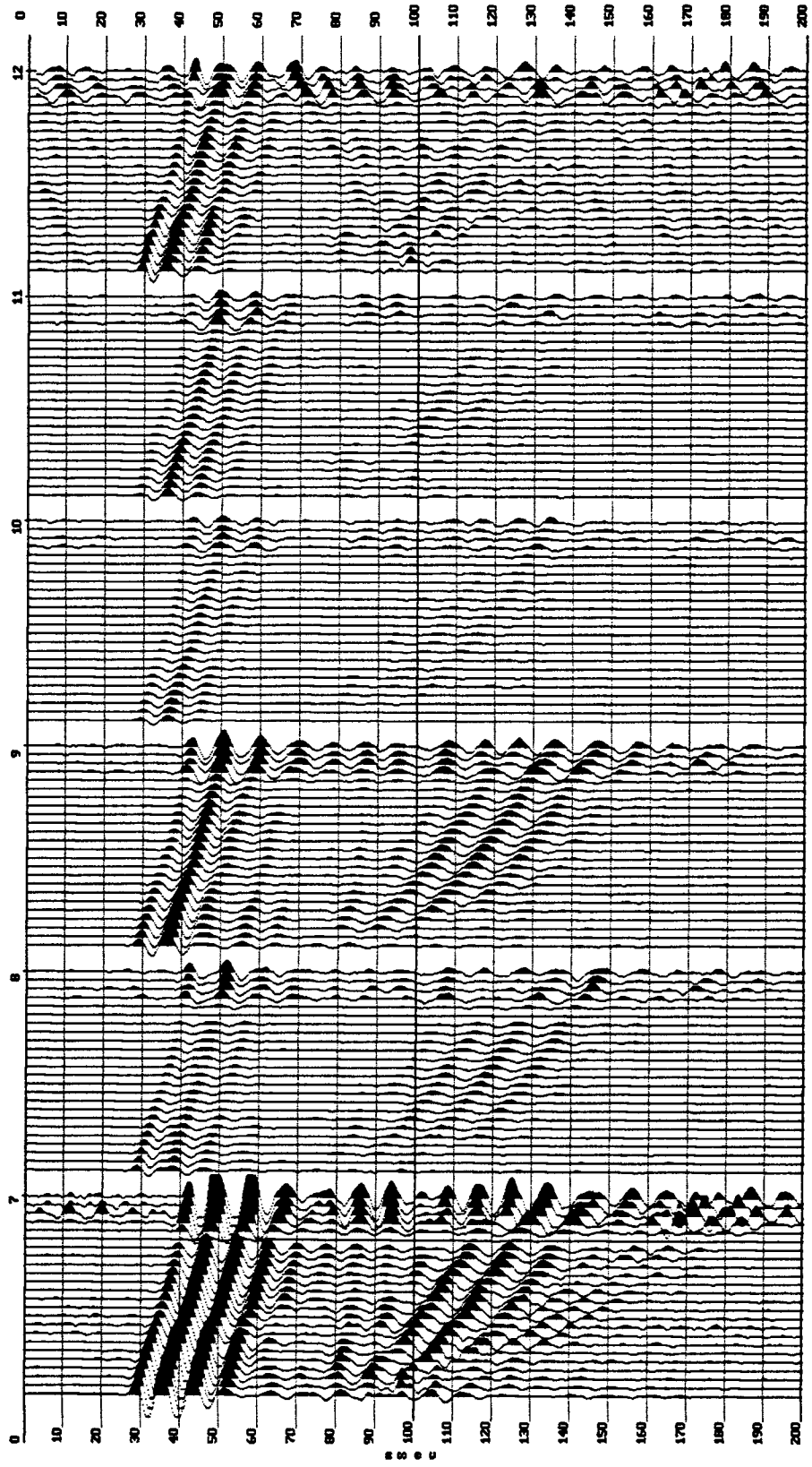
msec

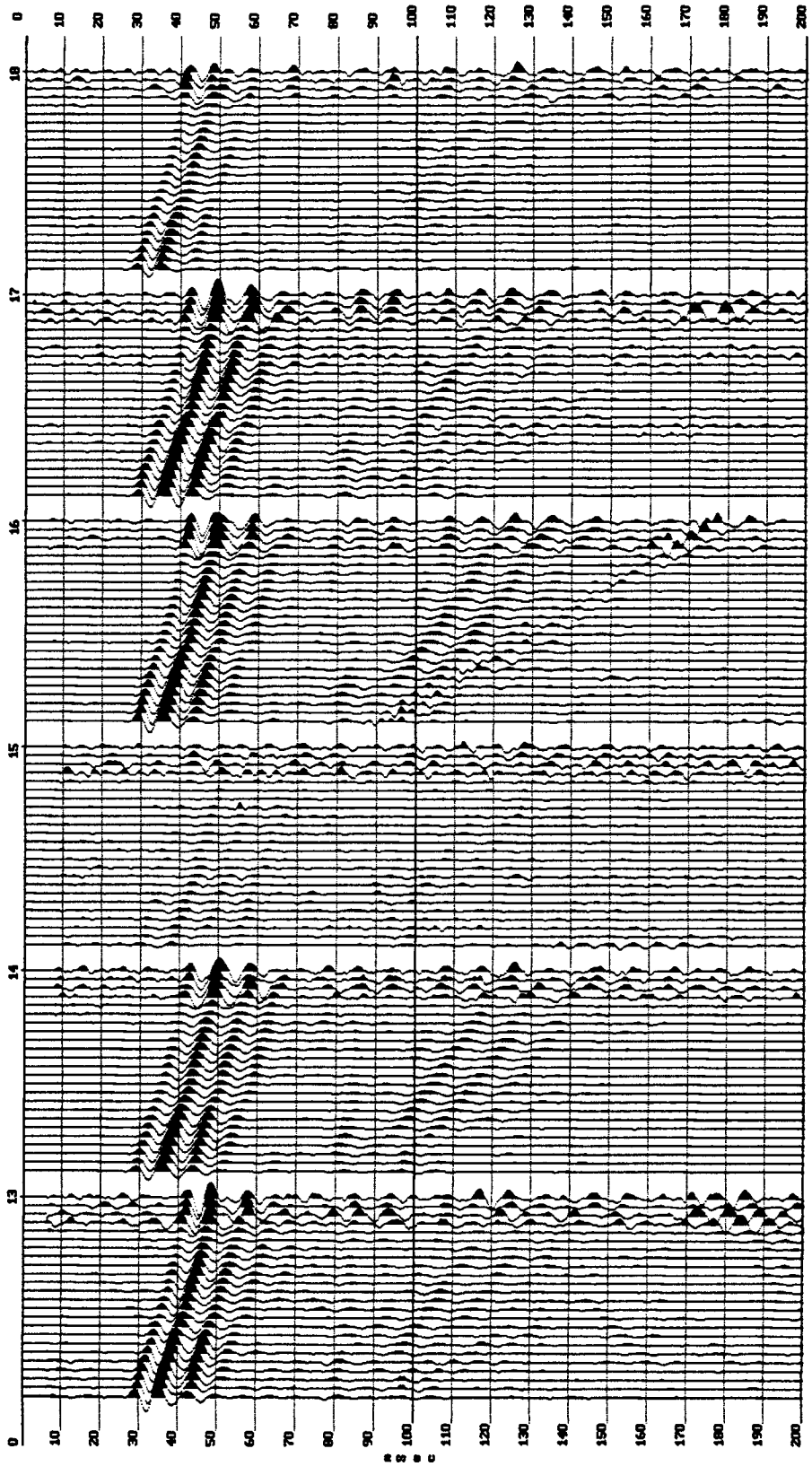
0
10
20
30
40
50
60
70
80
90
100
110
120
130
140
150
160
170
180
190
200
18
17
16
15
14
13
msec

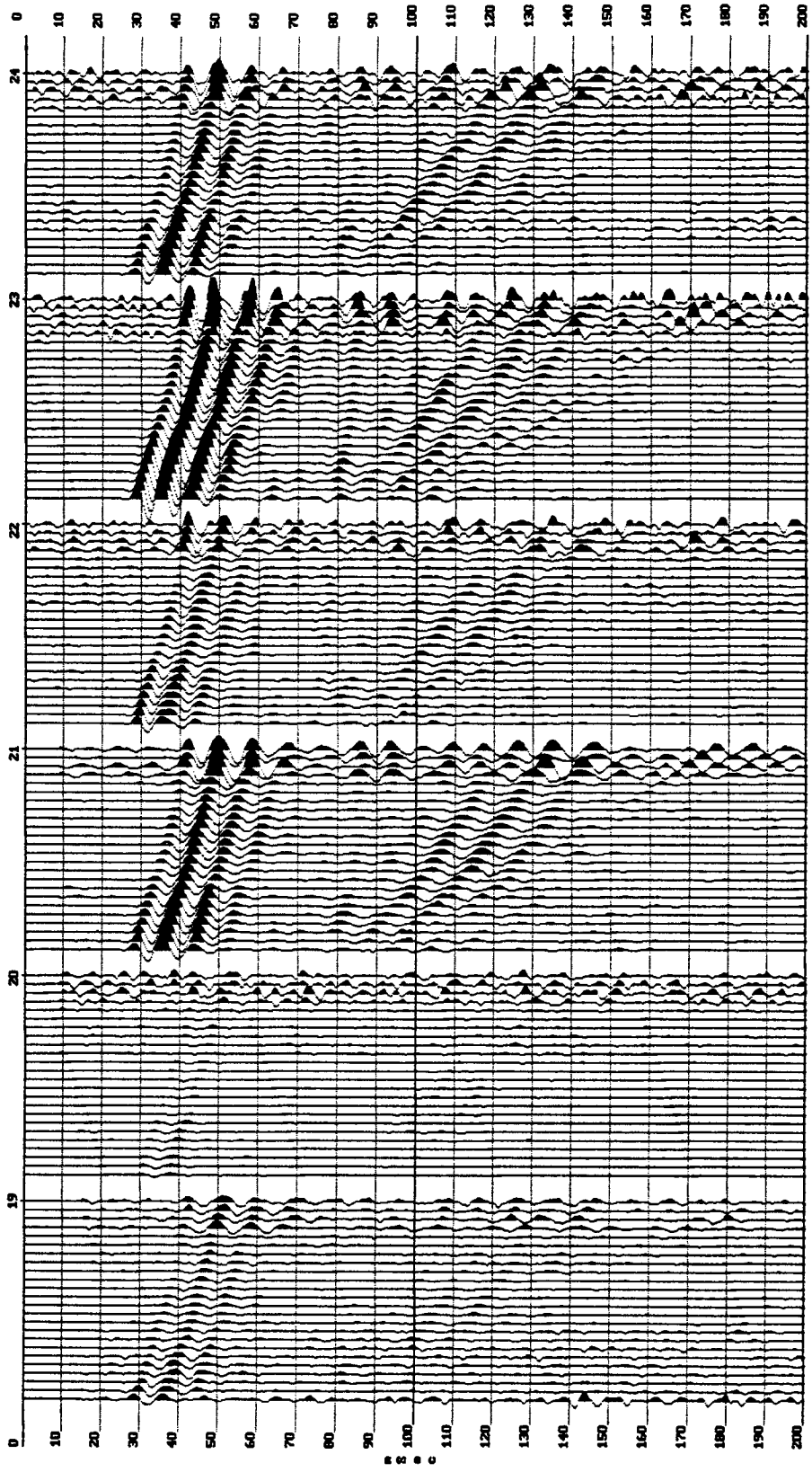
0
10
20
30
40
50
60
70
80
90
100
110
120
130
140
150
160
170
180
190
200
24
23
22
21
20
19
msec

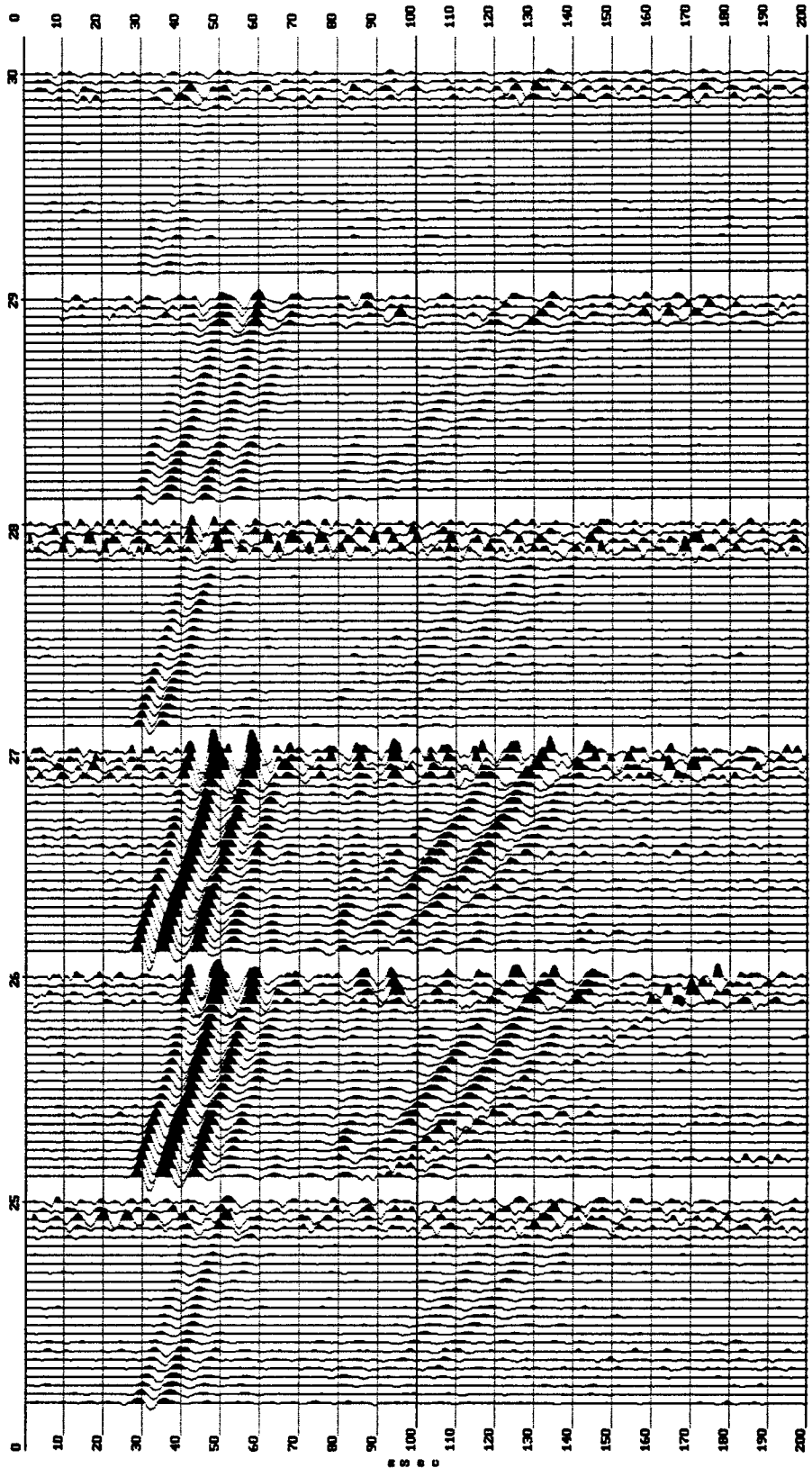
0
10
20
30
40
50
60
70
80
90
100
110
120
130
140
150
160
170
180
190
200
30
29
28
27
26
25

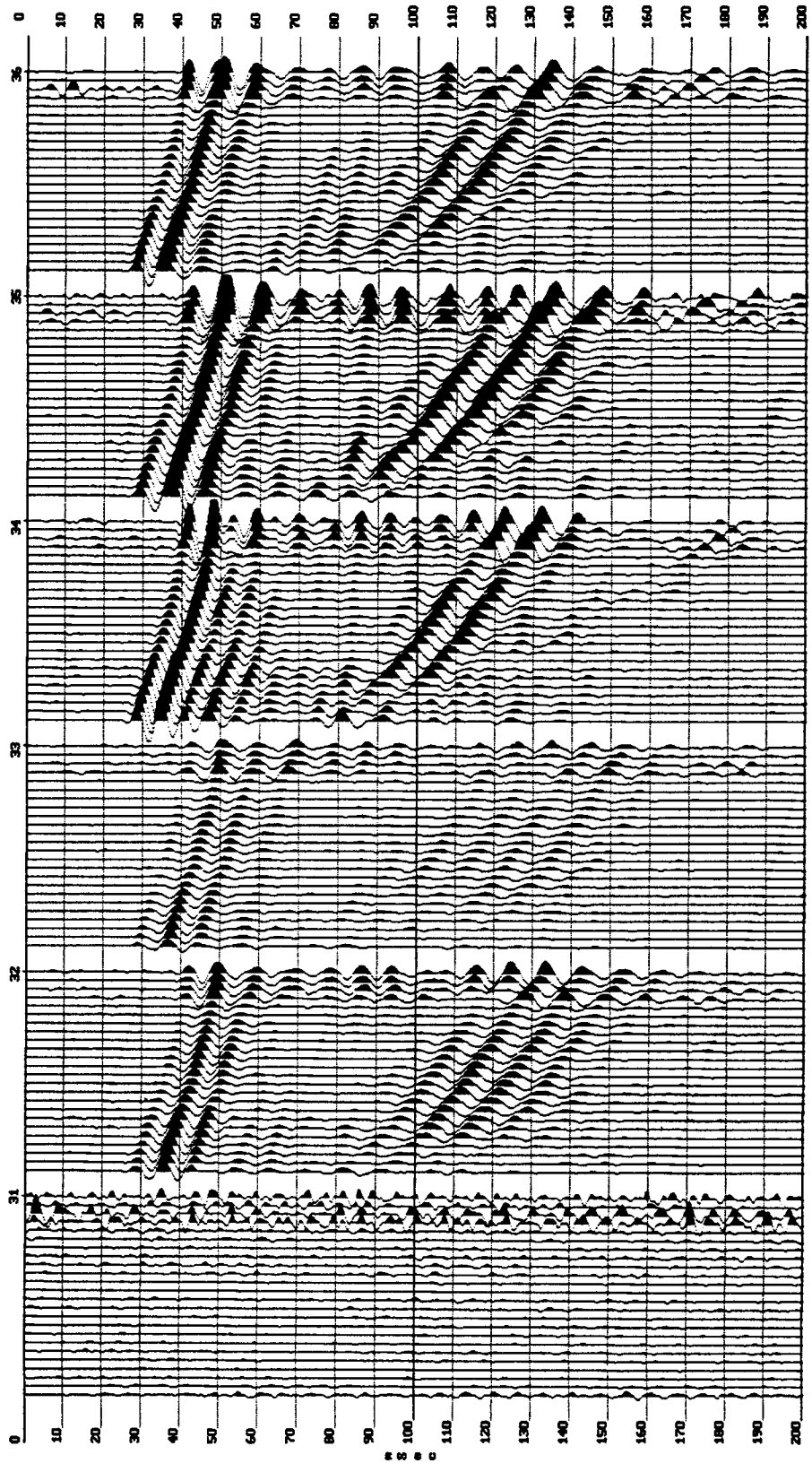
msec

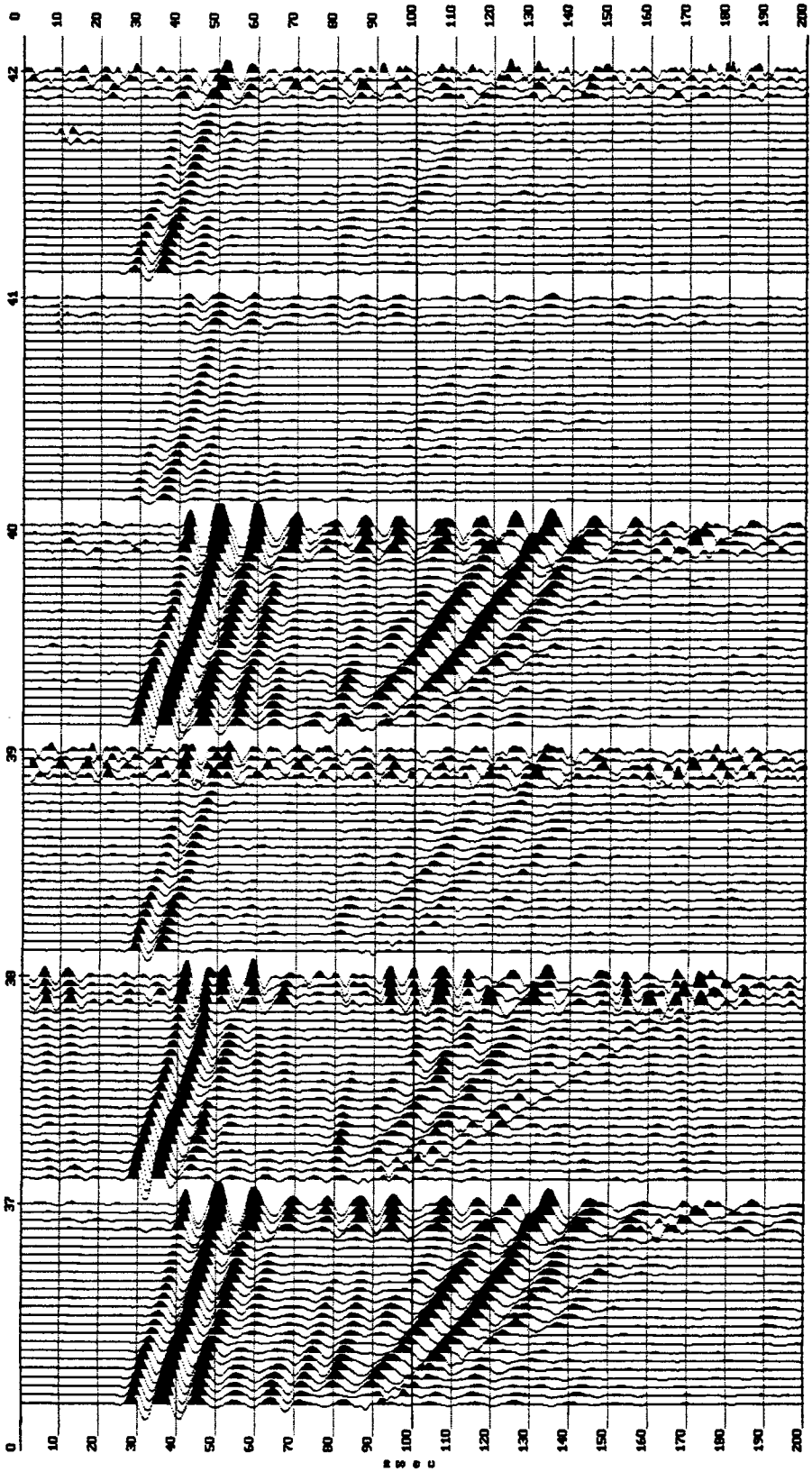
0
10
20
30
40
50
60
70
80
90
100
110
120
130
140
150
160
170
180
190
200
42
41
40
39
38
37
msec

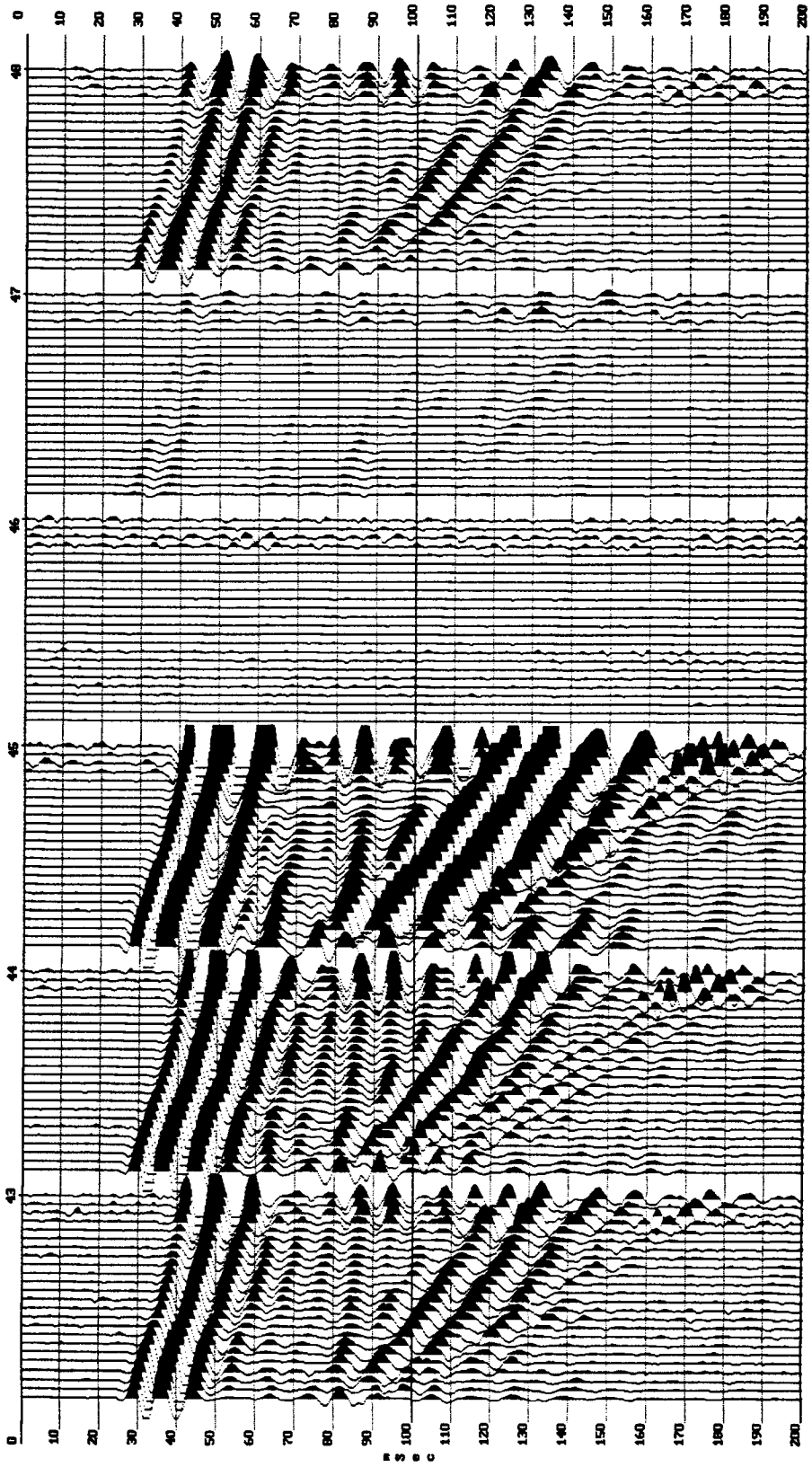
0
10
20
30
40
50
60
70
80
90
100
110
120
130
140
150
160
170
180
190
200
48
47
46
45
44
43
msec

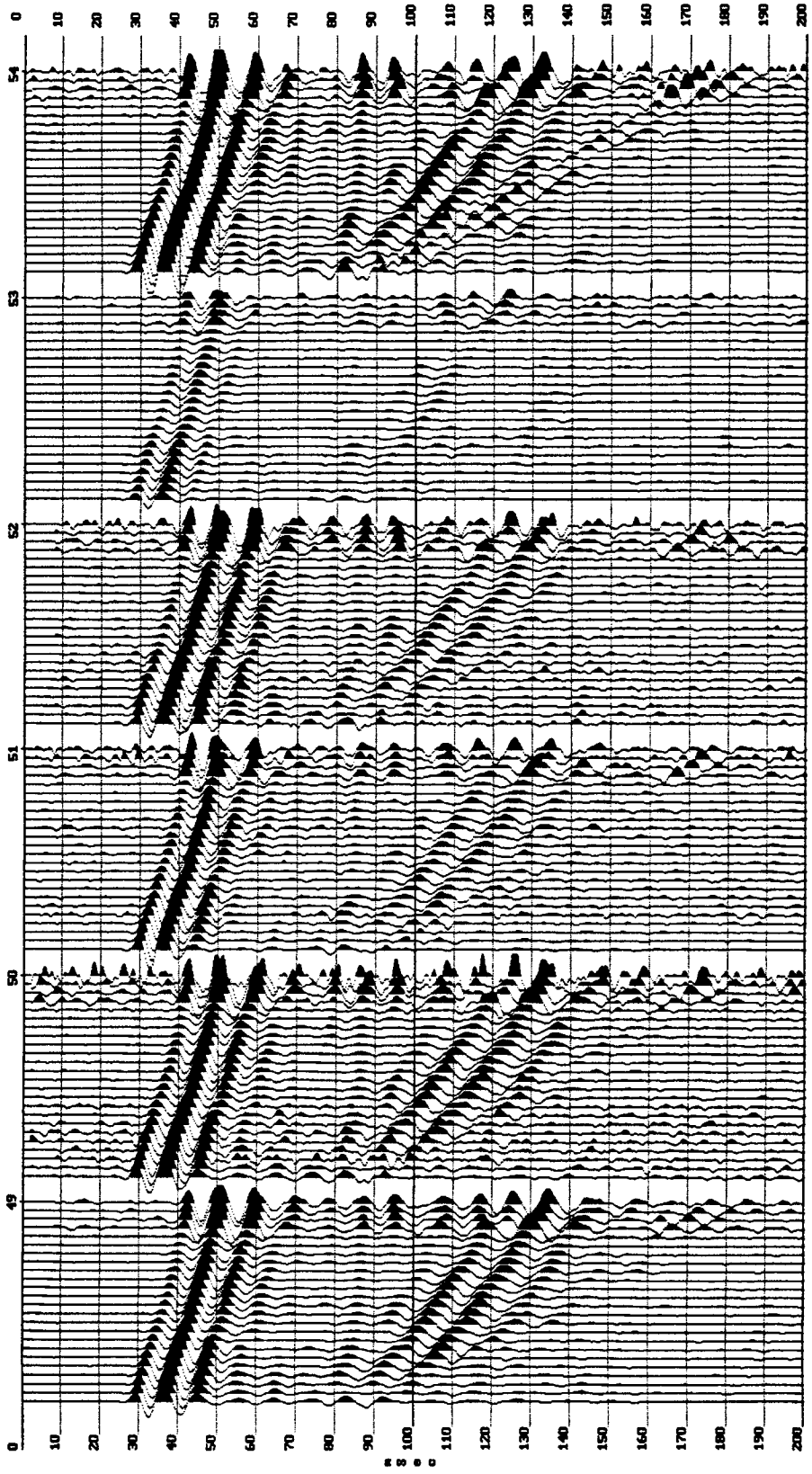
0
10
20
30
40
50
60
70
80
90
100
110
120
130
140
150
160
170
180
190
200
54
53
52
51
50
49
msec

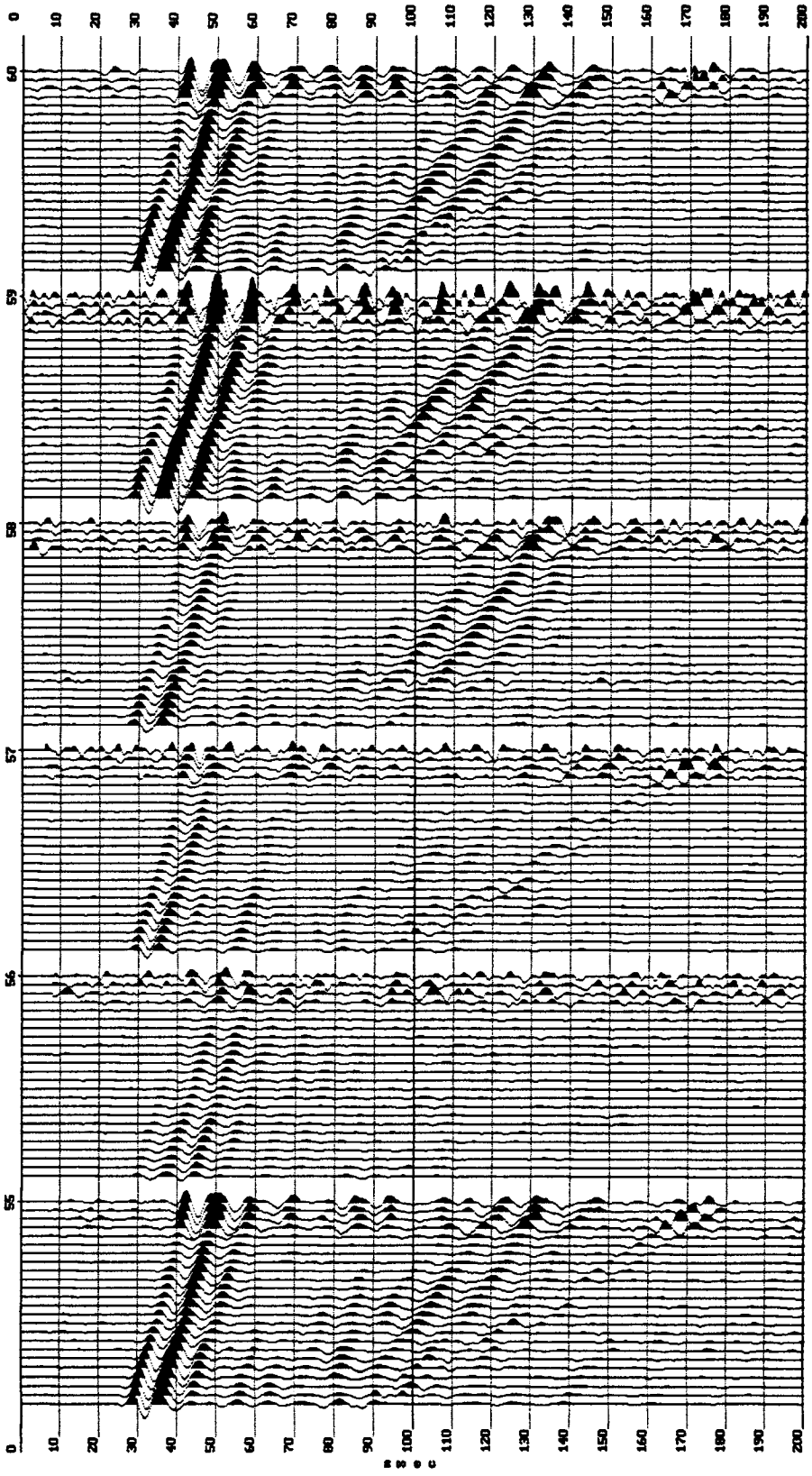
0
10
20
30
40
50
60
70
80
90
100
110
120
130
140
150
160
170
180
190
200
60
59
58
57
56
55
msec

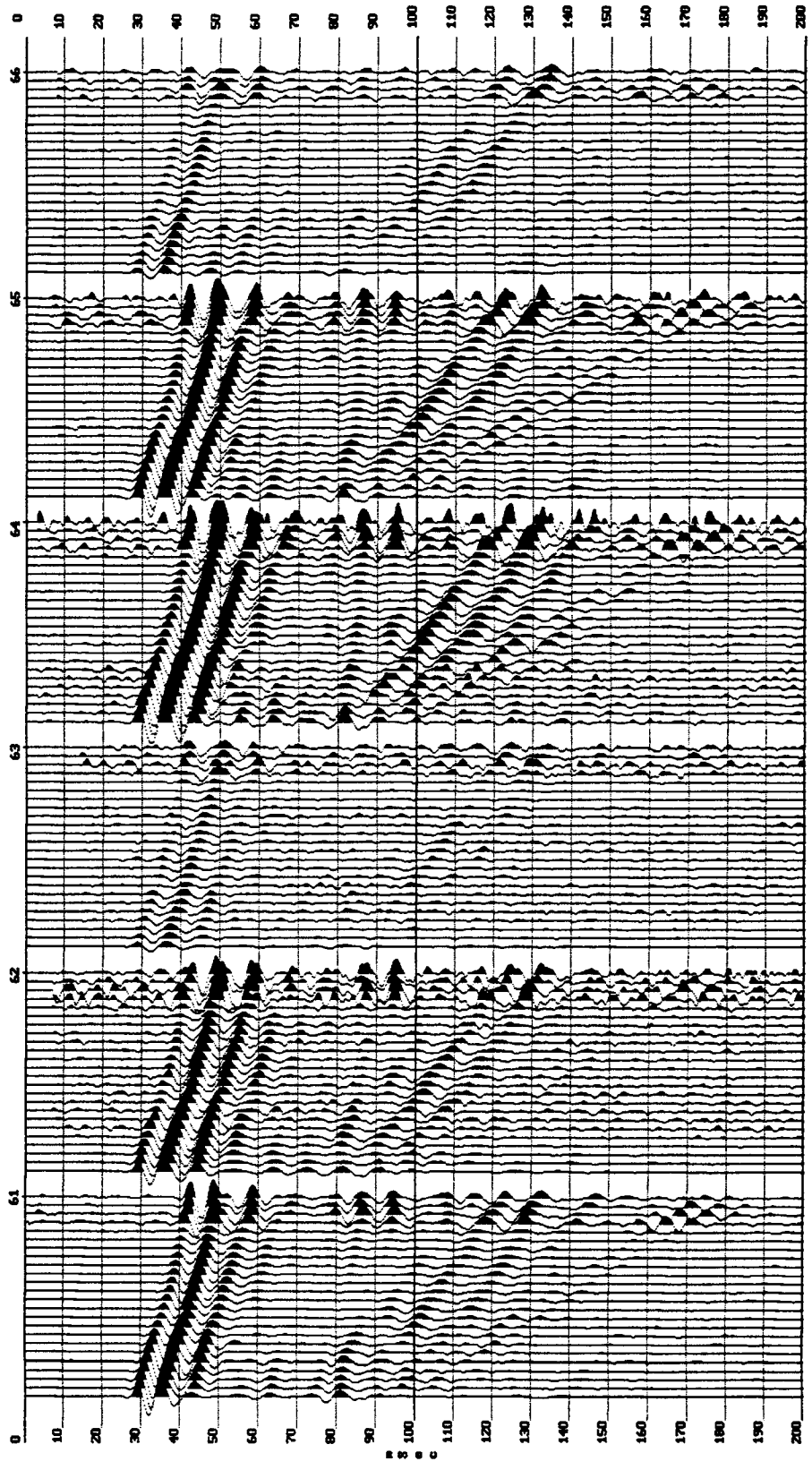
0
10
20
30
40
50
60
70
80
90
100
110
120
130
140
150
160
170
180
190
200
66
65
64
63
62
61
msec

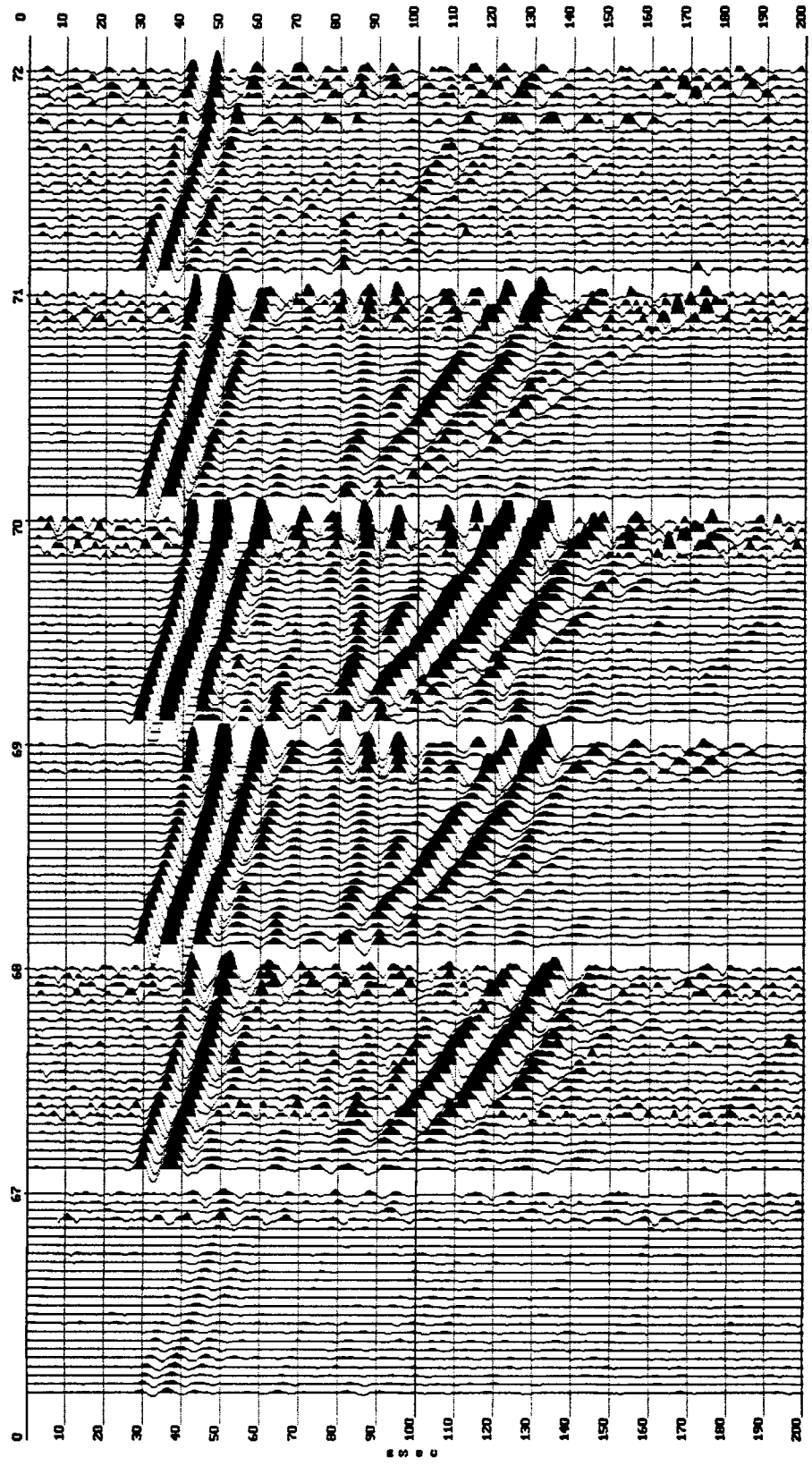
0
10
20
30
40
50
60
70
80
90
100
110
120
130
140
150
160
170
180
190
200
72
71
70
69
68
67
msec

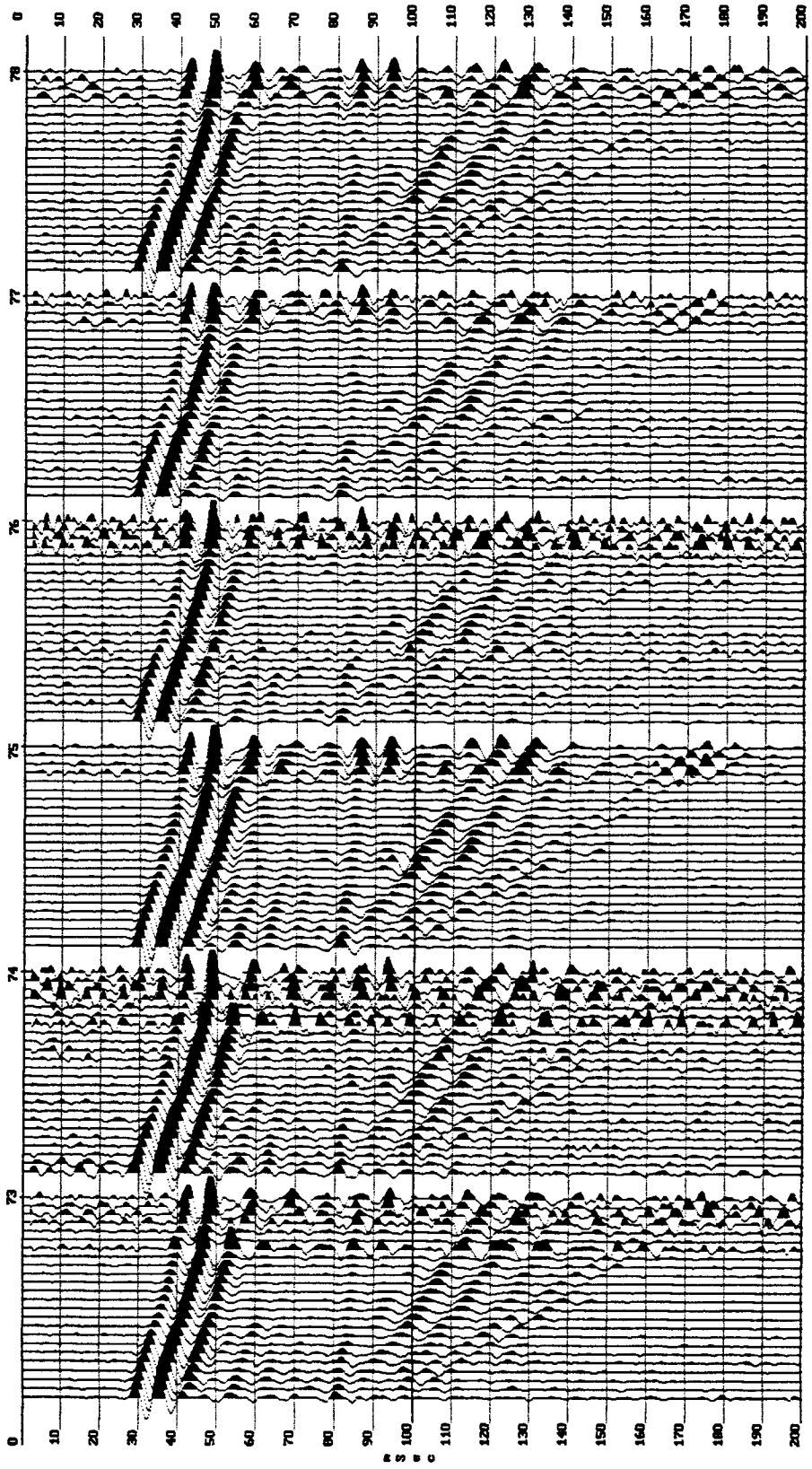
0
10
20
30
40
50
60
70
80
90
100
110
120
130
140
150
160
170
180
190
200
78
77
76
75
74
73
msec

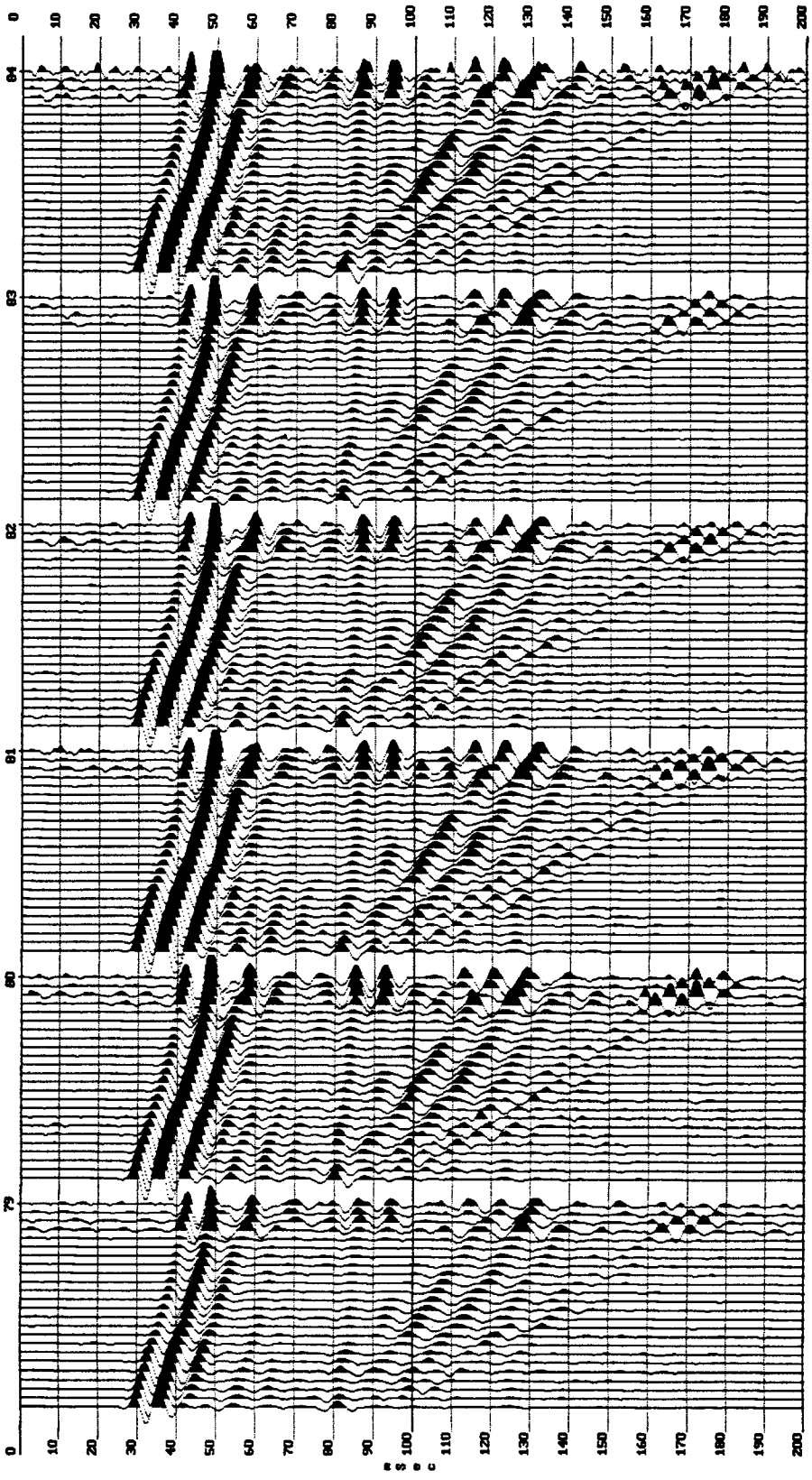
0
10
20
30
40
50
60
70
80
90
100
110
120
130
140
150
160
170
180
190
200
84
83
82
81
80
79
msec

0
10
20
30
40
50
60
70
80
90
100
110
120
130
140
150
160
170
180
190
200
90
89
88
87
86
85
msec

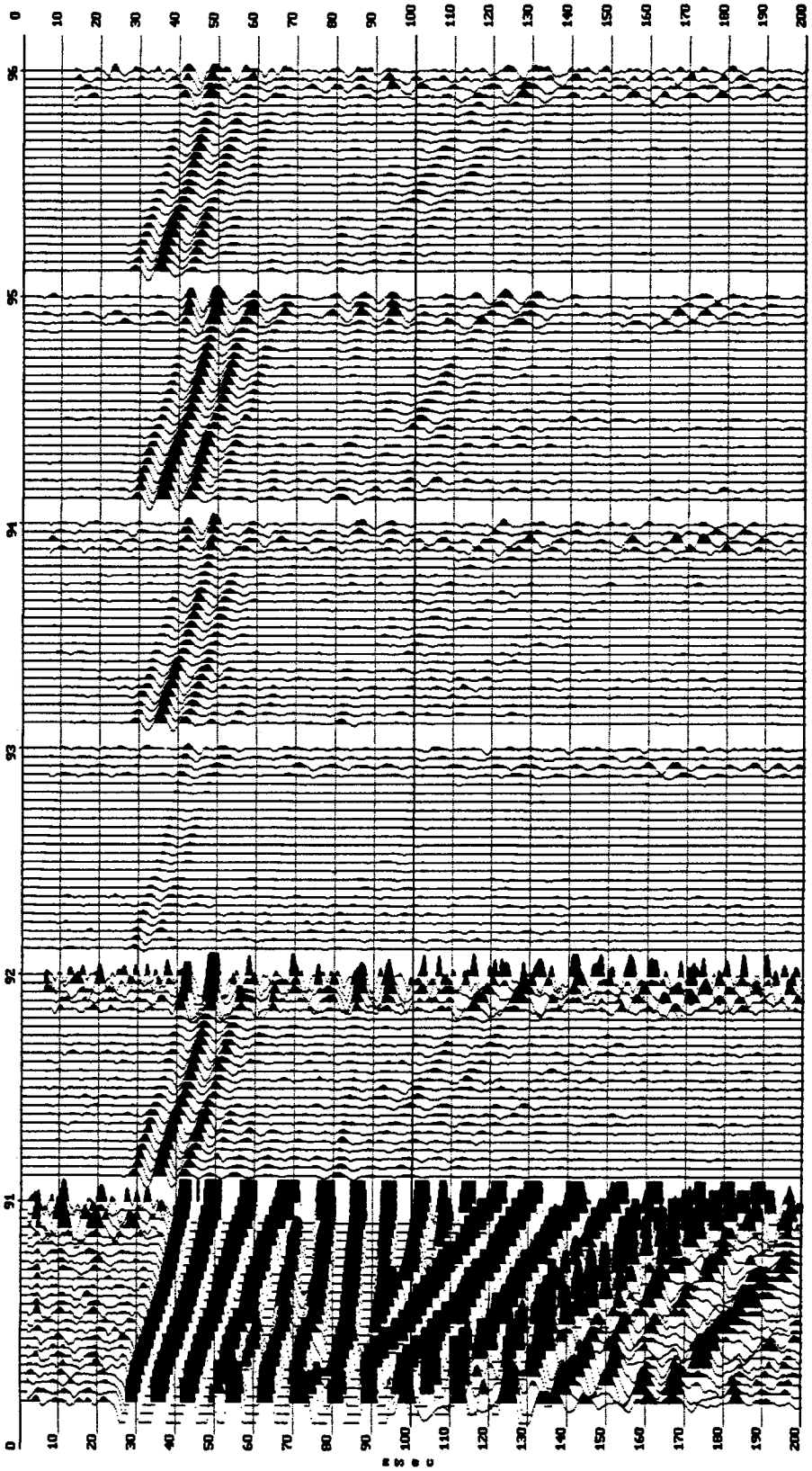
0
10
20
30
40
50
60
70
80
90
100
110
120
130
140
150
160
170
180
190
200
96
95
94
93
92
91
msec

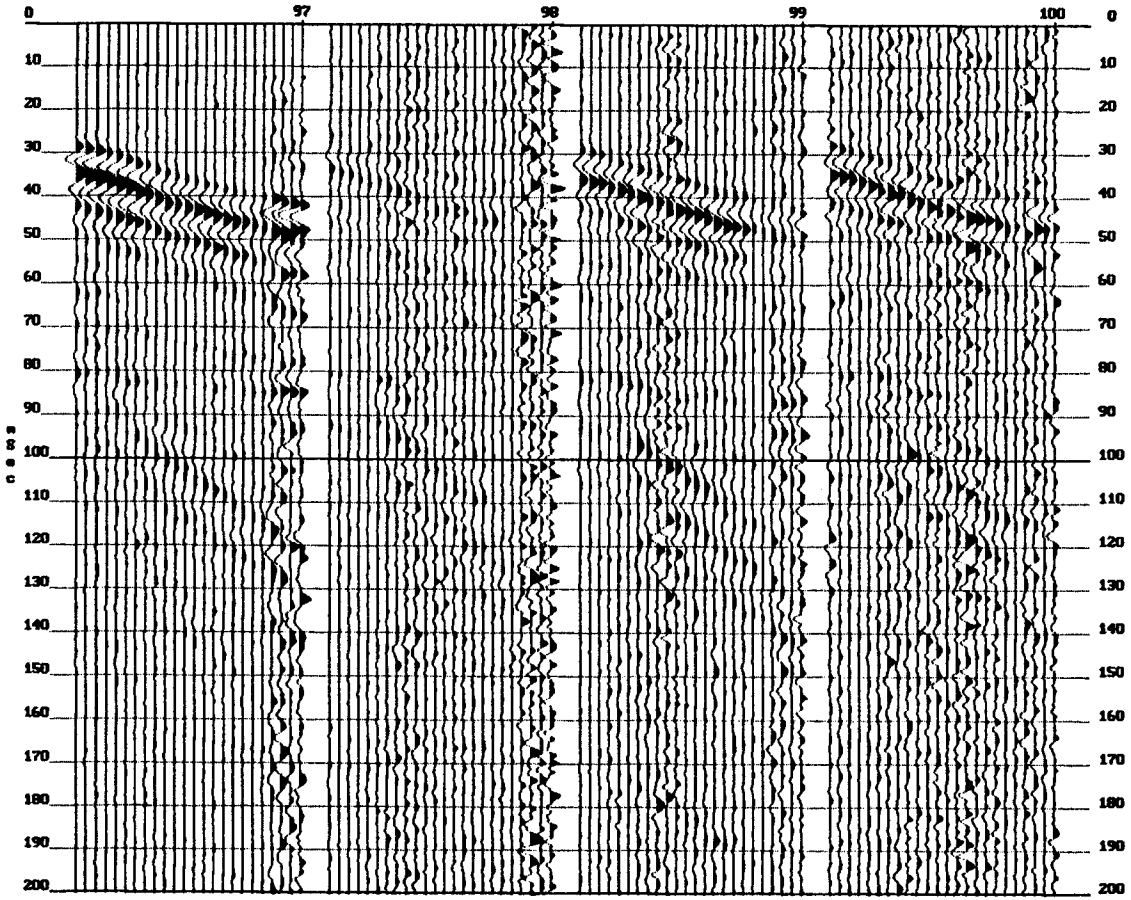
0
97
98
99
100
0
10
20
30
40
50
60
70
80
90
100
110
120
130
140
150
160
170
180
190
200
c e s s

Appendix D Snodgrass Ranch Seismic Data

Field files from the Snodgrass Ranch site, as they were collected. Data are roughly organized according to source energy. The data are shown in amplitude adjusted form; no trace normalization or AGC scaling has been performed. The gains for these data are constant: channel 1-7=74 dB, and channels 8-24=78 dB. A general feel for signal changes associated with parameters can be obtained from these plots. (Symbology is the same as that used in Appendix D)

Key for plate mass:

A=2.7 kg, 548 cm^2
B=10.9 kg, 548 cm^2
C=1.4 kg, 274 cm^2
D=2.7 kg, 274 cm^2
E=5.4 kg, 274 cm^2
F=10.9 kg, 274 cm^2
G=21.8 kg, 274 cm^2
H*=1.8 kg, 274 cm^2
I=2.7 kg, 137 cm^2
J=10.9 kg, 137 cm^2
K=5.4 kg, 0.48 m length, Auger Flight
L=10.9 kg, 0.78 m length, Auger Flight
M=10.9 kg, 0.9 m length, Downhole Plate

Key for Impact Mass (Combined hammer mass and extension mass, measured at impact with a scale):

N=5.0 kg
O=7.7 kg
P=10.4 kg
Q=12.7 kg
R= 30.06 Downhole Rifle
S=Manual Swing (Human)

Key for Impact Velocity:
T=5.5 m/s
U=8.5 m/s

Format for description:
File #, Plate Parameters, Impact Mass, Impact Velocity (Comments if needed)

File 1, A, O, U.
File 2, B, O, U.
File 3, C, O, U.
File 4, D, O, U.
File 5, E, O, U.
File 6, F, O, U.
File 7, G, O, U.
File 8, H, O, U.
File 9, I, O, U.
File 10, J, O, U.
File 11, NP, O, U.
File 12, A, P, U.
File 13, B, P, U.
File 14, C, P, U.
File 15, D, P, U.
File 16, E, P, U.
File 17, F, P, U.
File 18, G, P, U.
File 19, H, P, U.
File 20, I, P, U.

File 21, J, P, U.
File 22, NP, P, U.
File 27, A, Q, U.
File 28, B, Q, U.
File 29, C, Q, U.
File 30, D, Q, U.
File 31, E, Q, U.
File 32, F, Q, U.
File 33, G, Q, U.
File 34, H, Q, U.

File 35, I, Q, U.
File 36, J, Q, U.
File 37, NP, Q, U.
File 38, A, N, T.
File 39, B, N, T.
File 40, C, N, T.
File 41, D, N, T.
File 42, E, N, T.
File 43, F, N, T.
File 44, G, N, T.

File 45, H, N, T.
File 46, I, N, T.
File 47, J, N, T.
File 48, NP, N, T.
File 49, A, O, T.
File 50, B, O, T.
File 51, C, O, T.
File 52, D, O, T.
File 53, E, O, T.
File 54, F, O, T.

File 55, G, O, T.
File 56, H, O, T.
File 57, I, O, T.
File 58, J, O, T.
File 59, NP, O, T.
File 60, A, P, T.
File 61, B, P, T.
File 62, C, P, T.
File 63, D, P, T.
File 64, E, P, T.

File 65, F, P, T.
File 66, G, P, T.
File 67, H, P, T.
File 68, I, P, T.
File 69, J, P, T.
File 70, NP, P, T.
File 71, NP, P, T. (Repeat)
File 72, A, S. (Swinger 1)
File 73, B, S.
File 74, C, S.

File 75, D, S.
File 76, E, S.
File 77, F, S.
File 78, G, S.
File 79, H, S.
File 80, I, S.
File 81, J, S.
File 82, NP, S.
File 83,B, S, (Glancing Blow)
File 84, B, S. (Swinger 2)

File 85, F, S.
File 86, J, S.
File 87, M, P, T.
File 88, K, P, T.
File 89, L, P, T.
File 90, E, P, T.
File 91, F, P, T.
File 92, C, Dead Blow Hammer
File 93, C, Steel Alloy Hammer
File 94, B, P, T (Glancing Blow)

File 95, F, P, T. (Glancing Blow)
File 96, B, P, T. (Compaction Study)
File 97, B, P, T.
File 98, B, P, T.
File 99, B, P, T.
File 100, B, P, T.
File 101, B, P, T.
File 102, B, P, T.
File 103, B, P, T.
File 104, B, P, T.

File 105, B, P, T.
File 106, B, P, T.
File 107, B, P, T.
File 108, B, P, T.
File 109, B, P, T.
File 110, B, P, T.
File 111, B, P, T.
File 112, B, P, T.
File 113, B, P, T.
File 114, B, P, T.

File 115, B, P, T.
File 116, F, P, T. (Compaction)
File 117, F, P, T.
File 118, F, P, T.
File 119, F, P, T.
File 120, F, P, T.
File 121, F, P, T
File 122, F, P, T
File 123, F, P, T
File 124, F, P, T

File 125, F, P, T
File 126, F, P, T
File 127, F, P, T
File 128, F, P, T
File 129, F, P, T
File 130, F, P, T
File 131, F, P, T
File 132, F, P, T.
File 133, F, P, T.
File 134, F, P, T.

File 135, F, P, T.
File 136, J, P, T. (Compaction)
File 137, J, P, T
File 138, J, P, T
File 139, J, P, T
File 140, J, P, T
File 141, J, P, T
File 142, J, P, T
File 143, J, P, T
File 144, J, P, T

File 145, J, P, T
File 146, J, P, T
File 147, J, P, T
File 148, J, P, T.
File 149, J, P, T.
File 150, J, P, T.
File 151, J, P, T.

File 152, J, P, T.
File 153, J, P, T
File 154, J, P, T
File 155, J, P, T
File 156, S (Test Shot)
File 157, S. (New Hole)

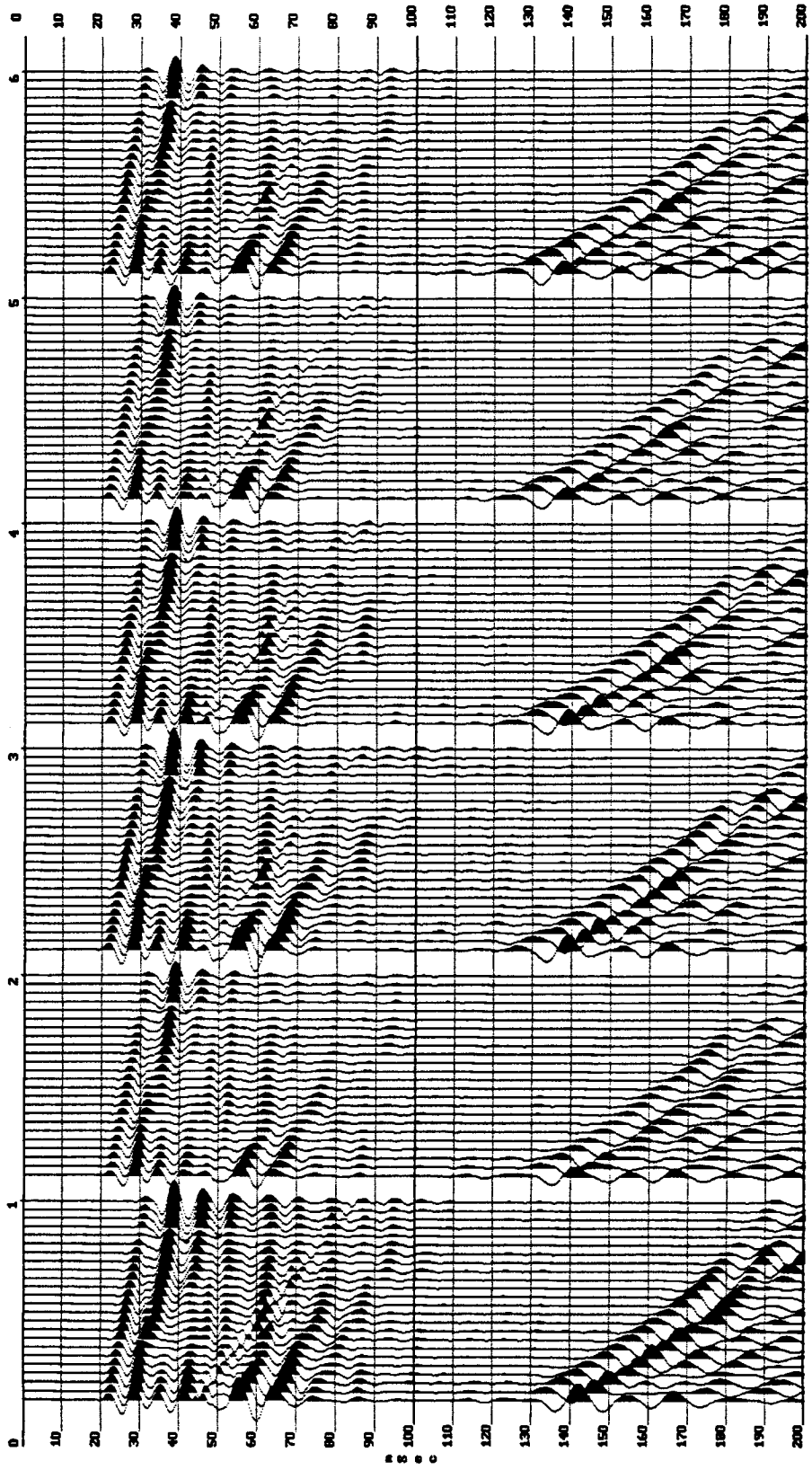
0
10
20
30
40
50
60
70
80
90
100
110
120
130
140
150
160
170
180
190
200
msec

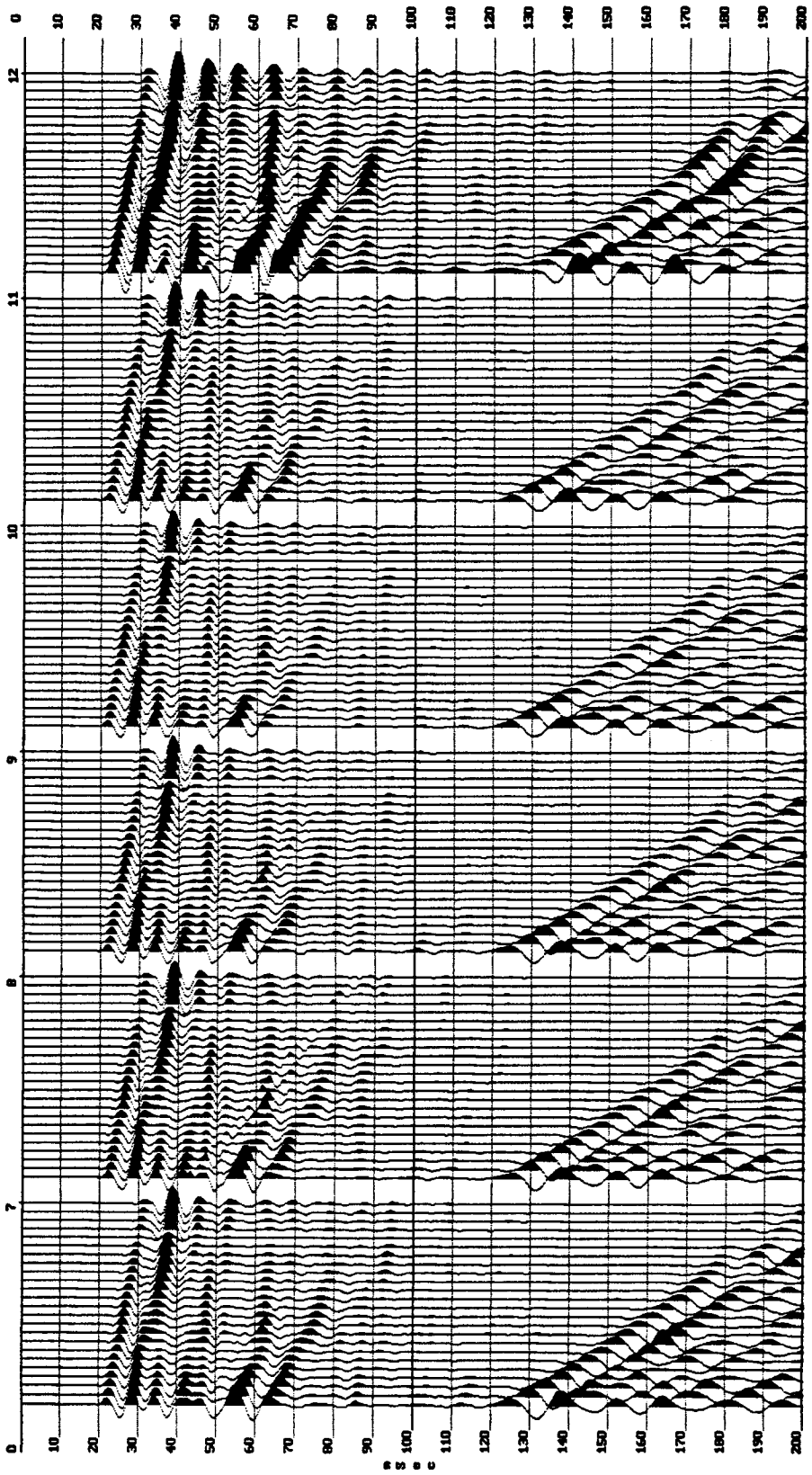
0
10
20
30
40
50
60
70
80
90
100
110
120
130
140
150
160
170
180
190
200
12
11
10
9
8
7
0
msec

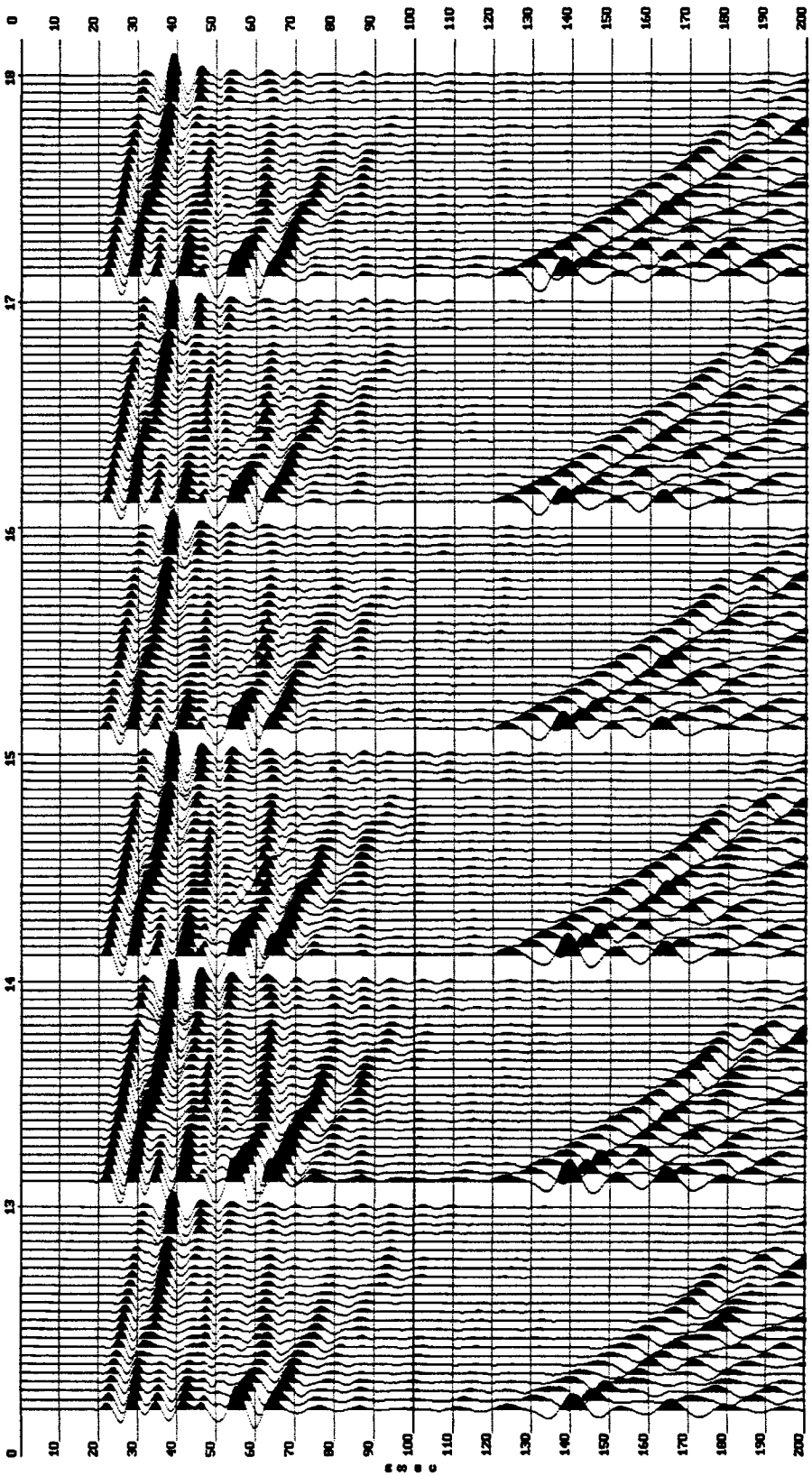
0
10
20
30
40
50
60
70
80
90
100
110
120
130
140
150
160
170
180
190
200
msec

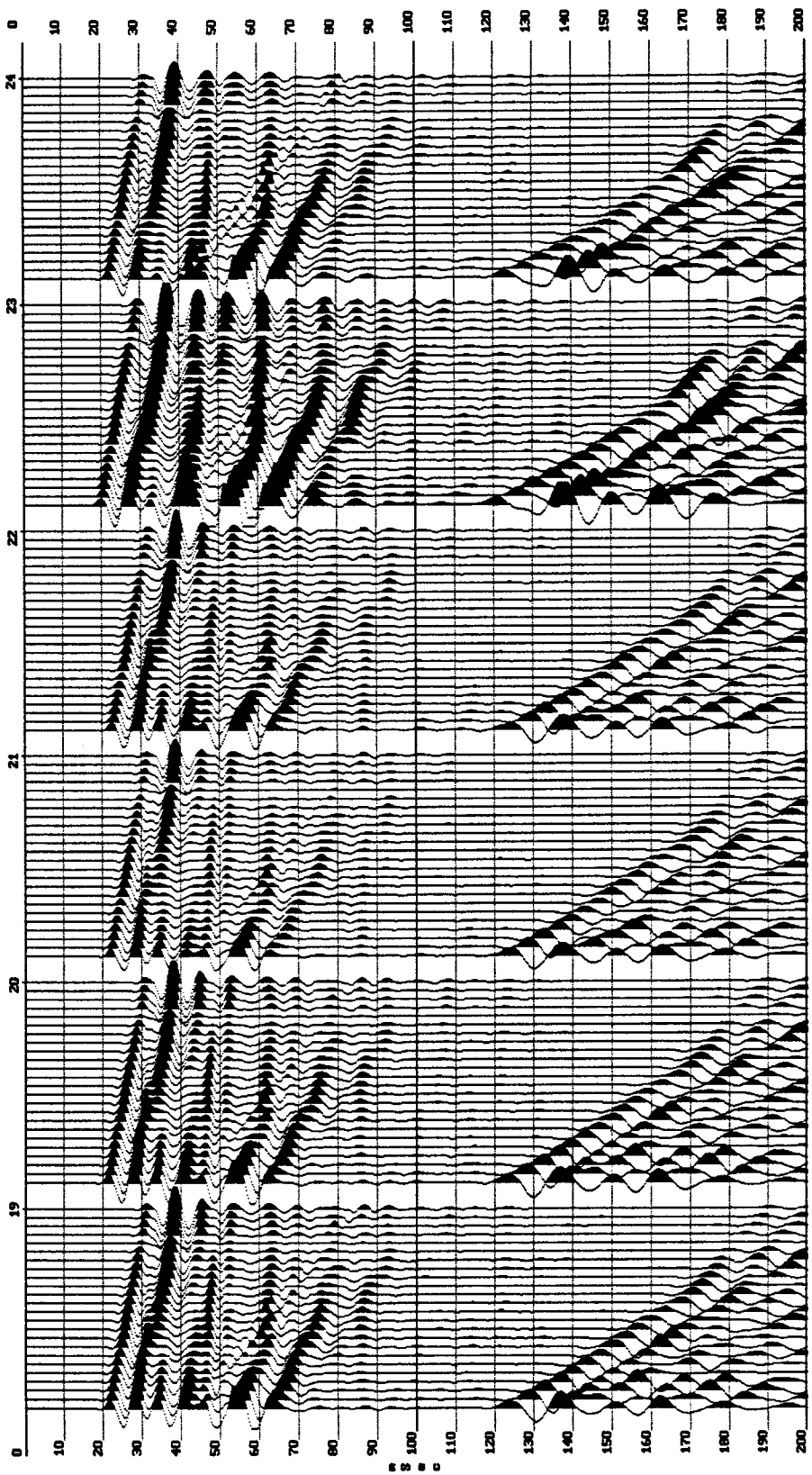
0
10
20
30
40
50
60
70
80
90
100
110
120
130
140
150
160
170
180
190
200
24
23
22
21
20
19
0

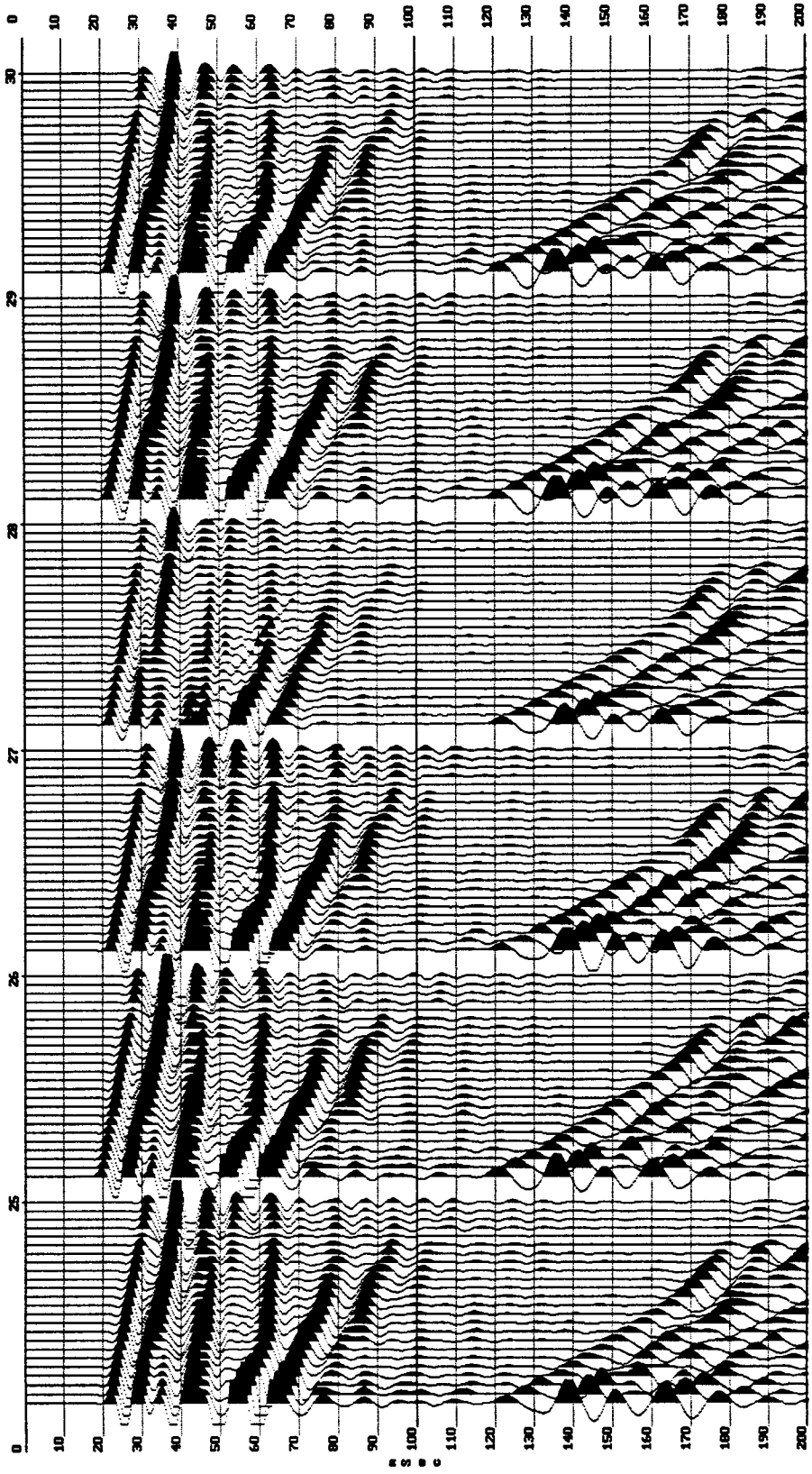
0
10
20
30
40
50
60
70
80
90
100
110
120
130
140
150
160
170
180
190
200
30
29
28
27
26
25
msec

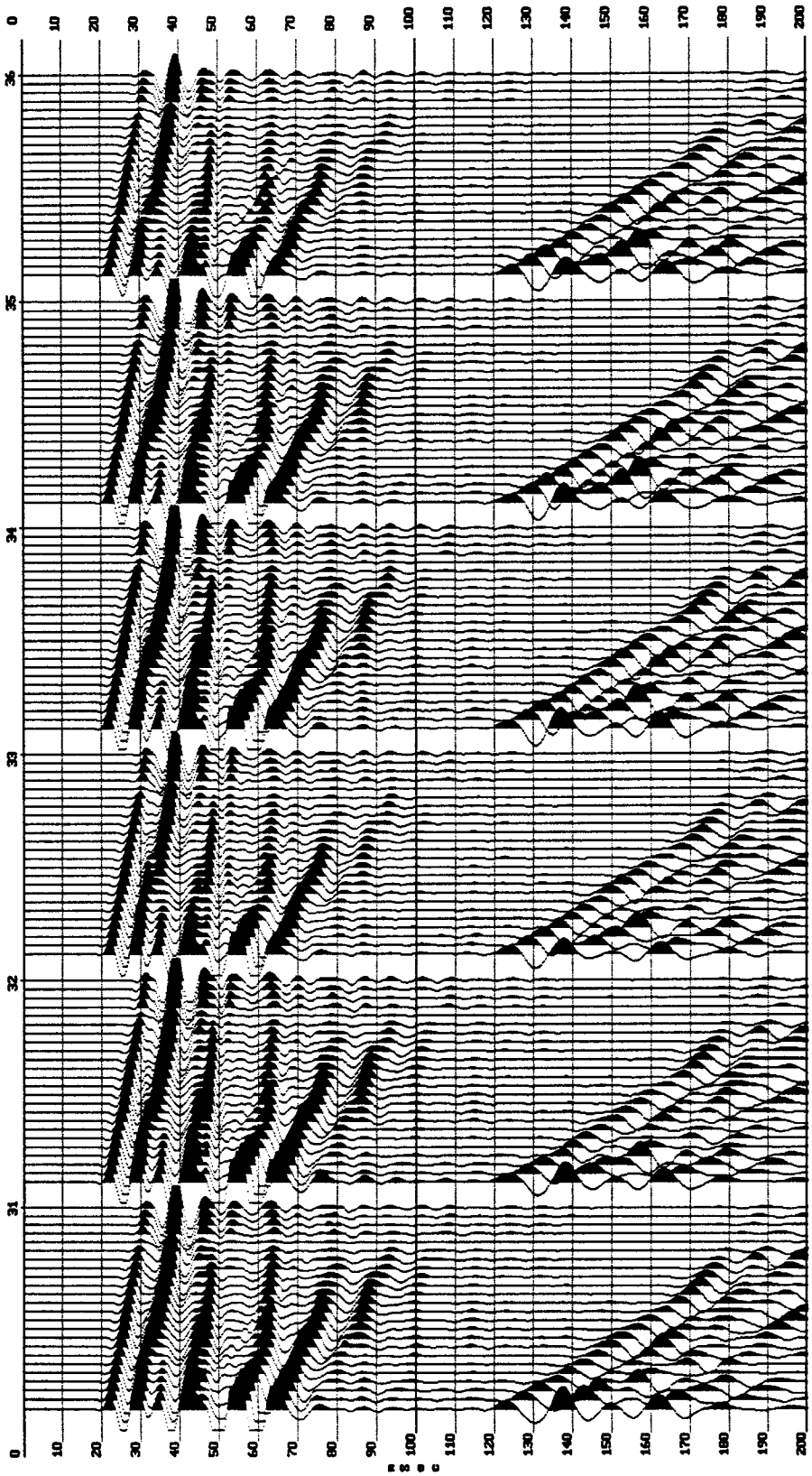
0
10
20
30
40
50
60
70
80
90
100
110
120
130
140
150
160
170
180
190
200
36
35
34
33
32
31
msec

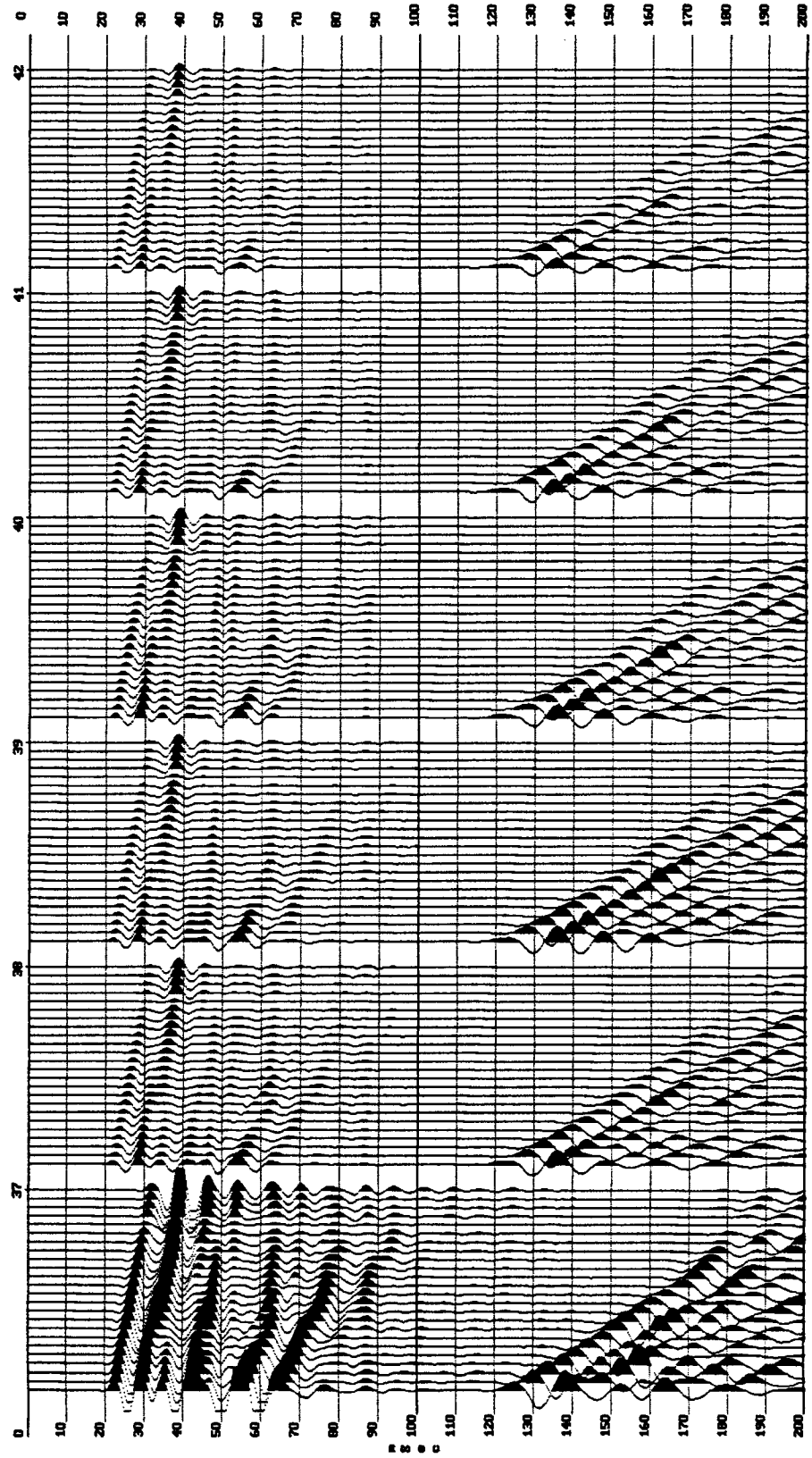
0
10
20
30
40
50
60
70
80
90
100
110
120
130
140
150
160
170
180
190
200
42
41
40
39
38
37
0
msec

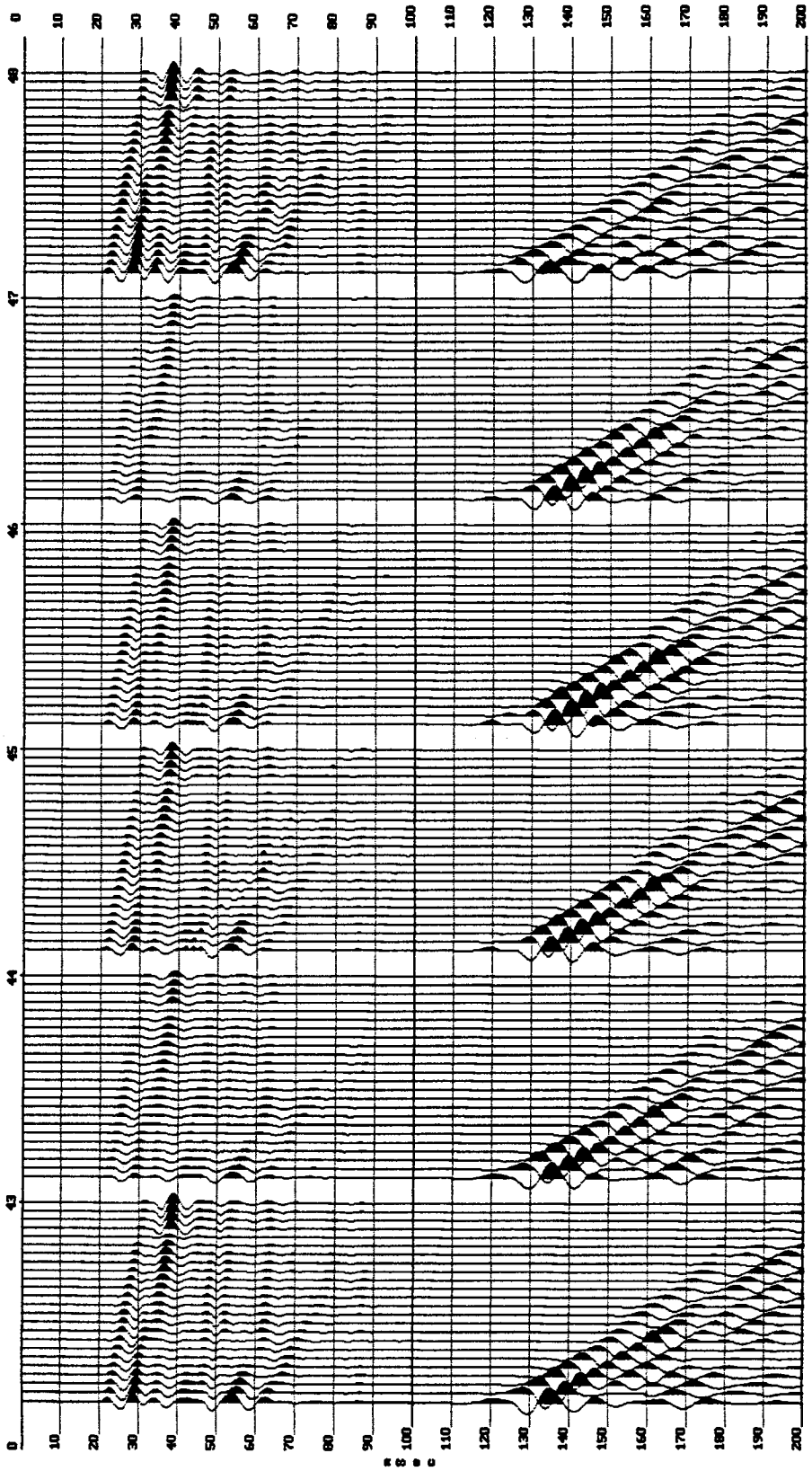
0
10
20
30
40
50
60
70
80
90
100
110
120
130
140
150
160
170
180
190
200
48
47
46
45
44
43
msec

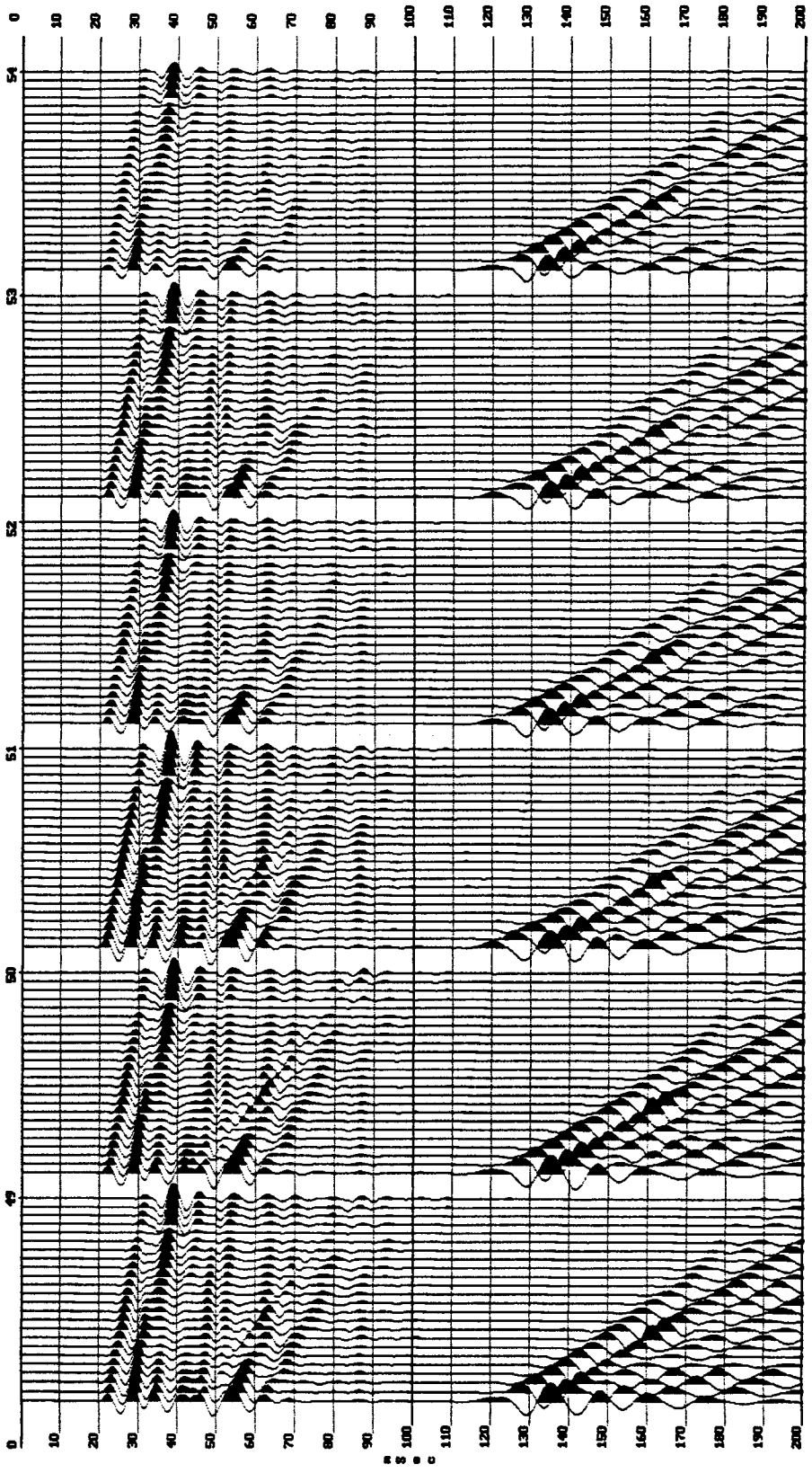
msec

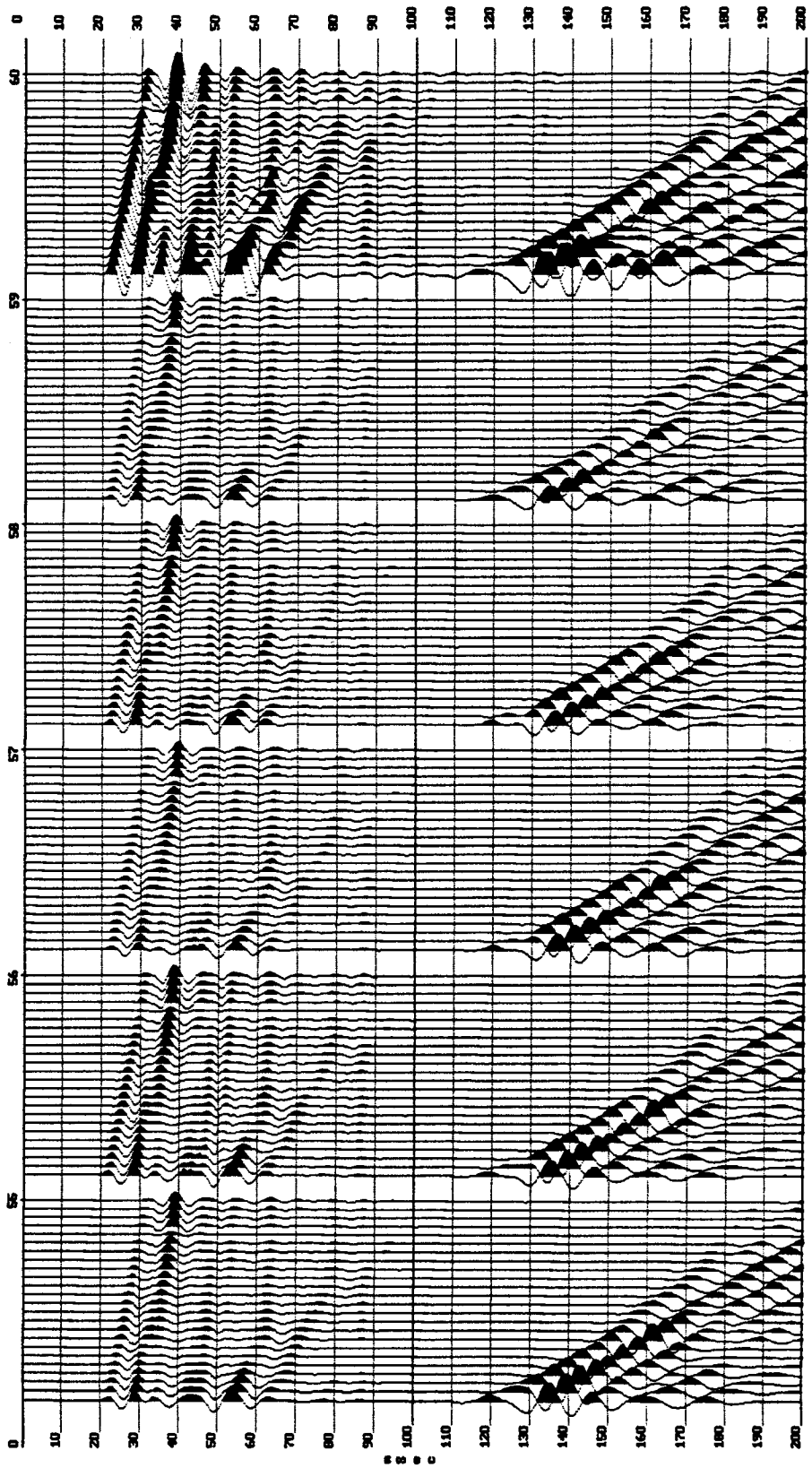
0
10
20
30
40
50
60
70
80
90
100
110
120
130
140
150
160
170
180
190
200
msec

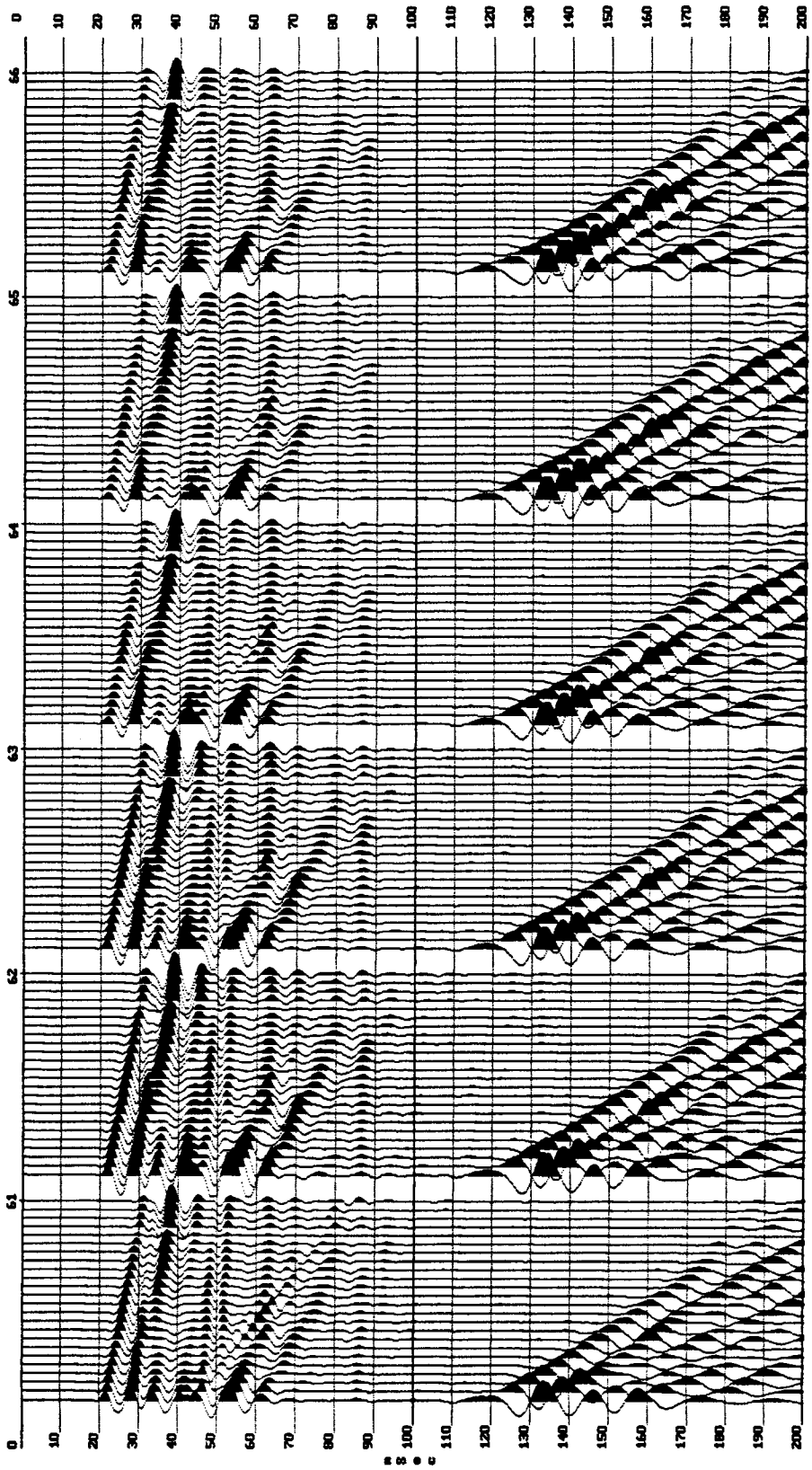
0
10
20
30
40
50
60
70
80
90
100
110
120
130
140
150
160
170
180
190
200
msec

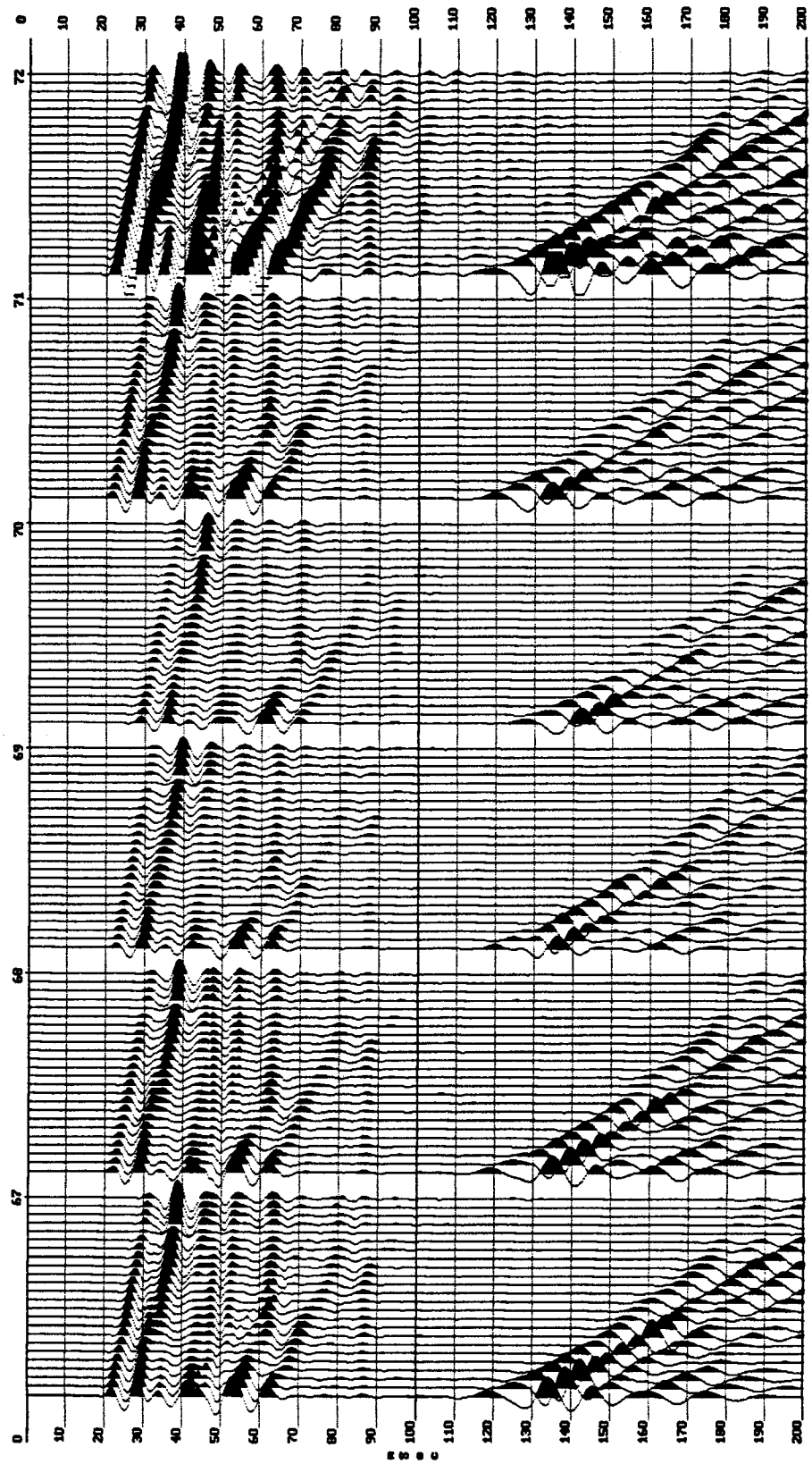
msec

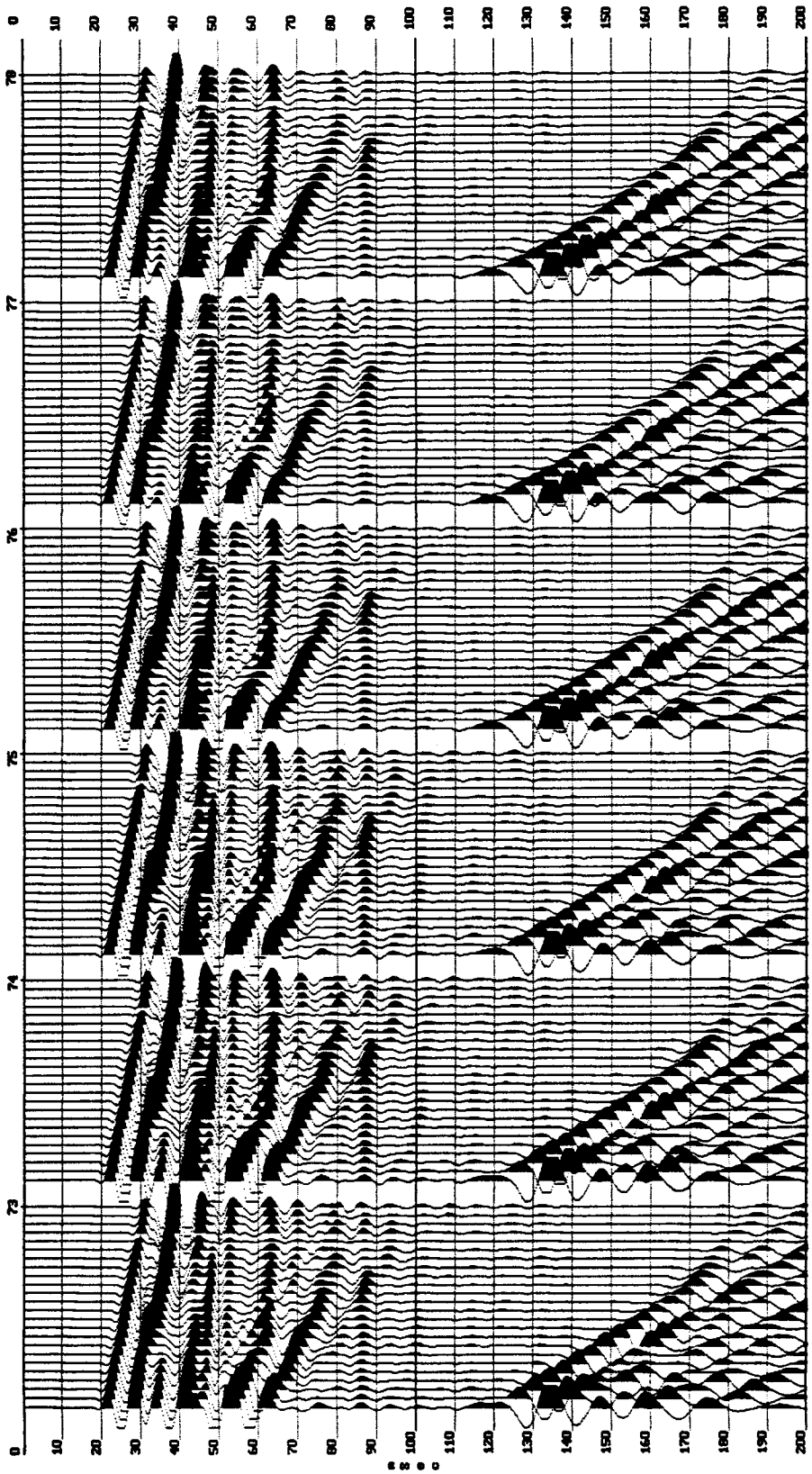
0
10
20
30
40
50
60
70
80
90
100
110
120
130
140
150
160
170
180
190
200
78
77
76
75
74
73
msec

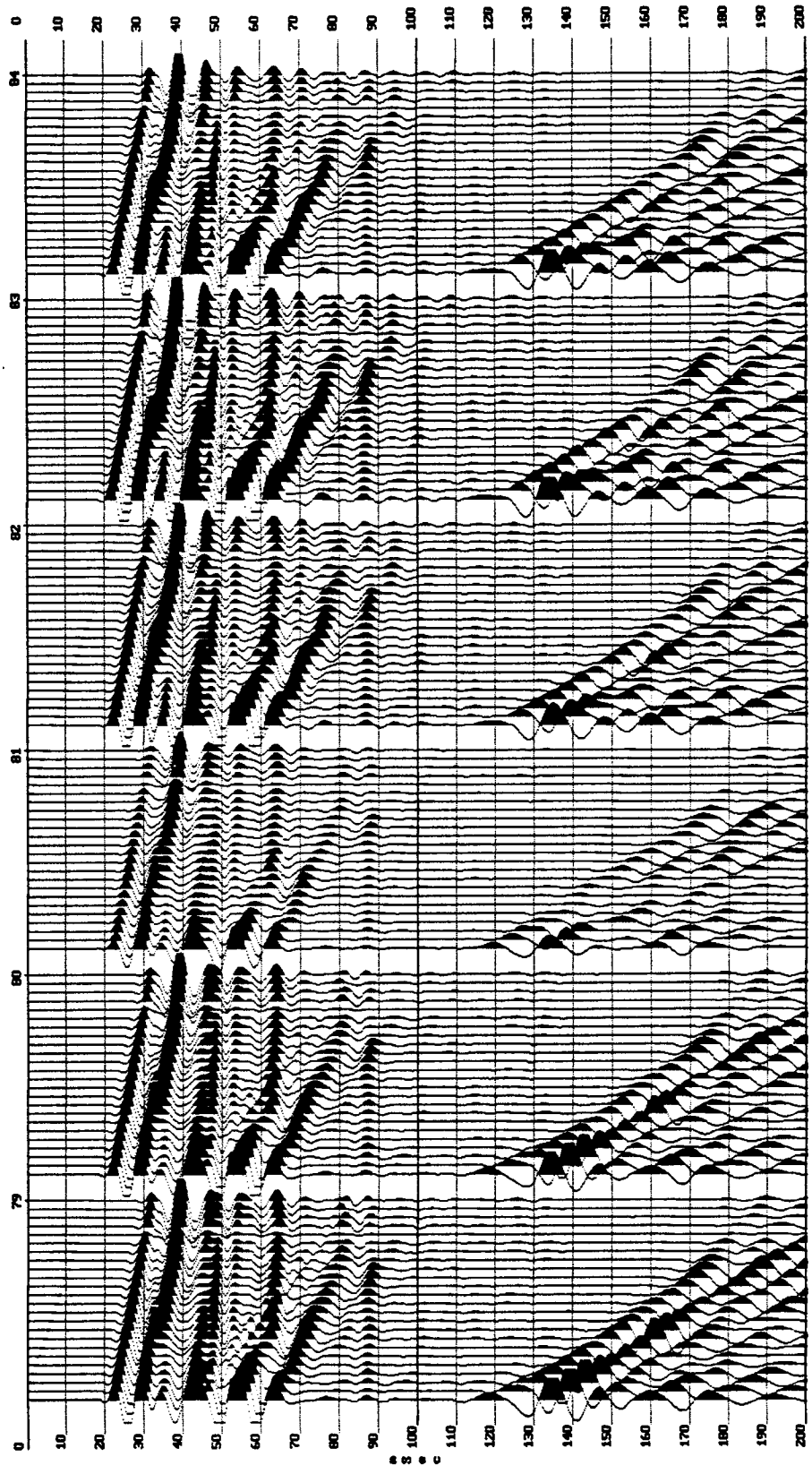
0
10
20
30
40
50
60
70
80
90
100
110
120
130
140
150
160
170
180
190
200
84
83
82
81
80
79
msec

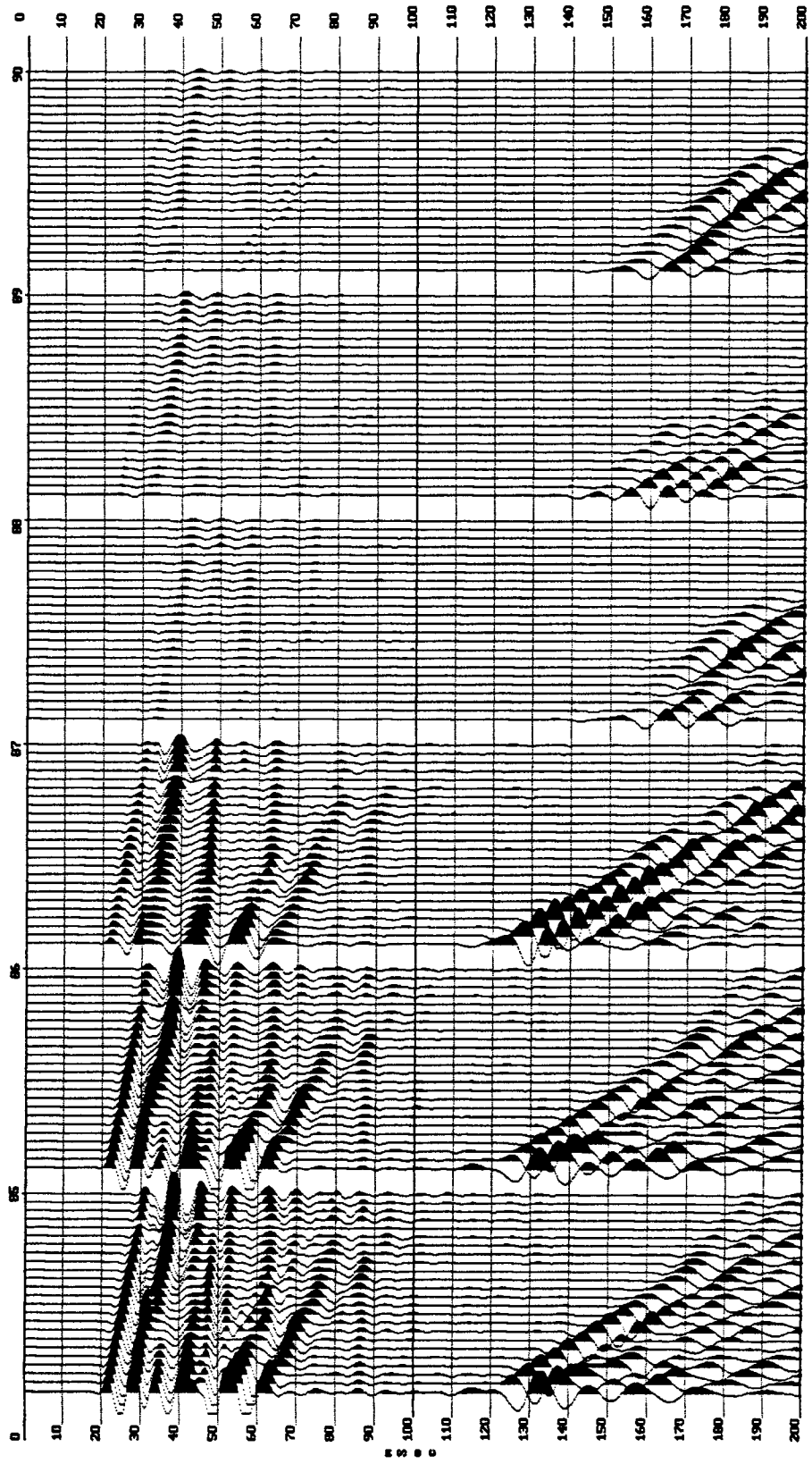
0
10
20
30
40
50
60
70
80
90
100
110
120
130
140
150
160
170
180
190
200
90
89
88
87
86
85
0

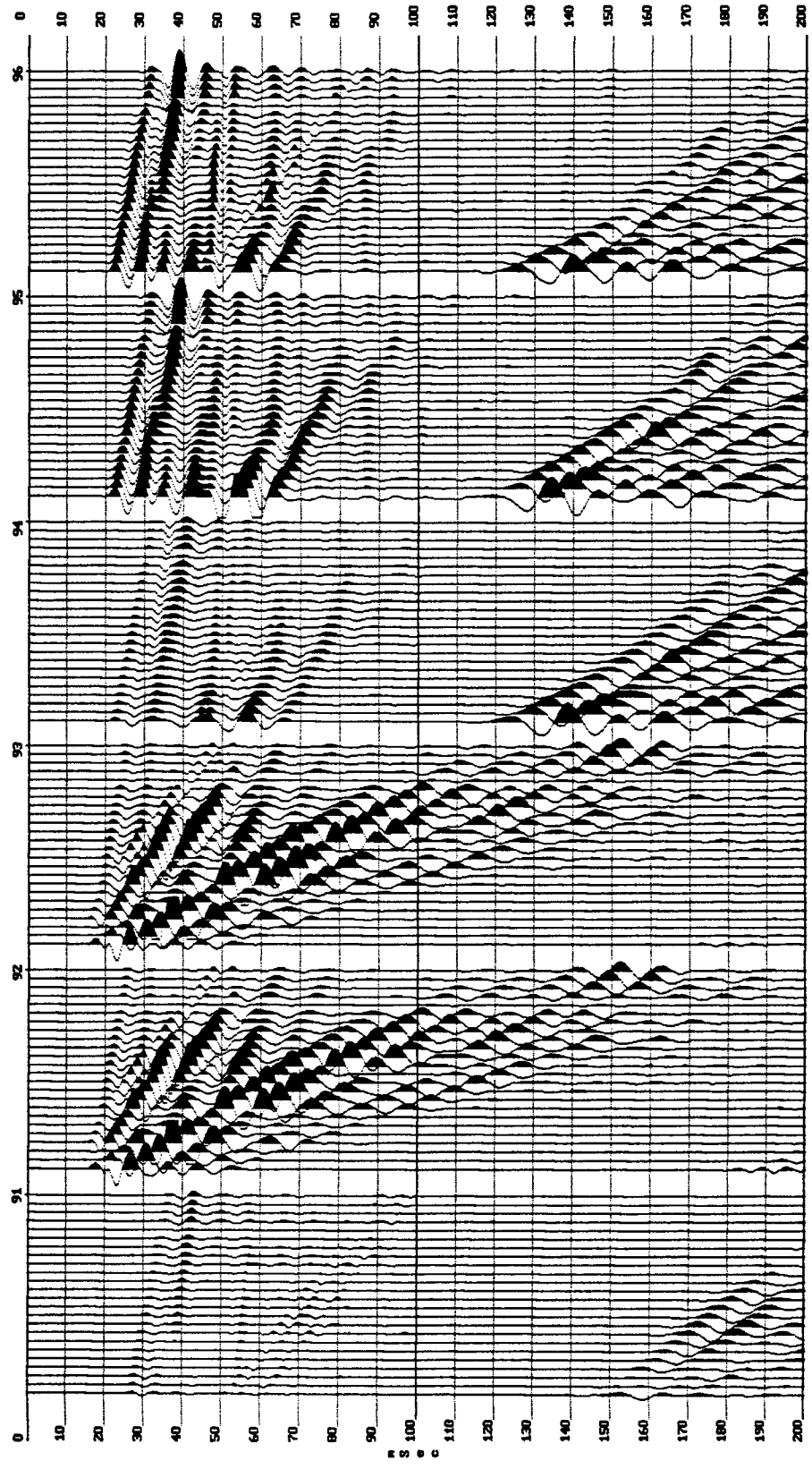
0
10
20
30
40
50
60
70
80
90
100
110
120
130
140
150
160
170
180
190
200
96
95
94
93
92
91
msec

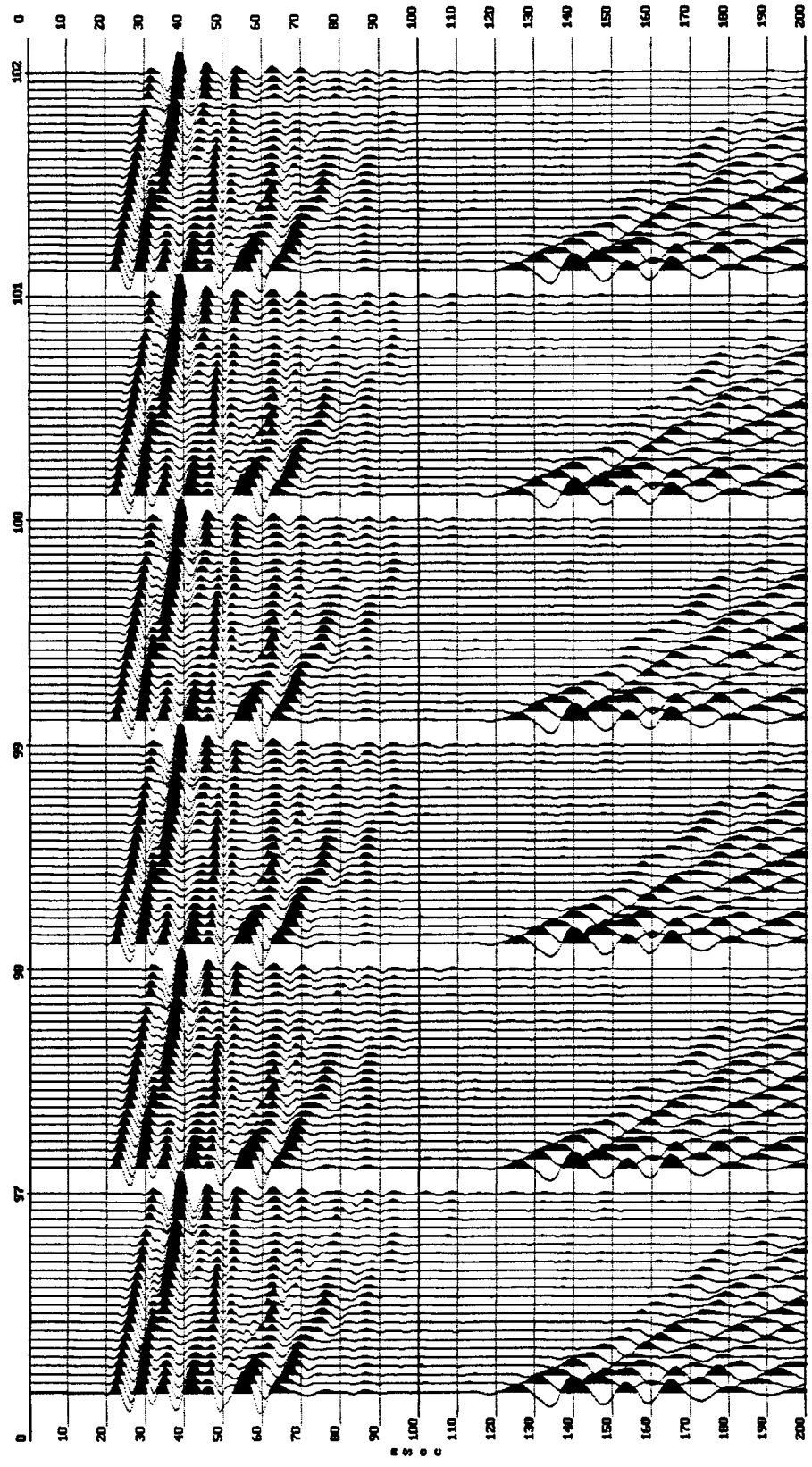
0
10
20
30
40
50
60
70
80
90
100
110
120
130
140
150
160
170
180
190
200
102
101
100
99
98
97
msec

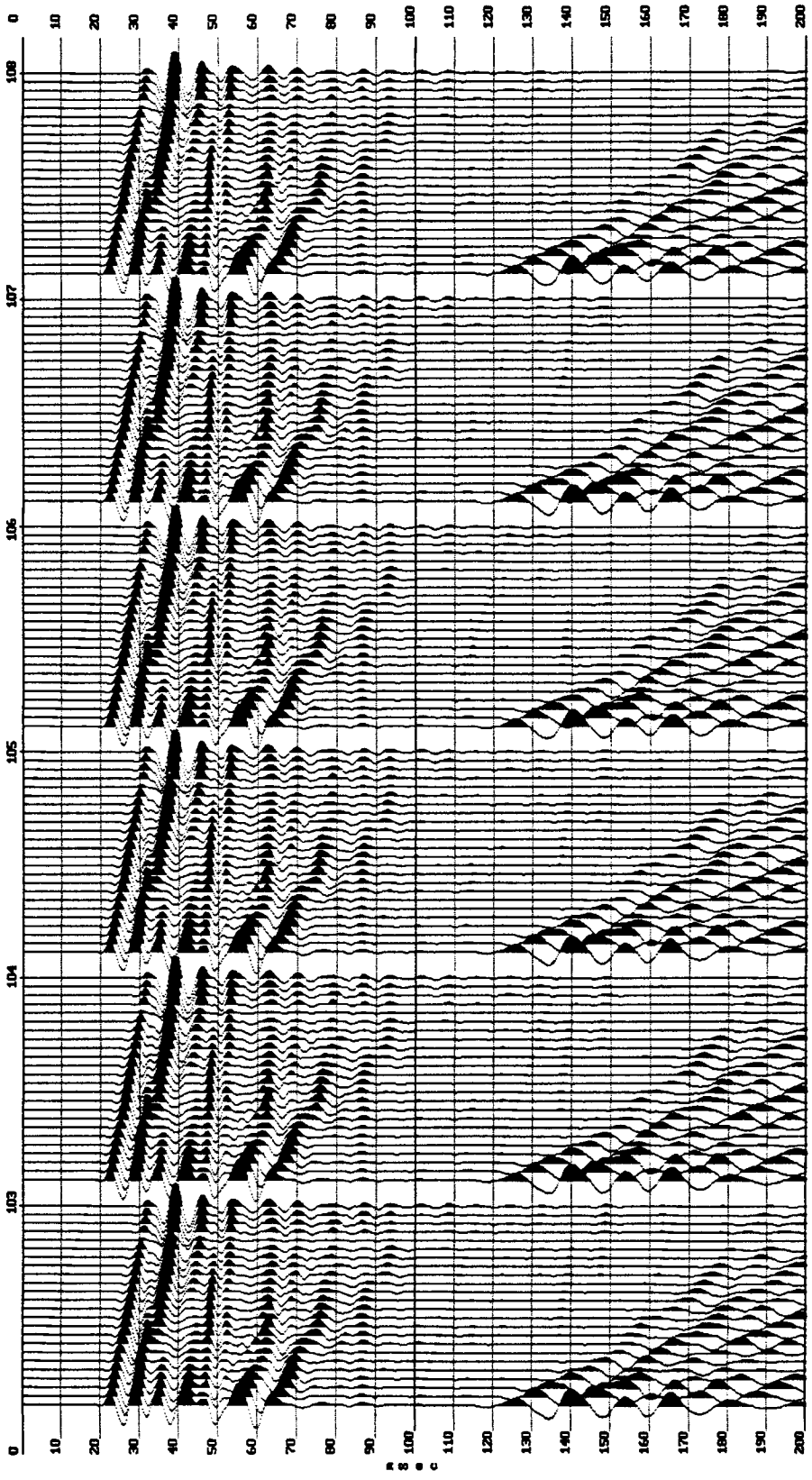
0
10
20
30
40
50
60
70
80
90
100
110
120
130
140
150
160
170
180
190
200
108
107
106
105
104
103
msec

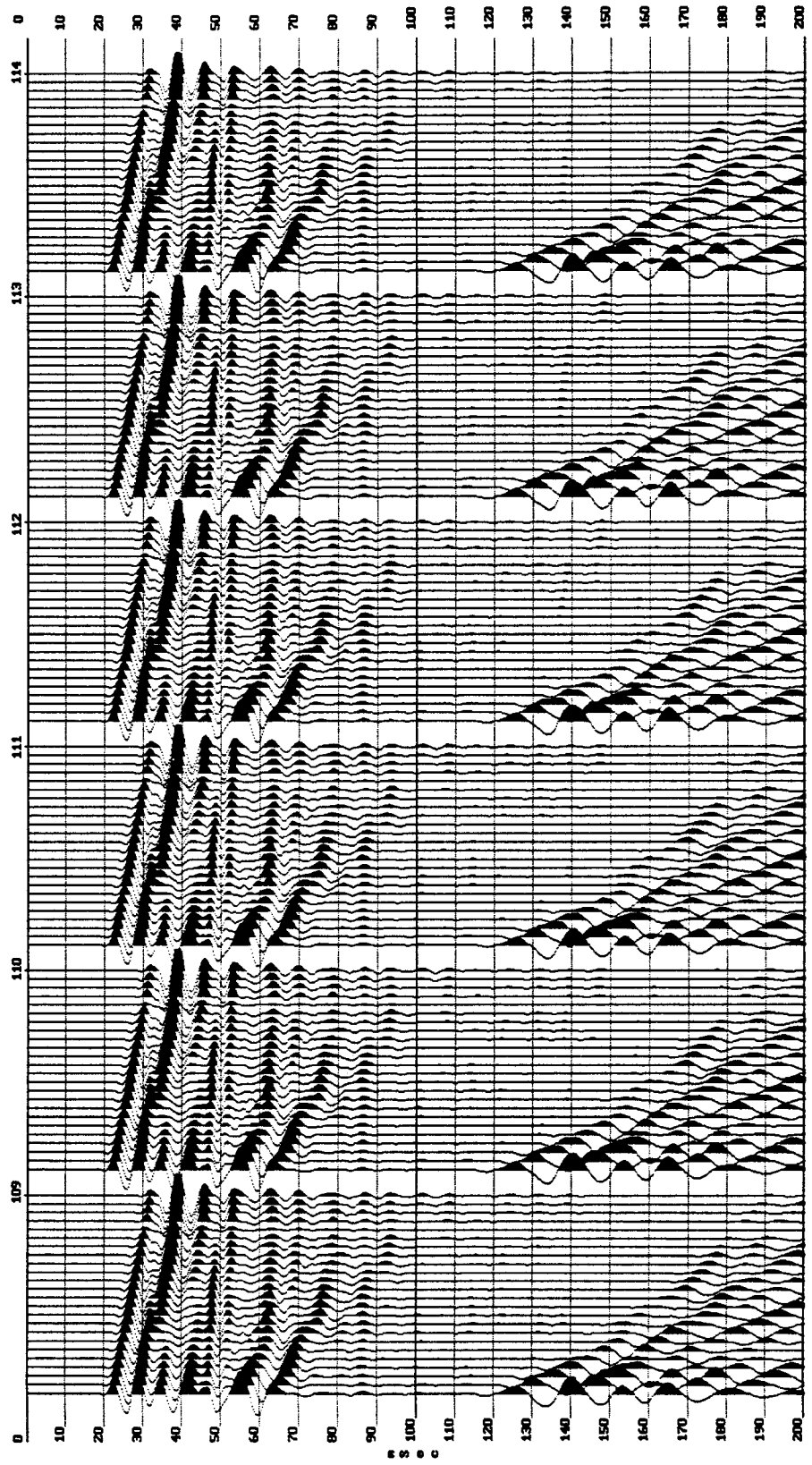
0
10
20
30
40
50
60
70
80
90
100
110
120
130
140
150
160
170
180
190
200
114
113
112
111
110
109
msec

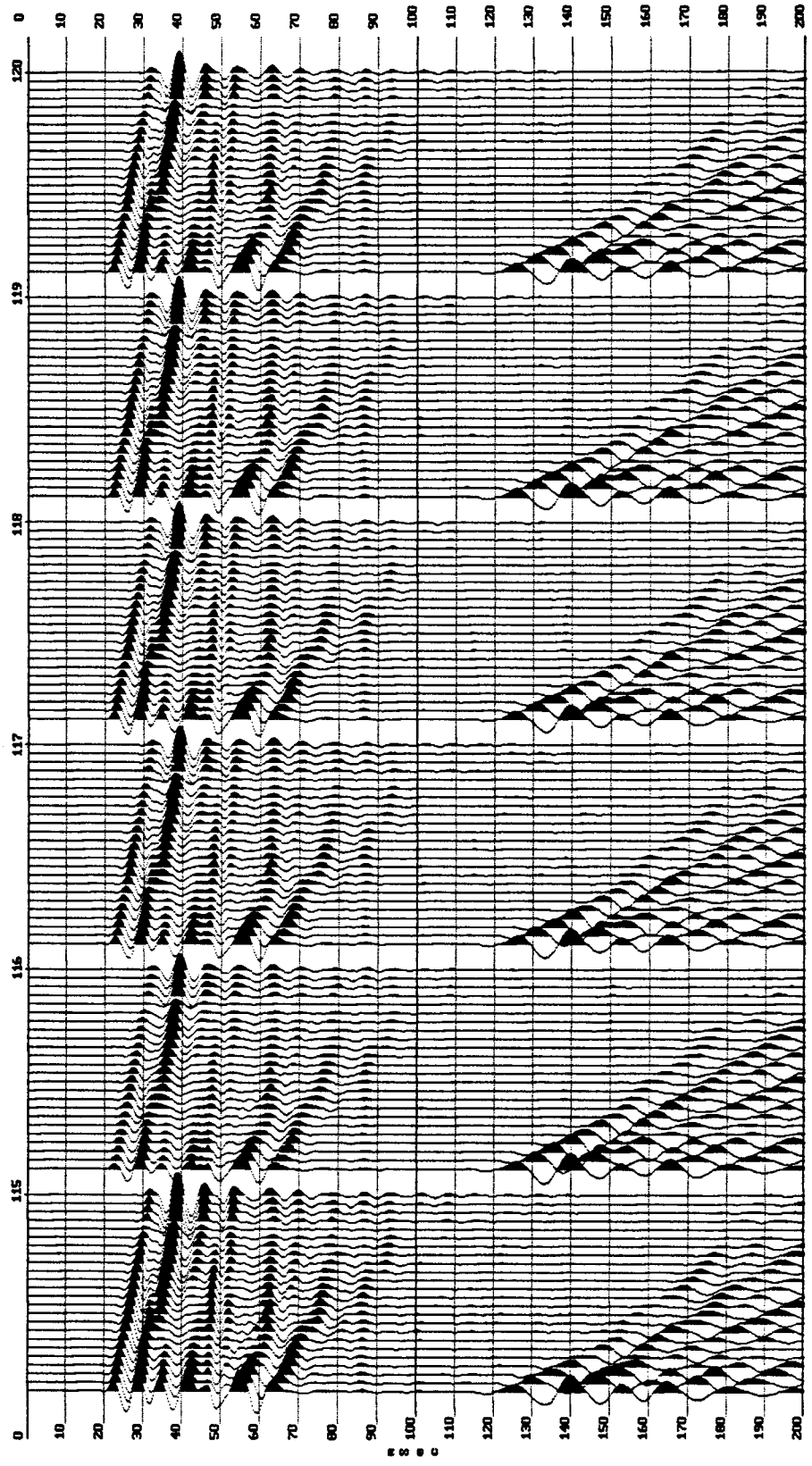
0
10
20
30
40
50
60
70
80
90
100
110
120
130
140
150
160
170
180
190
200
120
119
118
117
116
115
msec

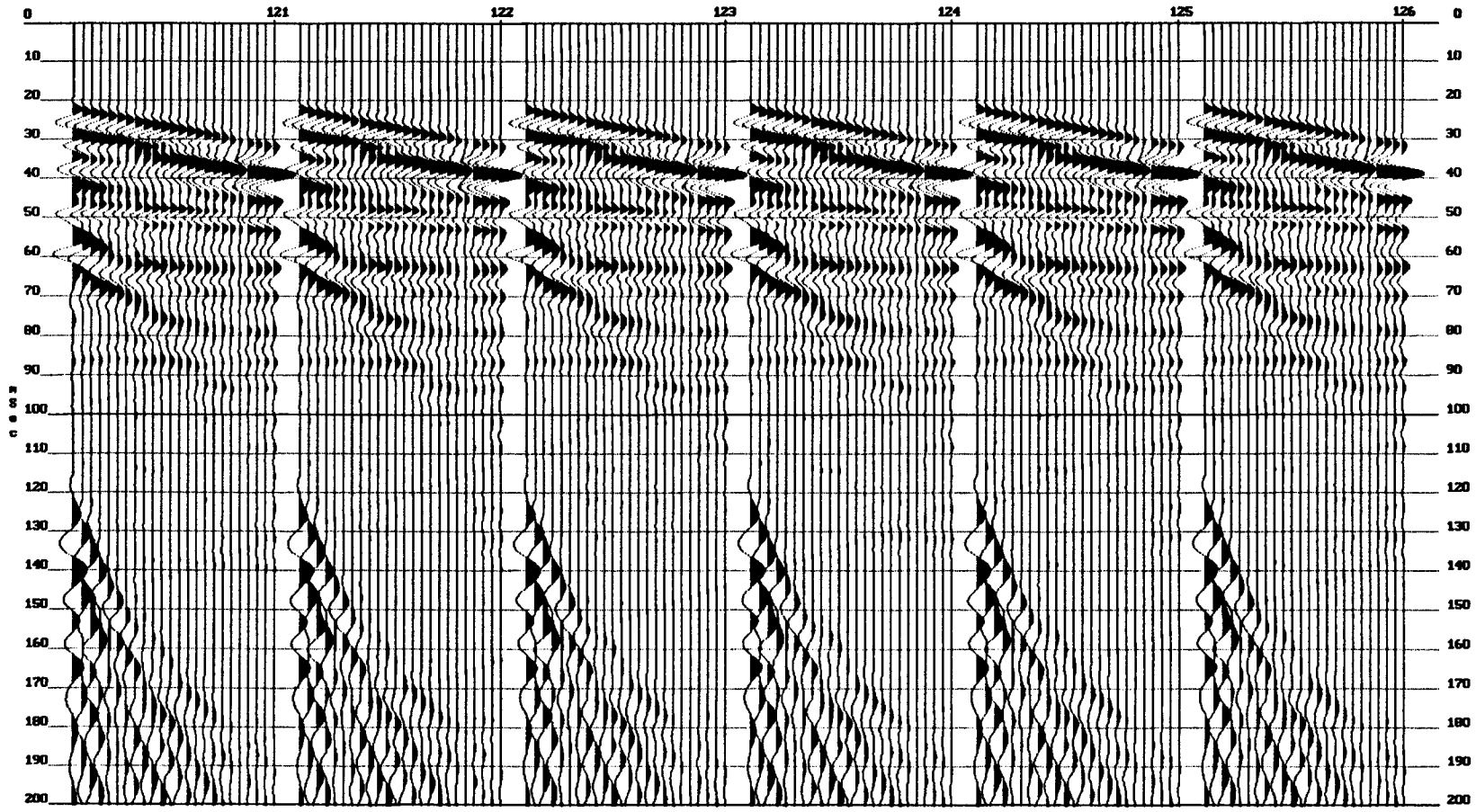
0
121
122
123
124
125
126
0
10
20
30
40
50
60
70
80
90
100
110
120
130
140
150
160
170
180
190
200

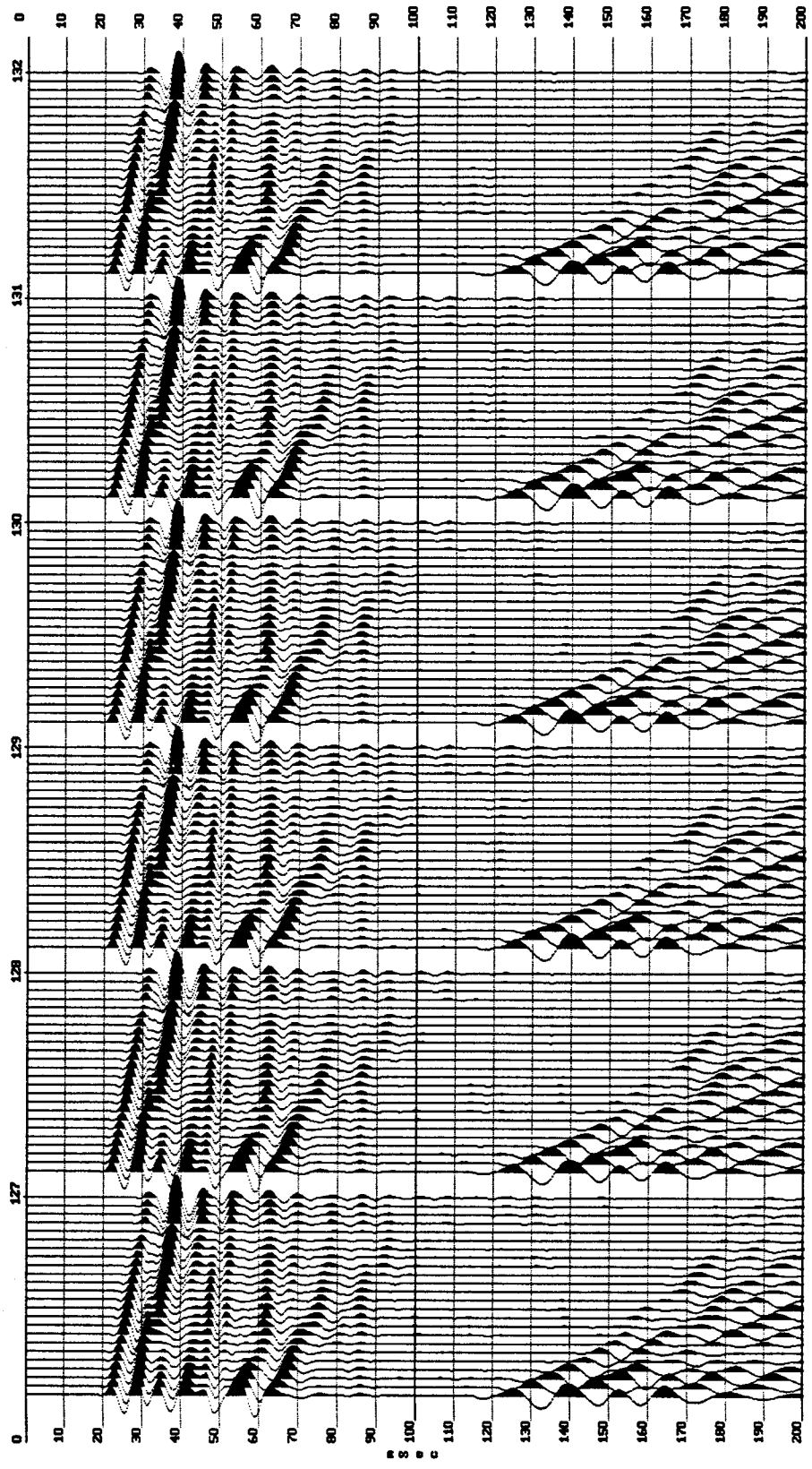
0
10
20
30
40
50
60
70
80
90
100
110
120
130
140
150
160
170
180
190
200
132
131
130
129
128
127
msec

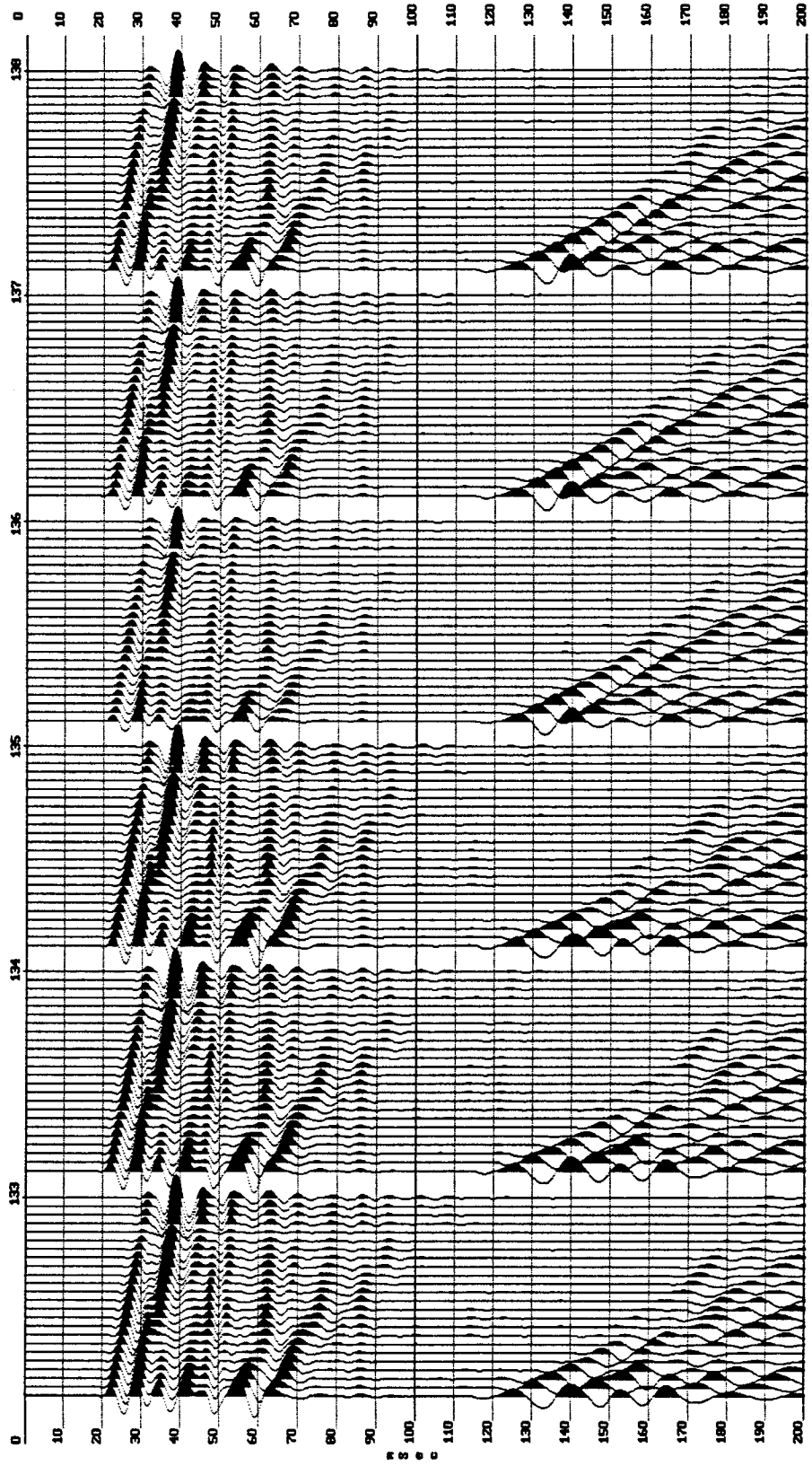
0
10
20
30
40
50
60
70
80
90
100
110
120
130
140
150
160
170
180
190
200
138
137
136
135
134
133
msec

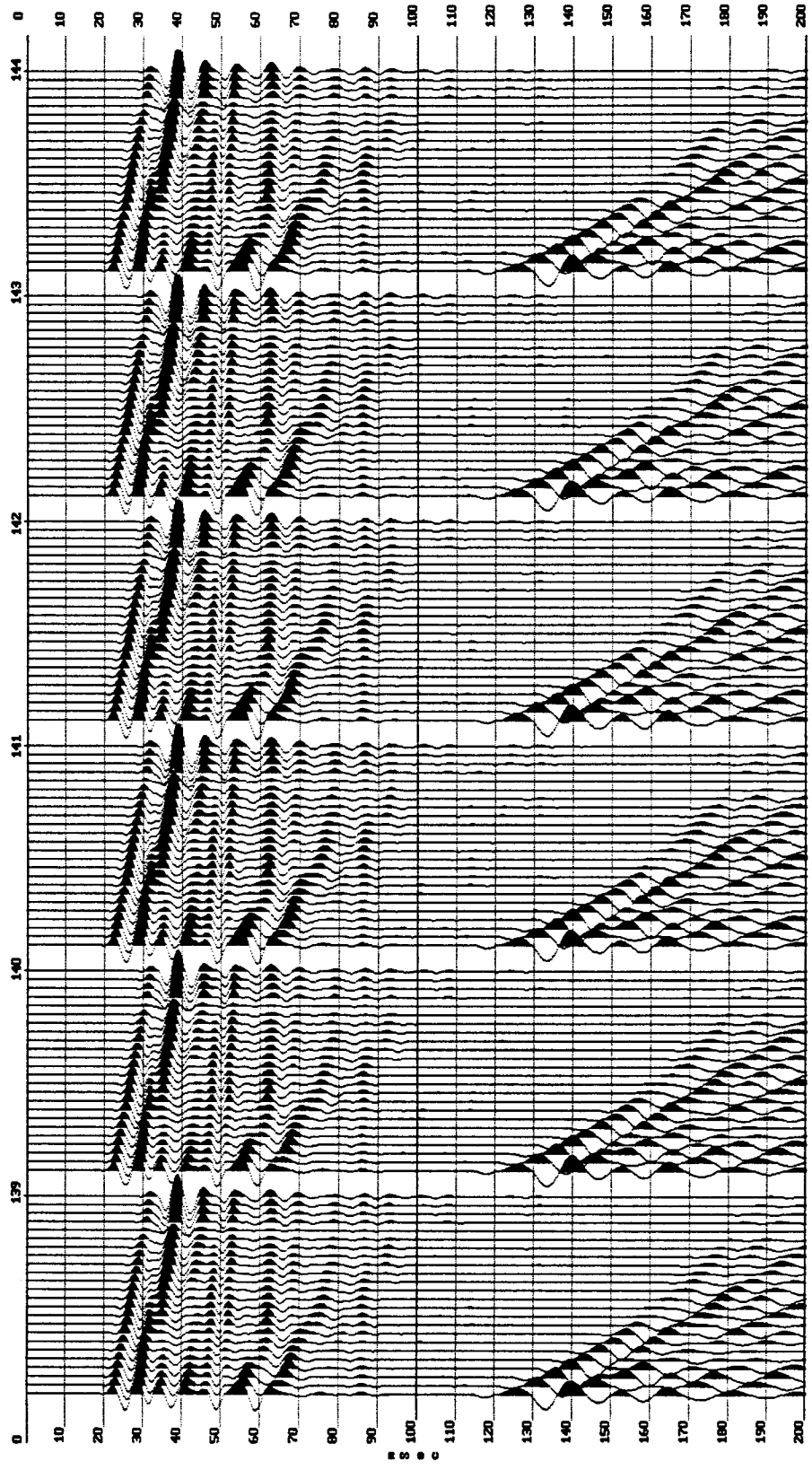
msec

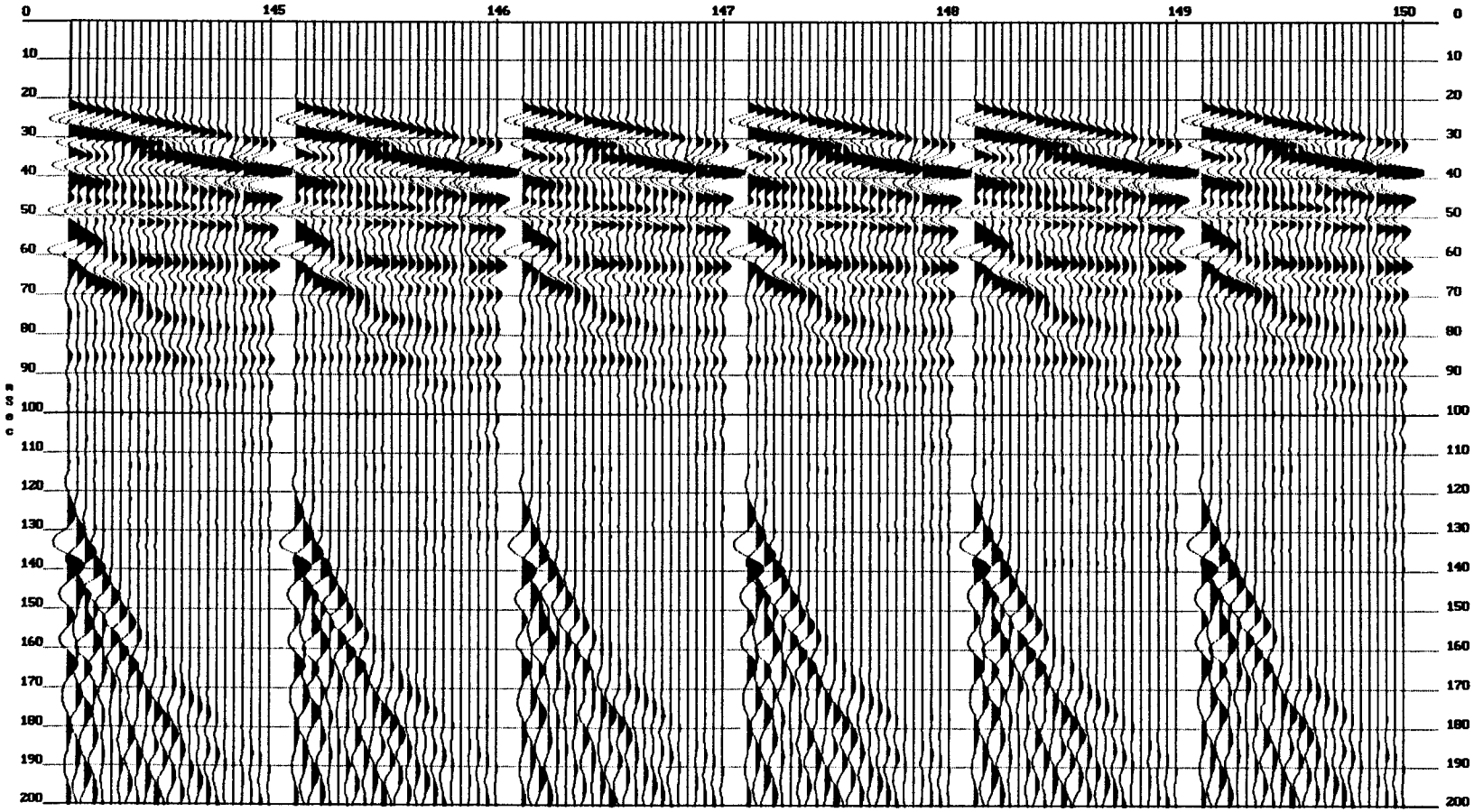
0
145
146
147
148
149
150
msec
10
20
30
40
50
60
70
80
90
100
110
120
130
140
150
160
170
180
190
200

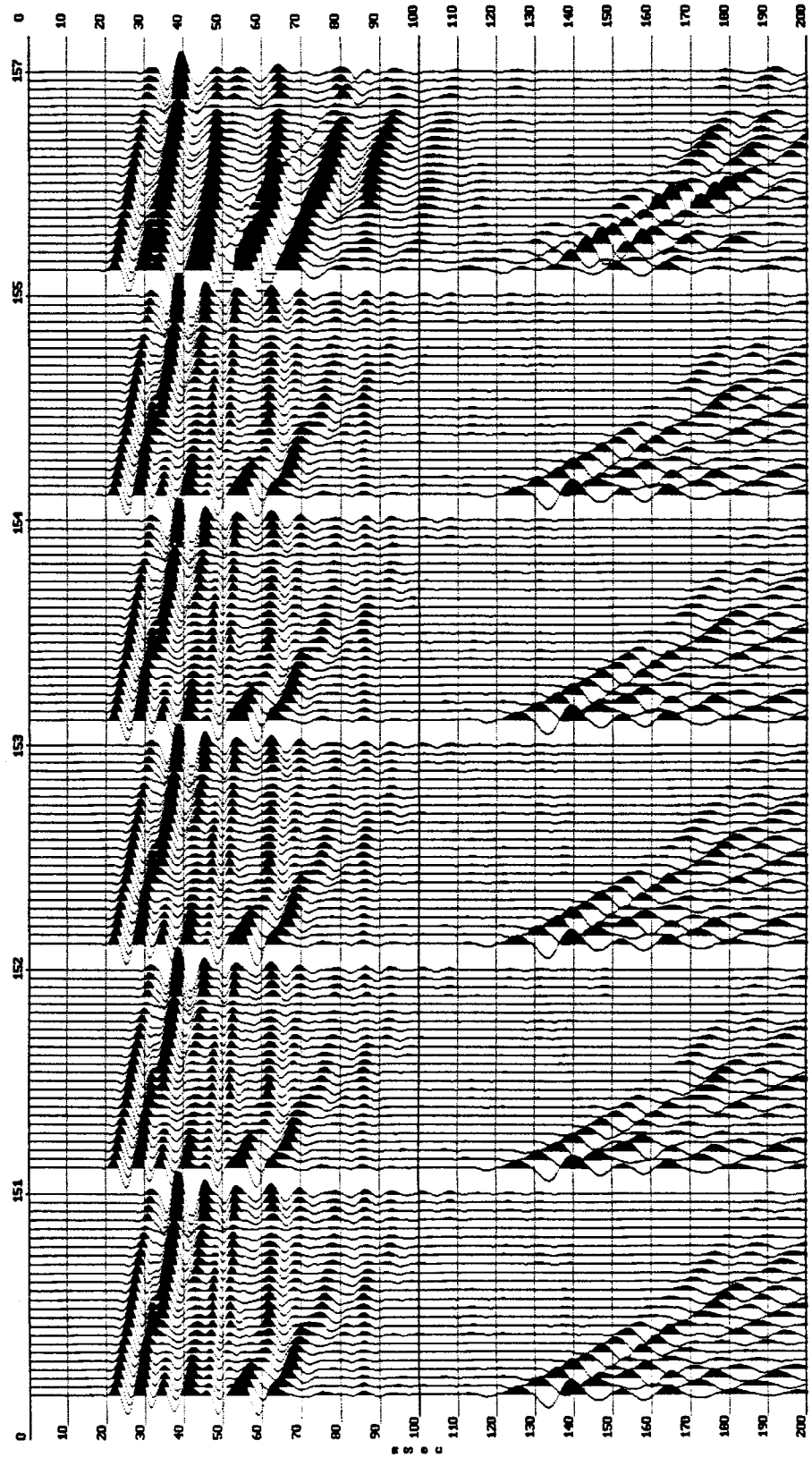
0
10
20
30
40
50
60
70
80
90
100
110
120
130
140
150
160
170
180
190
200
157
155
154
153
152
151
msec

Appendix E Sandpit Seismic Data

Field files from the Sandpit site, as they were collected. Data are roughly organized according to source energy. The data are shown in amplitude adjusted form; no trace normalization or AGC scaling has been performed. The gains are constant for these data: channels 1-13=94 dB, channels 14-24=98 dB. A general feel for signal changes associated with source parameters can be obtained from these plots. Symbology is the same as that used in Appendix D.

Key for plate mass:

A=2.7 kg, 548 cm^2
B=10.9 kg, 548 cm^2
C=1.4 kg, 274 cm^2
D=2.7 kg, 274 cm^2
E=5.4 kg, 274 cm^2
F=10.9 kg, 274 cm^2
G=21.8 kg, 274 cm^2
H*=1.8 kg, 274 cm^2
I=2.7 kg, 137 cm^2
J=10.9 kg, 137 cm^2
K=5.4 kg, 0.48 m length, Auger Flight
L=10.9 kg, 0.78 m length, Auger Flight
M=10.9 kg, 0.9 m length, Downhole Plate

Key for Impact Mass (Combined hammer mass and extension mass, measured at impact with a scale):

N=5.0 kg
O=7.7 kg
P=10.4 kg
Q=12.7 kg
R= 30.06 Downhole Rifle
S=Manual Swing (Human)

Key for Impact Velocity:

T=5.5 m/s
U=8.5 m/s

Format for description:
File #, Plate Parameters, Impact Mass, Impact Velocity (Comments if needed)

File 3, B, O, U.
File 4, A, O, U.
File 5, B, O, U.
File 6, C, O, U.
File 7, D, O, U.
File 8, E, O, U.
File 9, F, O, U.
File 10, G, O, U.
File 11, H, O, U.
File 12, I, O, U.
File 13, J, O, U.
File 14, NP, O, U.
File 15, A, P, U.
File 16, B, P, U.
File 17, C, P, U.
File 18, D, P, U.
File 19, E, P, U.
File 20, F, P, U.
File 21, G, P, U.
File 22, H, P, U.(Air plane noise)
File 23, H, P, U.
File 24, I, P, U.
File 25, J, P, U.
File 26, NP, P, U.

File 27, A, Q, U.
File 28, B, Q, U.
File 29, C, Q, U.
File 30, D, Q, U.
File 31, E, Q, U. (Bounced)
File 32, E, Q, U.
File 33, F, Q, U.
File 34, G, Q, U.
File 35, H, Q, U.
File 36, I, Q, U.
File 37, J, Q, U.
File 38, NP, Q, U.

File 39, A, N, T. (Bounced)
File 40, A, N, T.
File 41, (Noise Test)
File 42, B, N, T.
File 43, D, N, T.
File 44, C, N, T.
File 45, E, N, T. (Train Noise)
File 46, F, N, T.
File 47, G, N, T.
File 48, H, N, T.
File 49, I, N, T.
File 50, J, N, T.
File 51, NP, N, T.

File 52, A, O, T.
File 53, B, O, T.
File 54, C, O, T.
File 55, D, O, T.
File 56, E, O, T.
File 57, F, O, T.
File 58, G, O, T.
File 59, H, O, T.
File 60, I, O, T.
File 61, J, O, T.
File 62, NP, O, T.

File 63, A, P, T.
File 64, B, P, T.
File 65, C, P, T.
File 66, D, P, T.
File 67, E, P, T.
File 68, F, P, T.
File 69, G, P, T.
File 70, H, P, T.
File 71, I, P, T.
File 72, J, P, T.
File 73, NP, P, T.

File 74, A, S. (5.4 kg)
File 75, A, S.
File 76, B, S.
File 77, C, S.
File 78, D, S.
File 79, E, S.
File 80, F, S.
File 81, G, S.
File 82, H, S.
File 83, I, S.
File 84, J, S.
File 85, NP, S.
File 86, I, S.

File 87, B, P, T. (Compaction)
File 88, B, P, T.
File 90, B, P, T.
File 91, B, P, T.
File 92, B, P, T.
File 93, B, P, T.
File 95, B, P, T.
File 96, B, P, T.
File 97, B, P, T.
File 98, B, P, T.
File 99, B, P, T.
File 100, B, P, T.
File 101, B, P, T.
File 102, B, P, T.
File 103, B, P, T.
File 104, B, P, T.
File 105, B, P, T.
File 106, B, P, T.
File 107, B, P, T.

File 108, F, P, T. (Compaction)
File 109, F, P, T.
File 110, F, P, T.
File 111, F, P, T.
File 112, F, P, T.
File 113, F, P, T.
File 114, F, P, T.
File 115, F, P, T.
File 116, F, P, T.
File 117, F, P, T.
File 118, F, P, T.
File 119, F, P, T.
File 120, F, P, T.
File 121, F, P, T.
File 122, F, P, T.
File 123, F, P, T.
File 124, F, P, T.
File 125, F, P, T.
File 126, F, P, T.
File 127, F, P, T.

File 128, J, P, T.(Compaction)
File 130, J, P, T.
File 131, J, P, T.
File 132, J, P, T.
File 133, J, P, T.
File 134, J, P, T.
File 135, J, P, T.
File 136, J, P, T.
File 137, J, P, T.
File 138, J, P, T.
File 139, J, P, T.
File 140, J, P, T.
File 141, J, P, T.
File 142, J, P, T.
File 143, J, P, T.
File 144, J, P, T.
File 145, J, P, T.
File 147, J, P, T.

File 148, R. (3rd Shot in Hole)
File 149, R. (1st Shot in Hole)
File 150, Dead Blow Hammer.(0.9 kg)
File 151, Steel Alloy Hammer (0.9 kg).
File 152, B, O, T. (Glancing Blow)
File 153, F, O, T. (Glancing Blow)
File 154, J, O, T. (Glancing Blow)

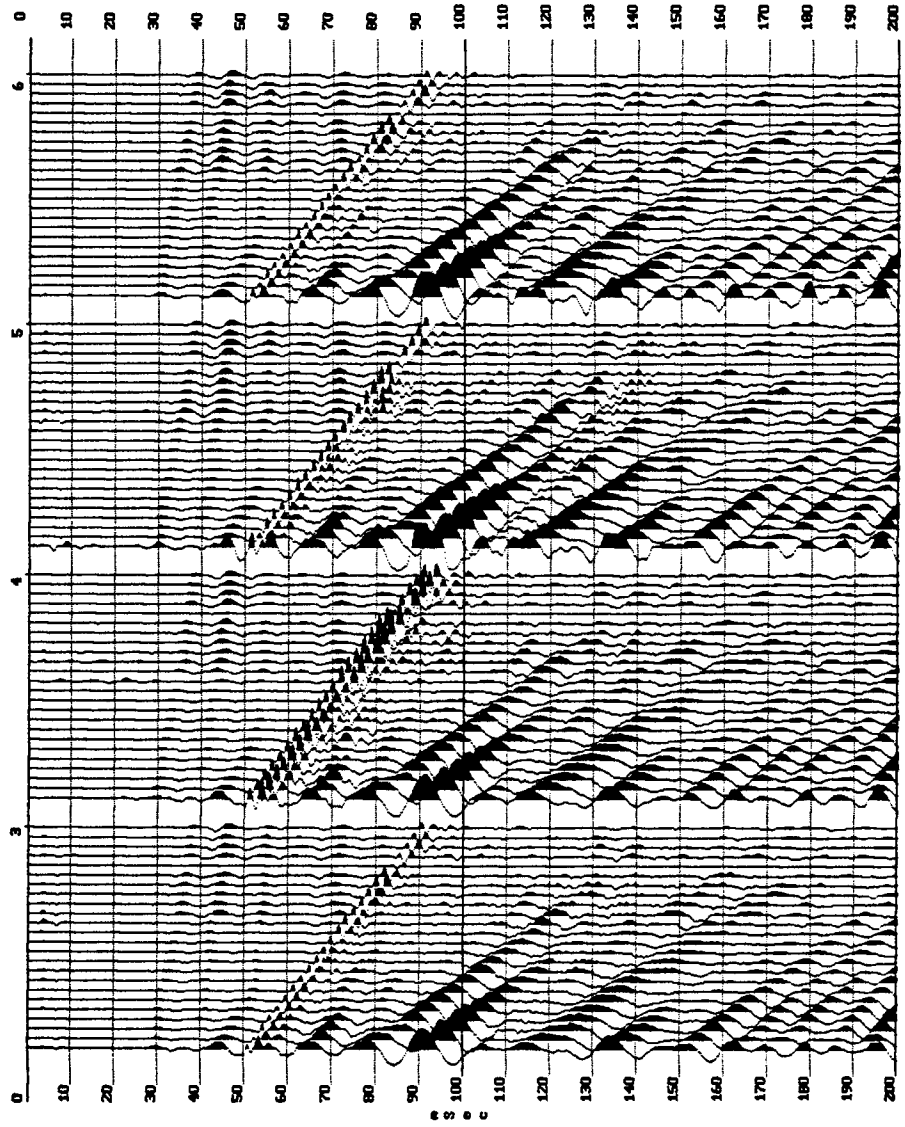
0
10
20
30
40
50
60
70
80
90
100
110
120
130
140
150
160
170
180
190
200
msec

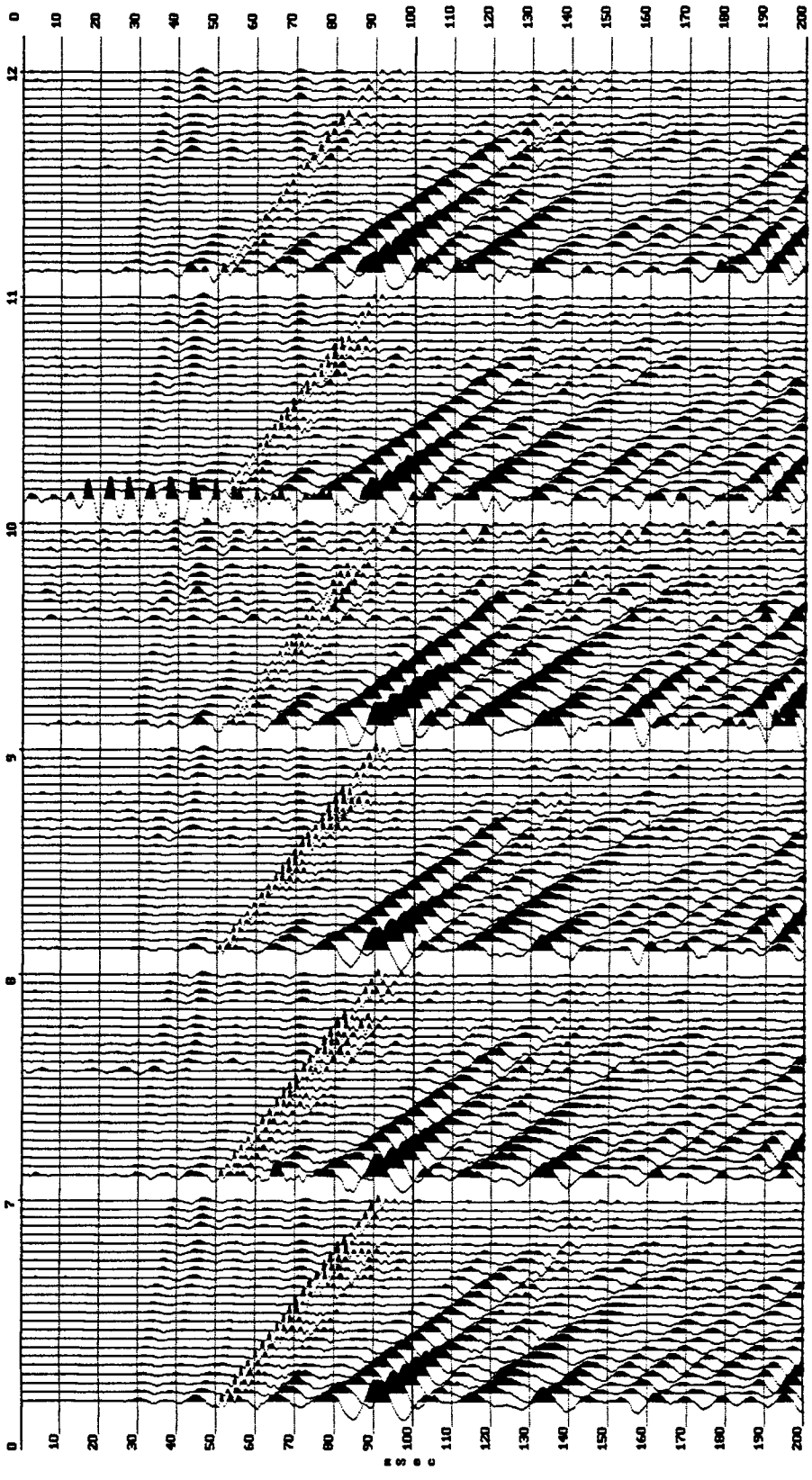
0
10
20
30
40
50
60
70
80
90
100
110
120
130
140
150
160
170
180
190
200
12
11
10
9
8
7
0
msec

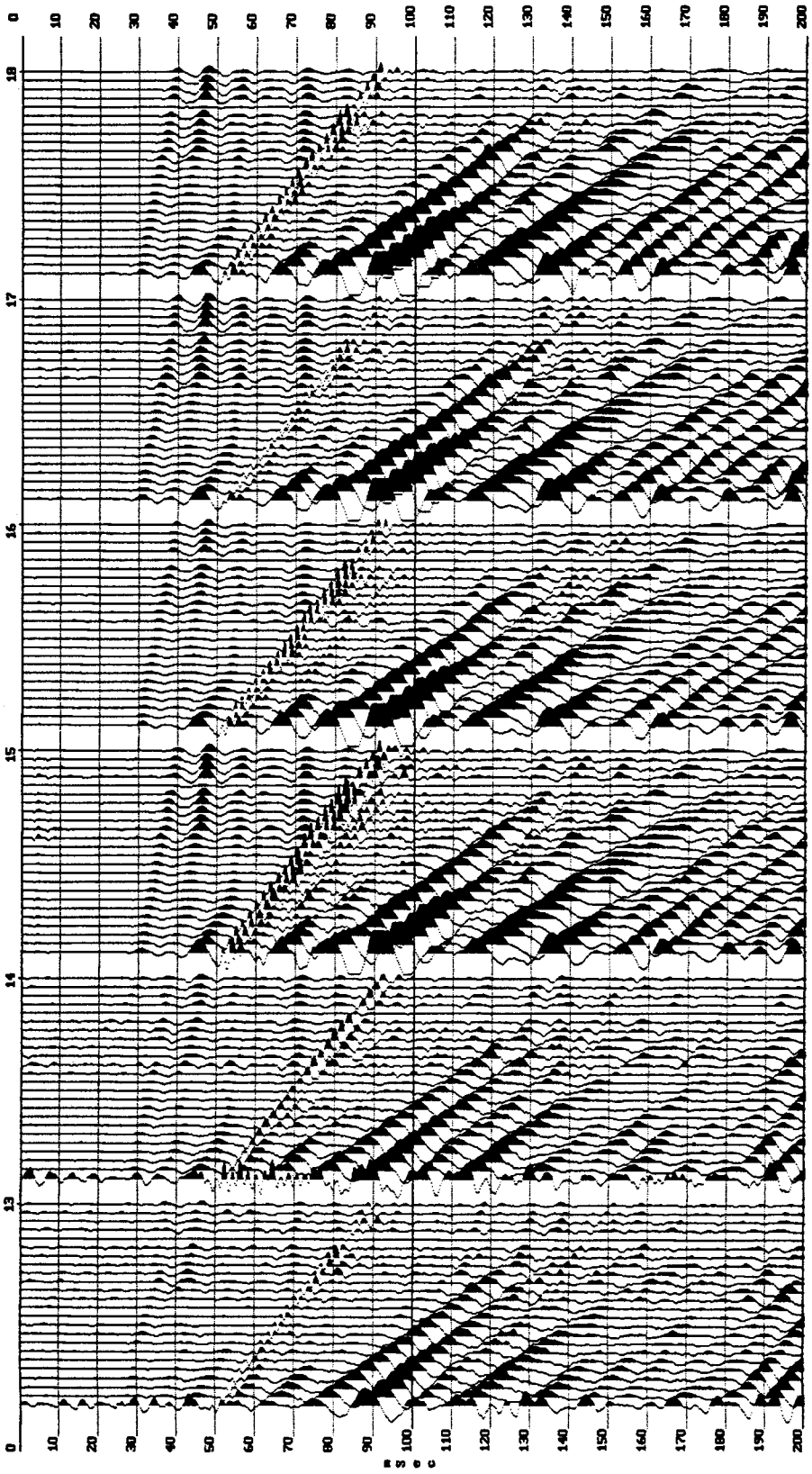
0
10
20
30
40
50
60
70
80
90
100
110
120
130
140
150
160
170
180
190
200
18
17
16
15
14
13
msec

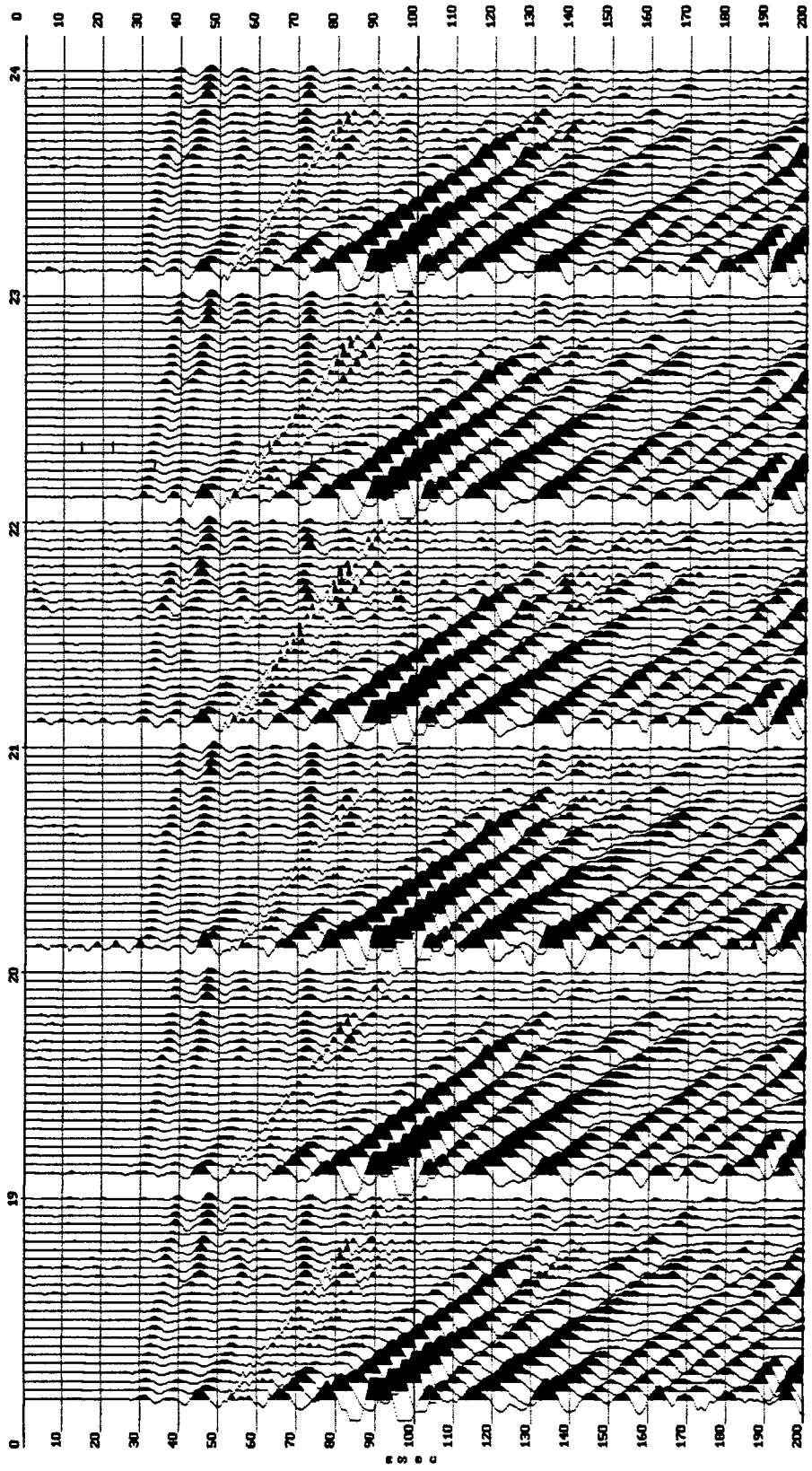
0
10
20
30
40
50
60
70
80
90
100
110
120
130
140
150
160
170
180
190
200
24
23
22
21
20
19
msec

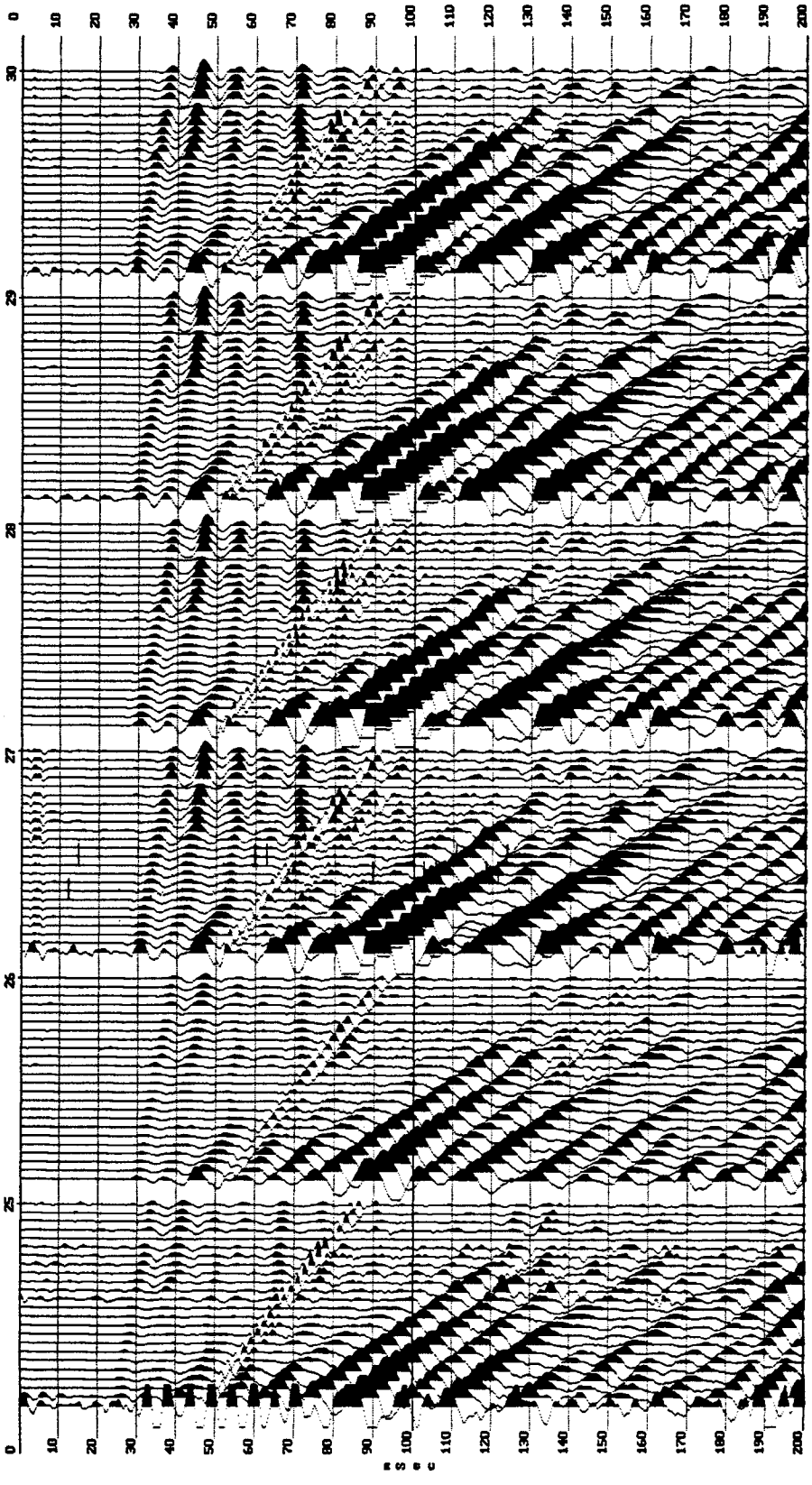
0
10
20
30
40
50
60
70
80
90
100
110
120
130
140
150
160
170
180
190
200
30
29
28
27
26
25
0
msec

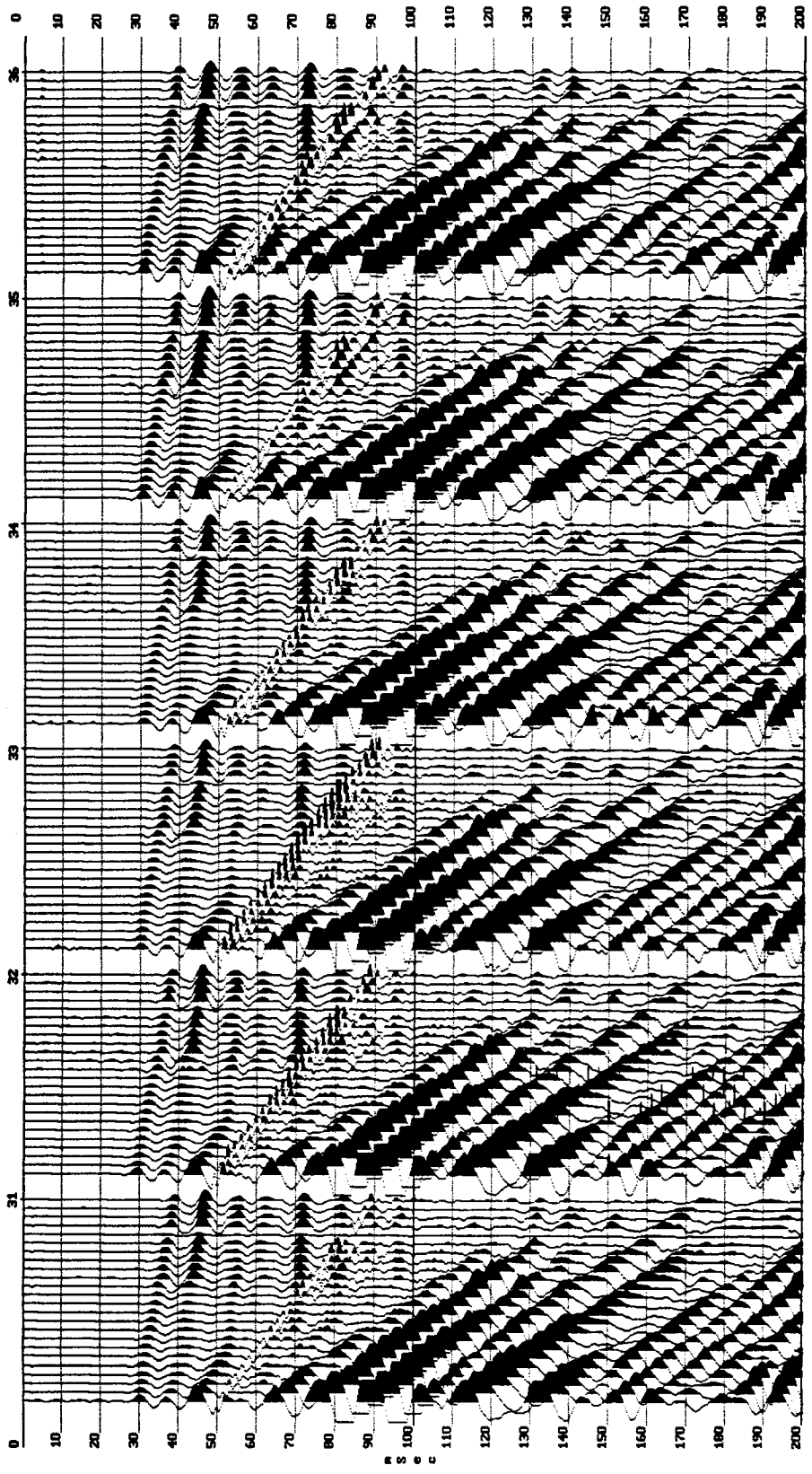
0
10
20
30
40
50
60
70
80
90
100
110
120
130
140
150
160
170
180
190
200
36
35
34
33
32
31
msec

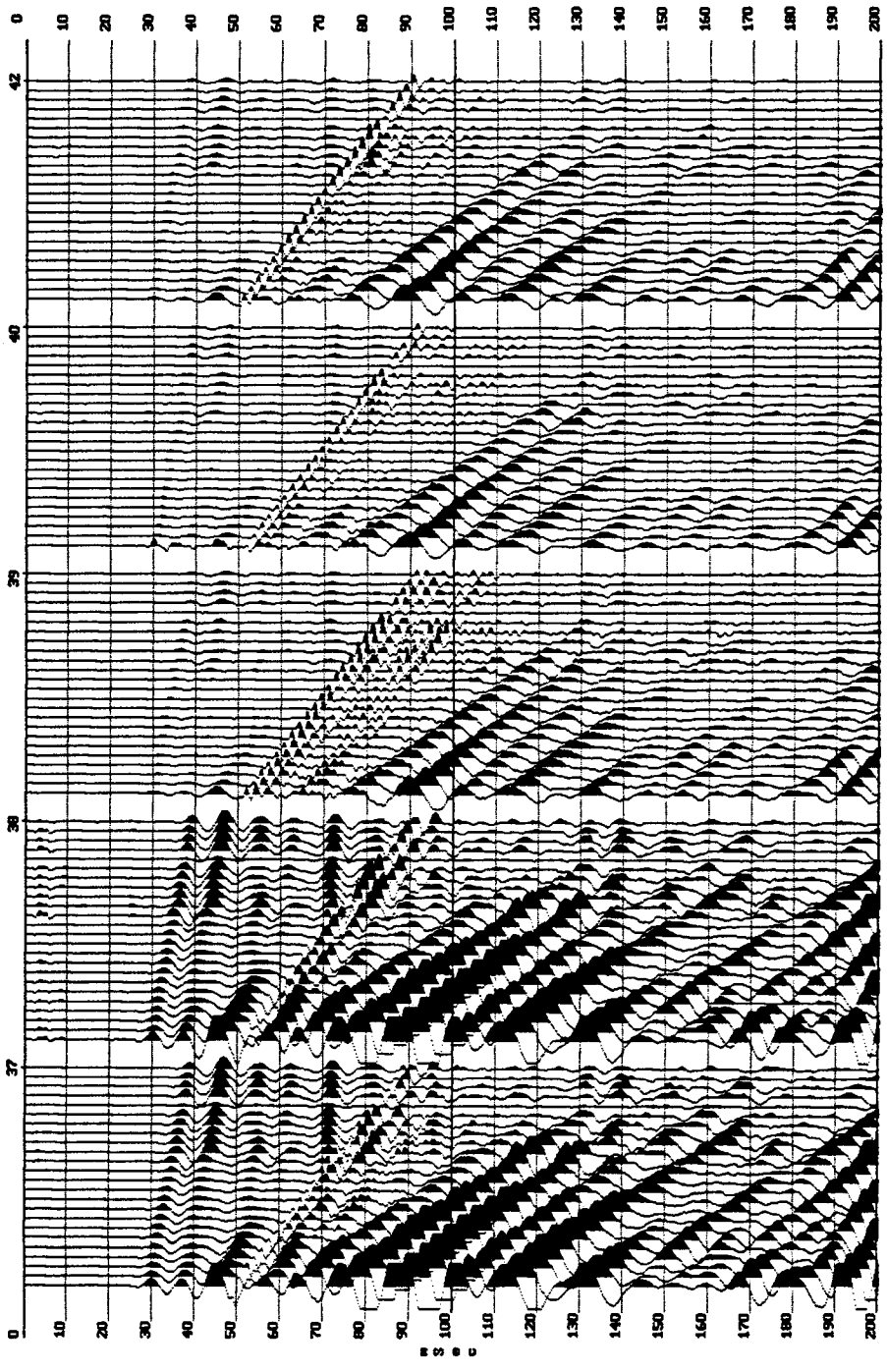
0
10
20
30
40
50
60
70
80
90
100
110
120
130
140
150
160
170
180
190
200
42
40
39
38
37
msec

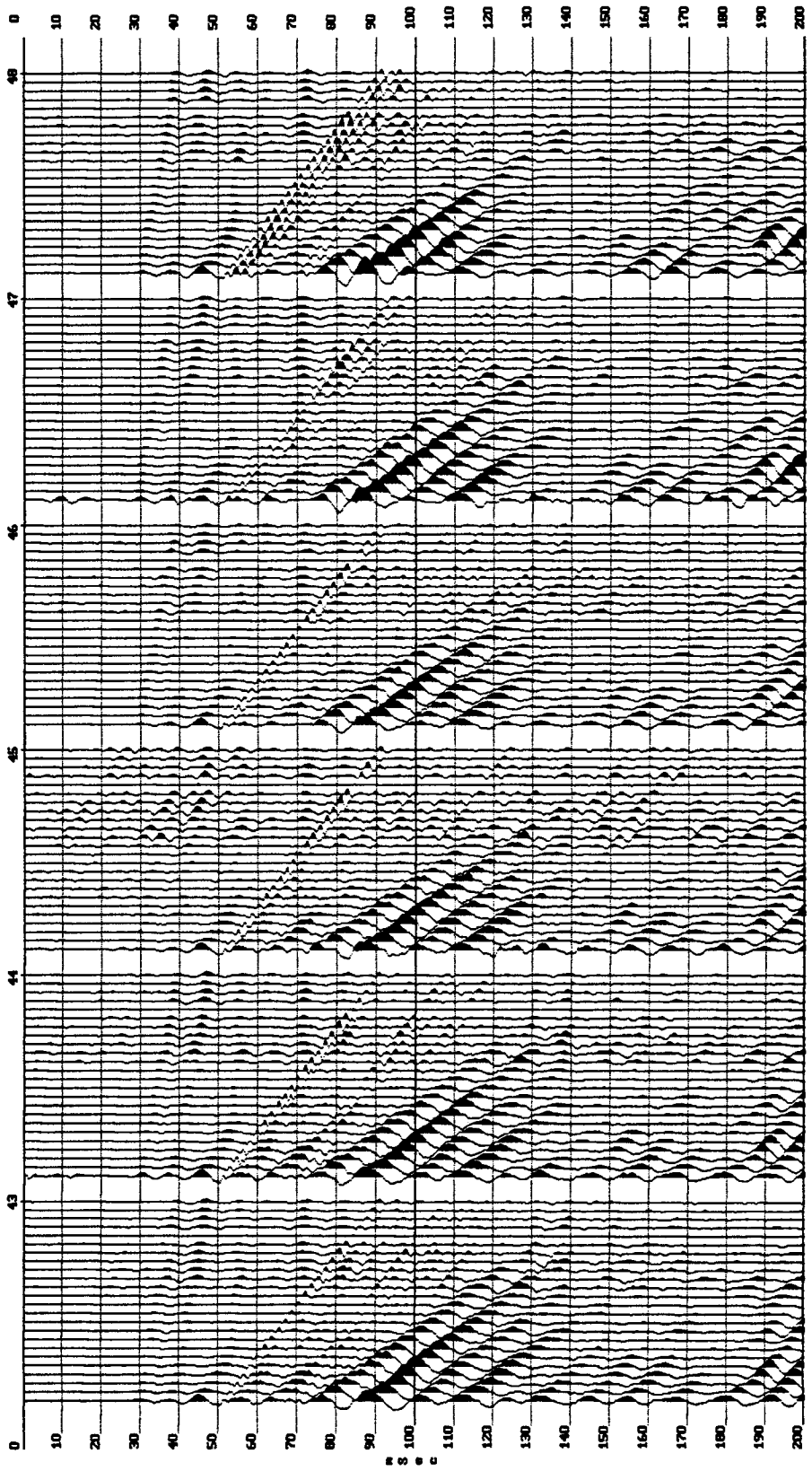
0
10
20
30
40
50
60
70
80
90
100
110
120
130
140
150
160
170
180
190
200
48
47
46
45
44
43
msec

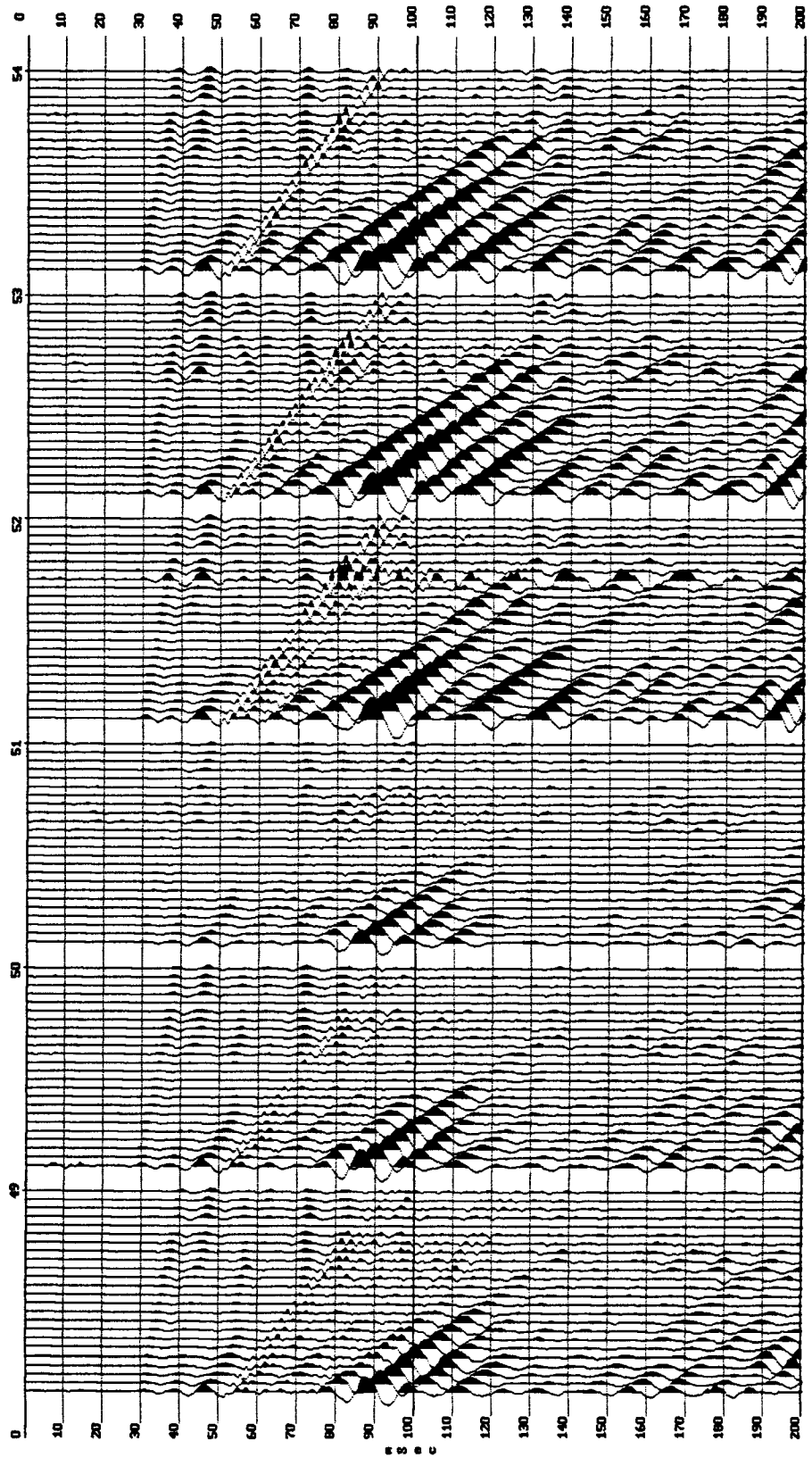
0
10
20
30
40
50
60
70
80
90
100
110
120
130
140
150
160
170
180
190
200
54
53
52
51
50
49
msec

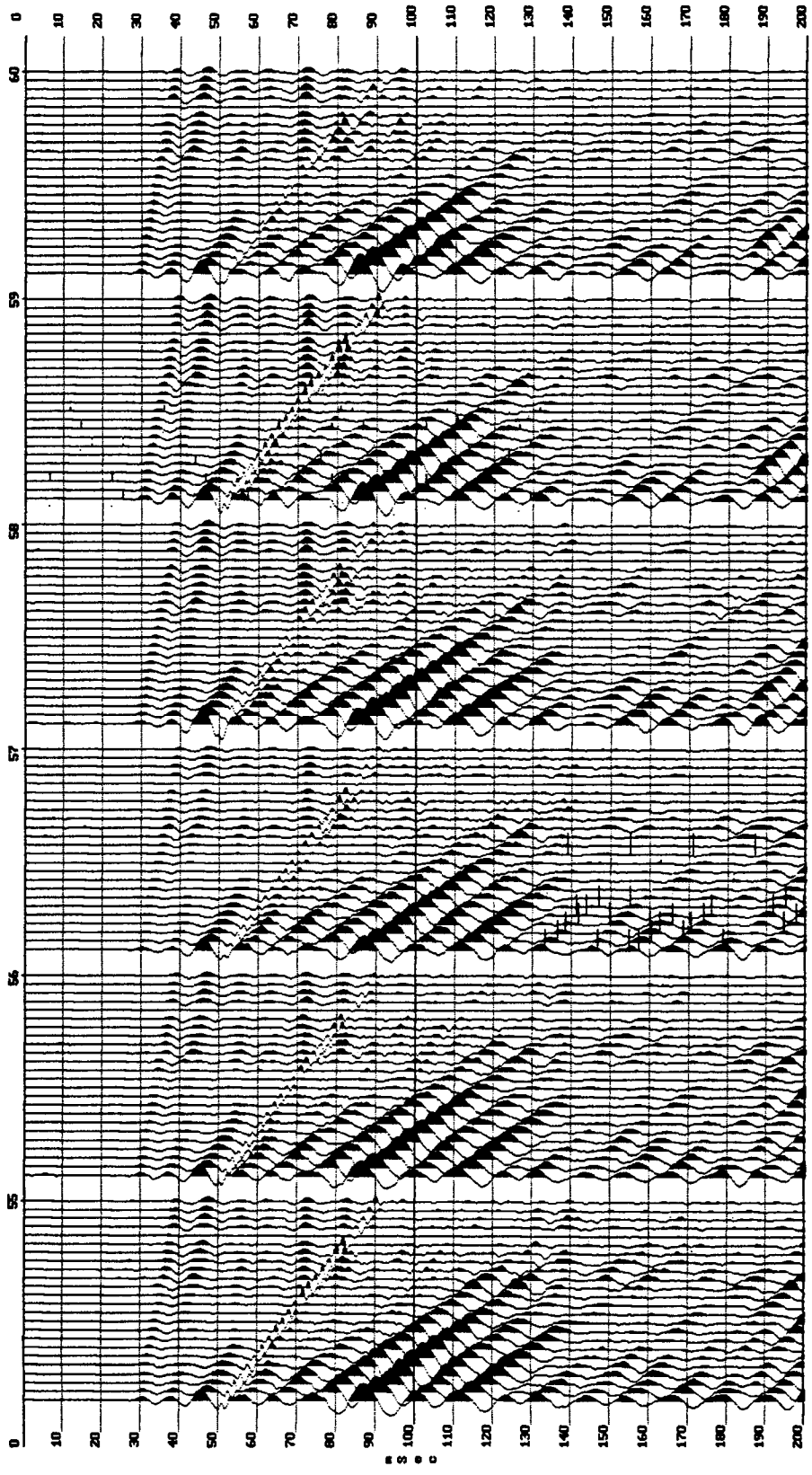
0
10
20
30
40
50
60
70
80
90
100
110
120
130
140
150
160
170
180
190
200
60
59
58
57
56
55
0
msec

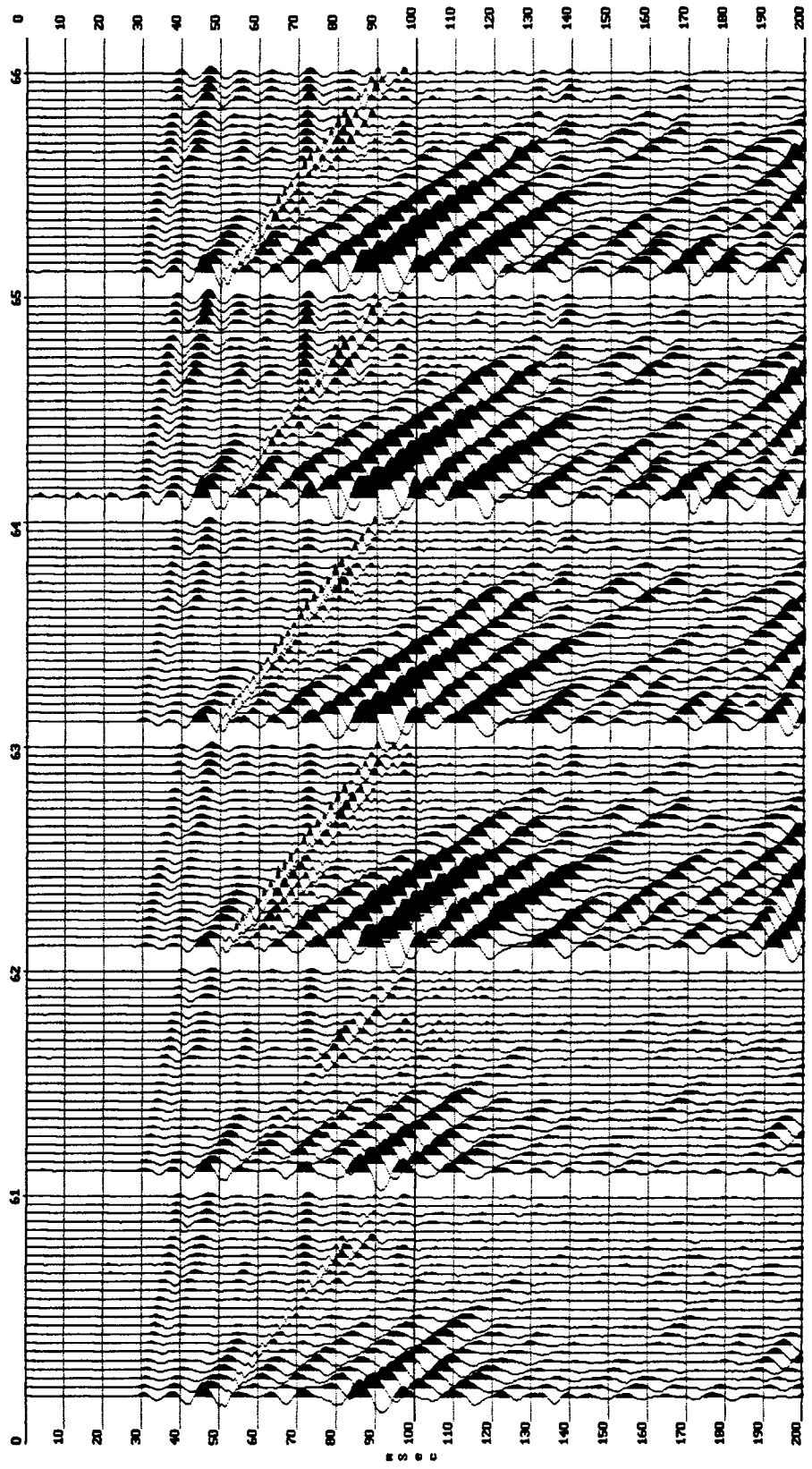
0
10
20
30
40
50
60
70
80
90
100
110
120
130
140
150
160
170
180
190
200
66
65
64
63
62
61
msec

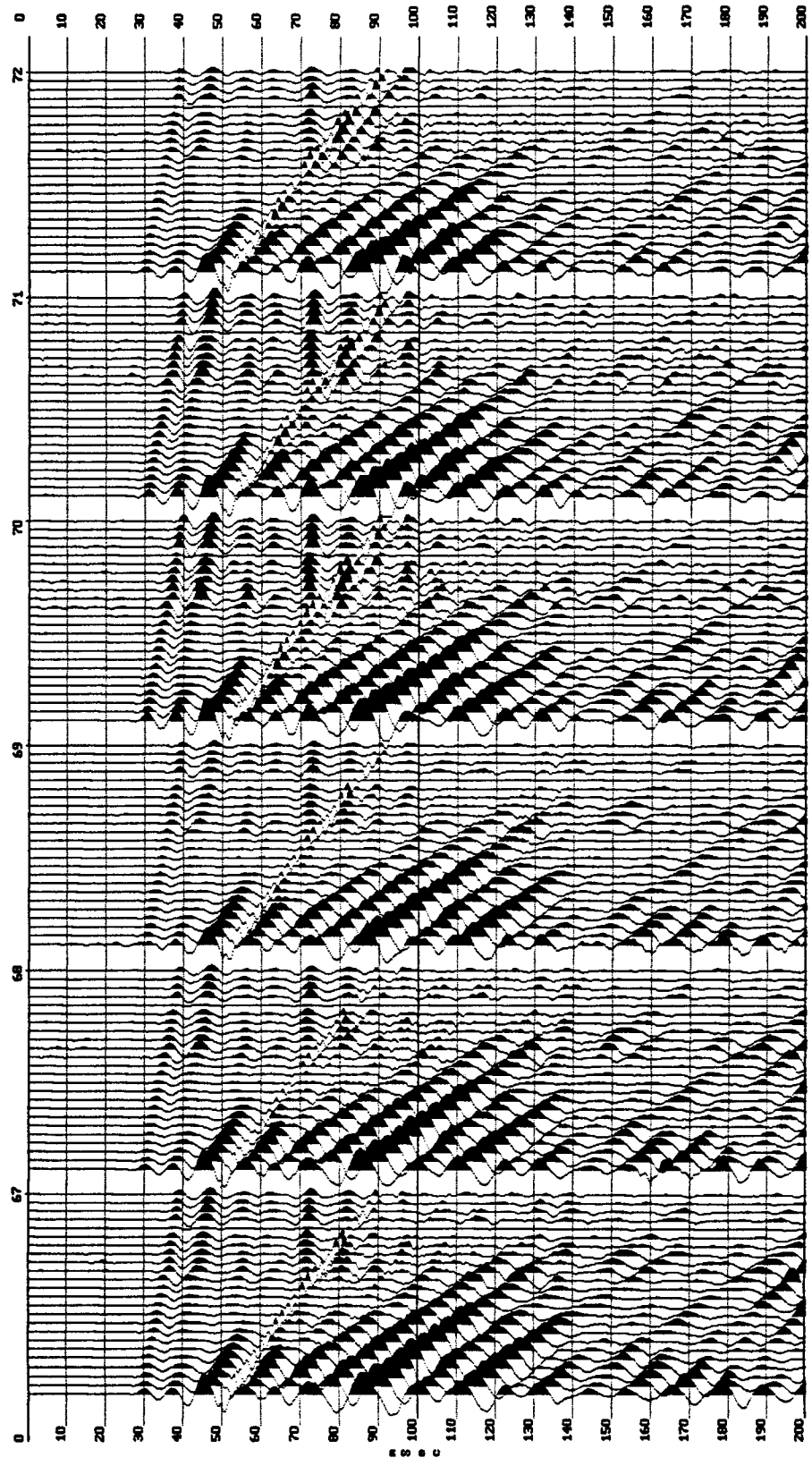
0
10
20
30
40
50
60
70
80
90
100
110
120
130
140
150
160
170
180
190
200
72
71
70
69
68
67
0

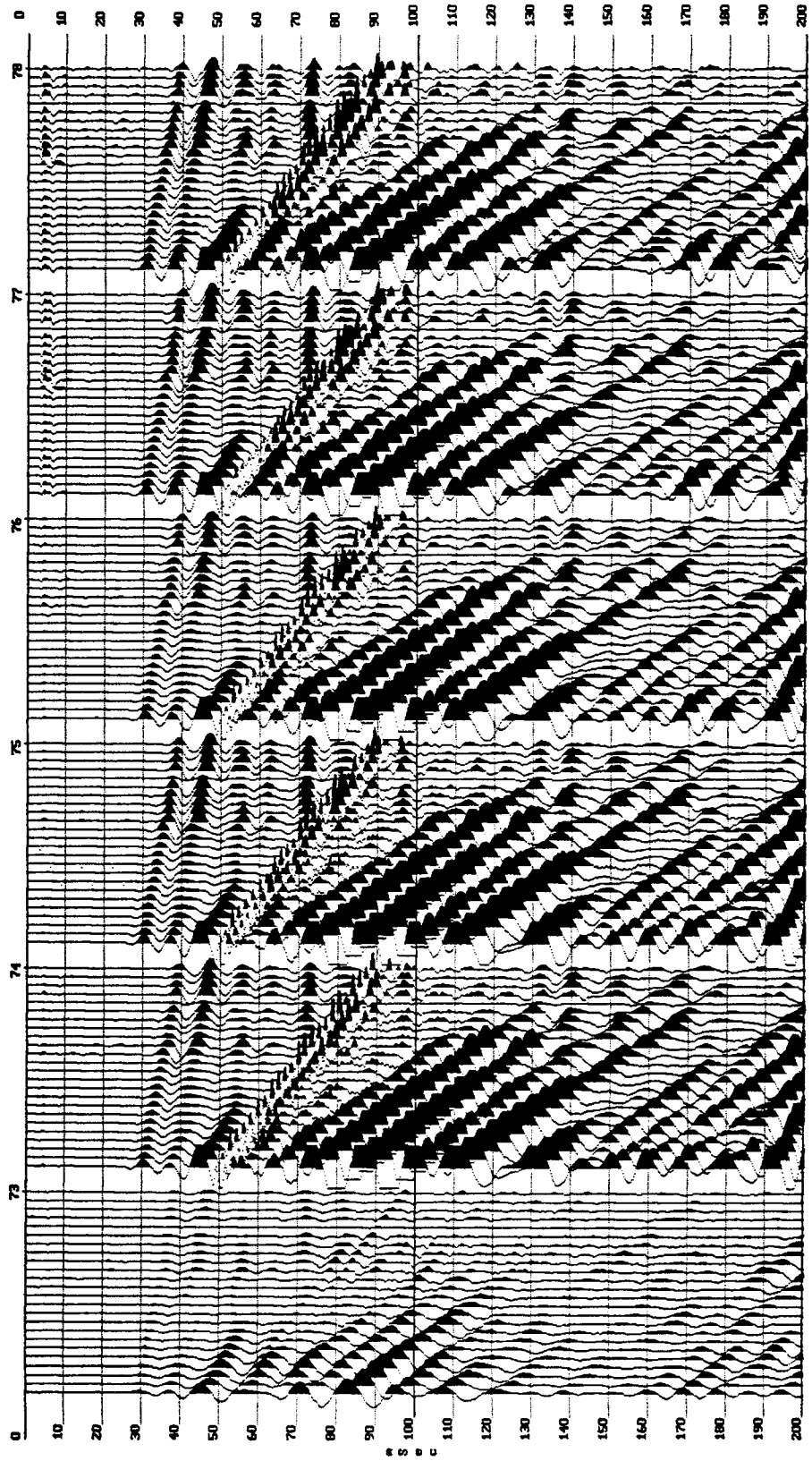
0
10
20
30
40
50
60
70
80
90
100
110
120
130
140
150
160
170
180
190
200
78
77
76
75
74
73
msec

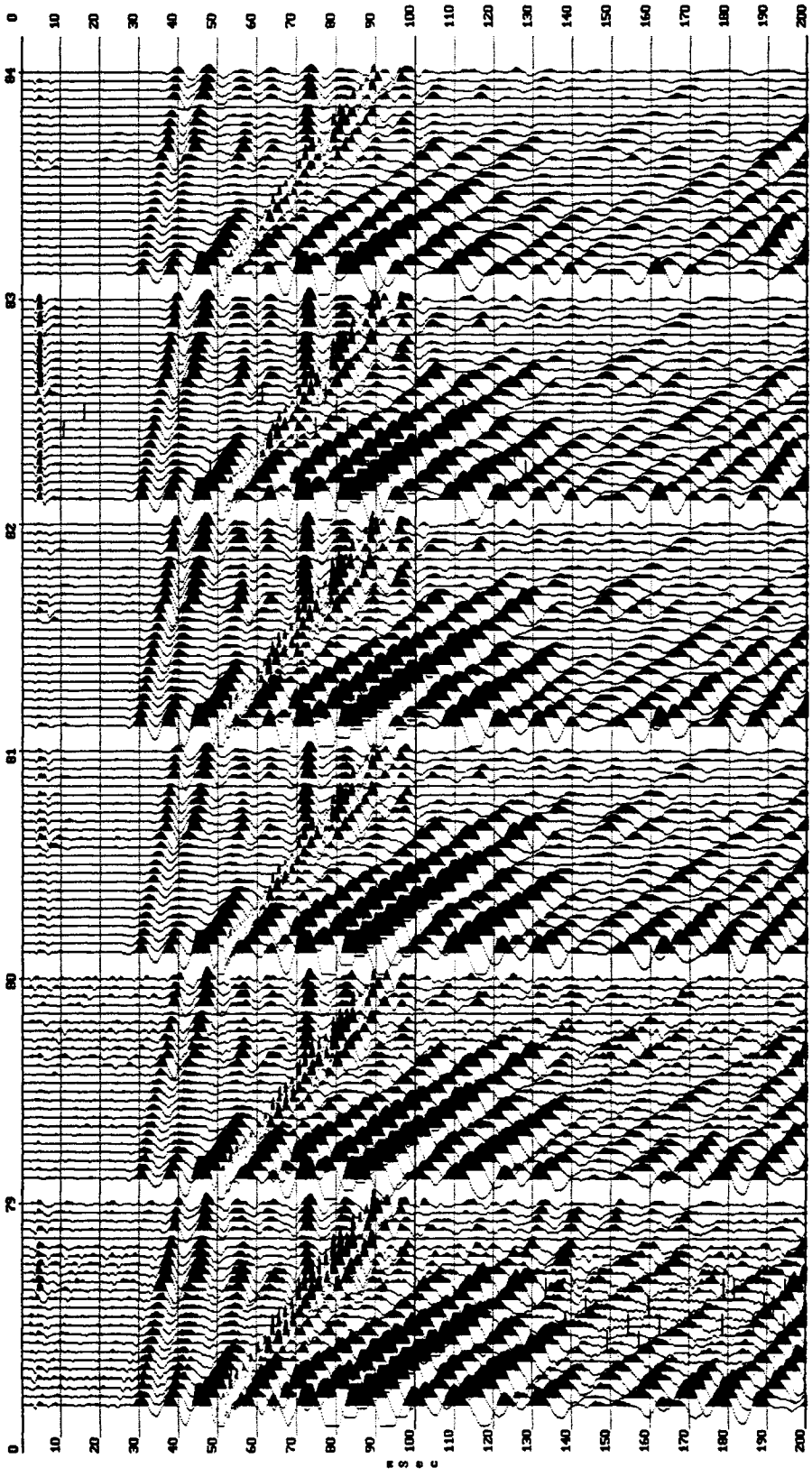
0
10
20
30
40
50
60
70
80
90
100
110
120
130
140
150
160
170
180
190
200
84
83
82
81
80
79
0
msec

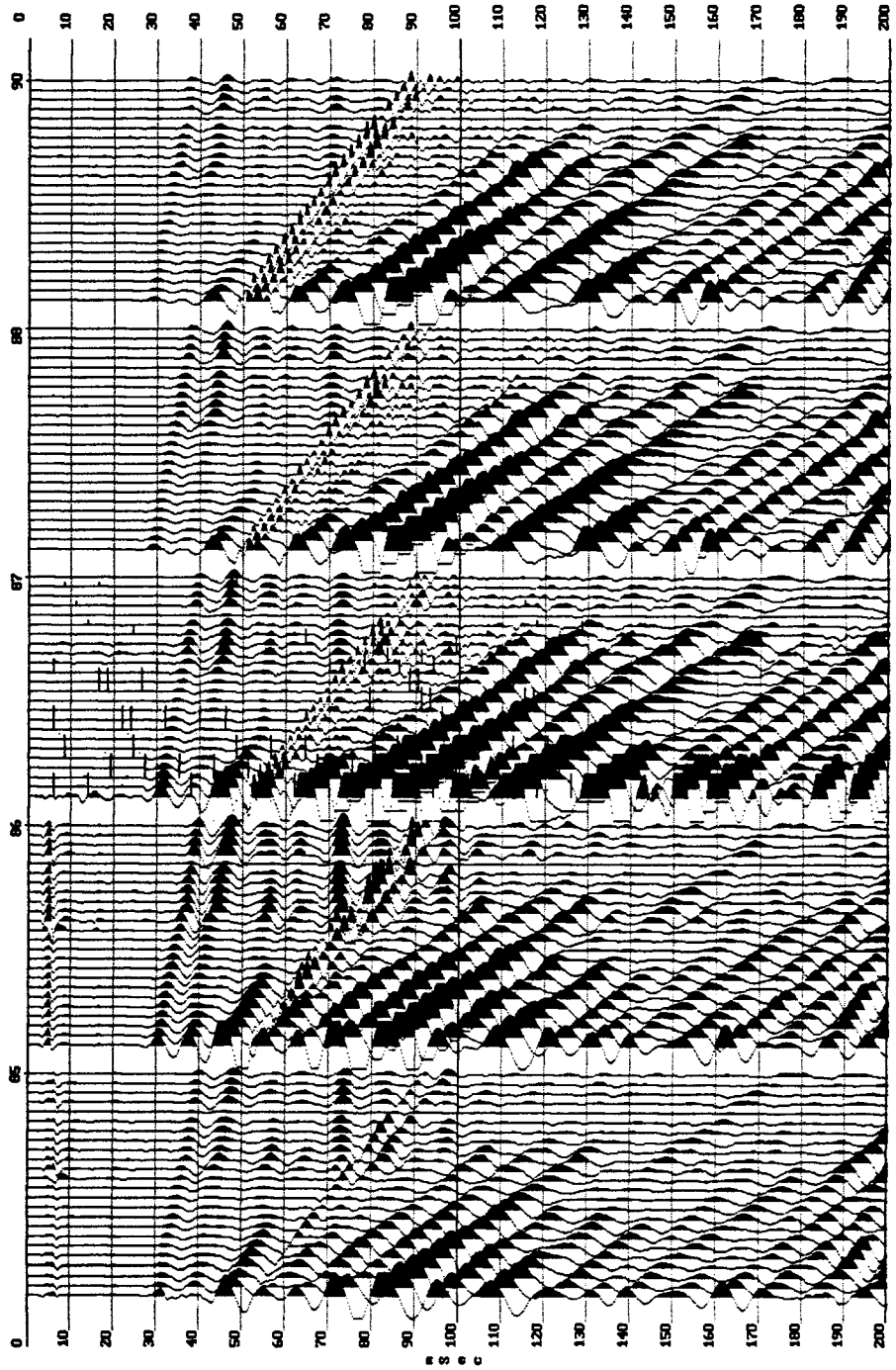
0
10
20
30
40
50
60
70
80
90
100
110
120
130
140
150
160
170
180
190
200
90
88
87
86
85
msec

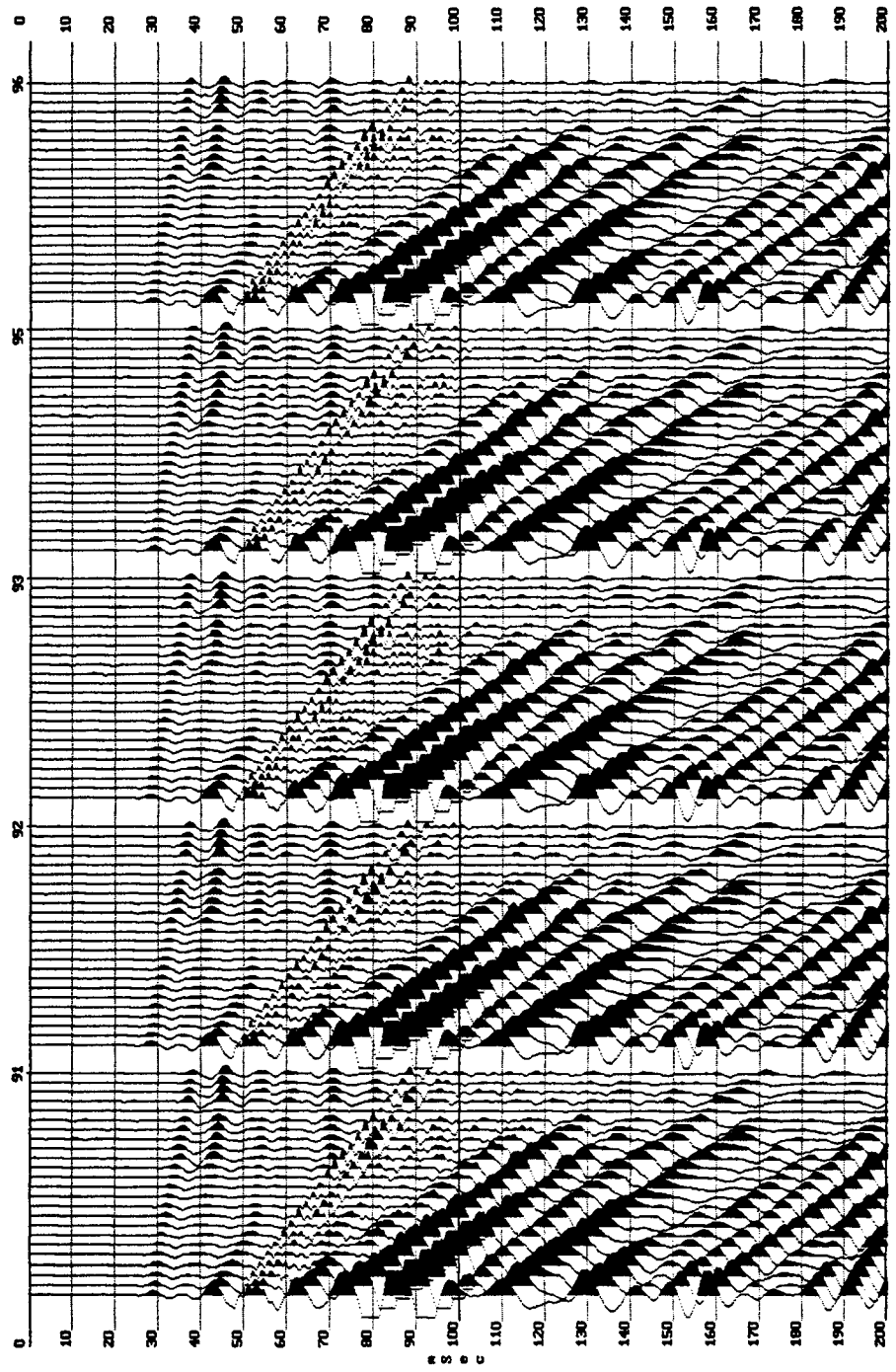
0
10
20
30
40
50
60
70
80
90
100
110
120
130
140
150
160
170
180
190
200
96
95
93
92
91
msec

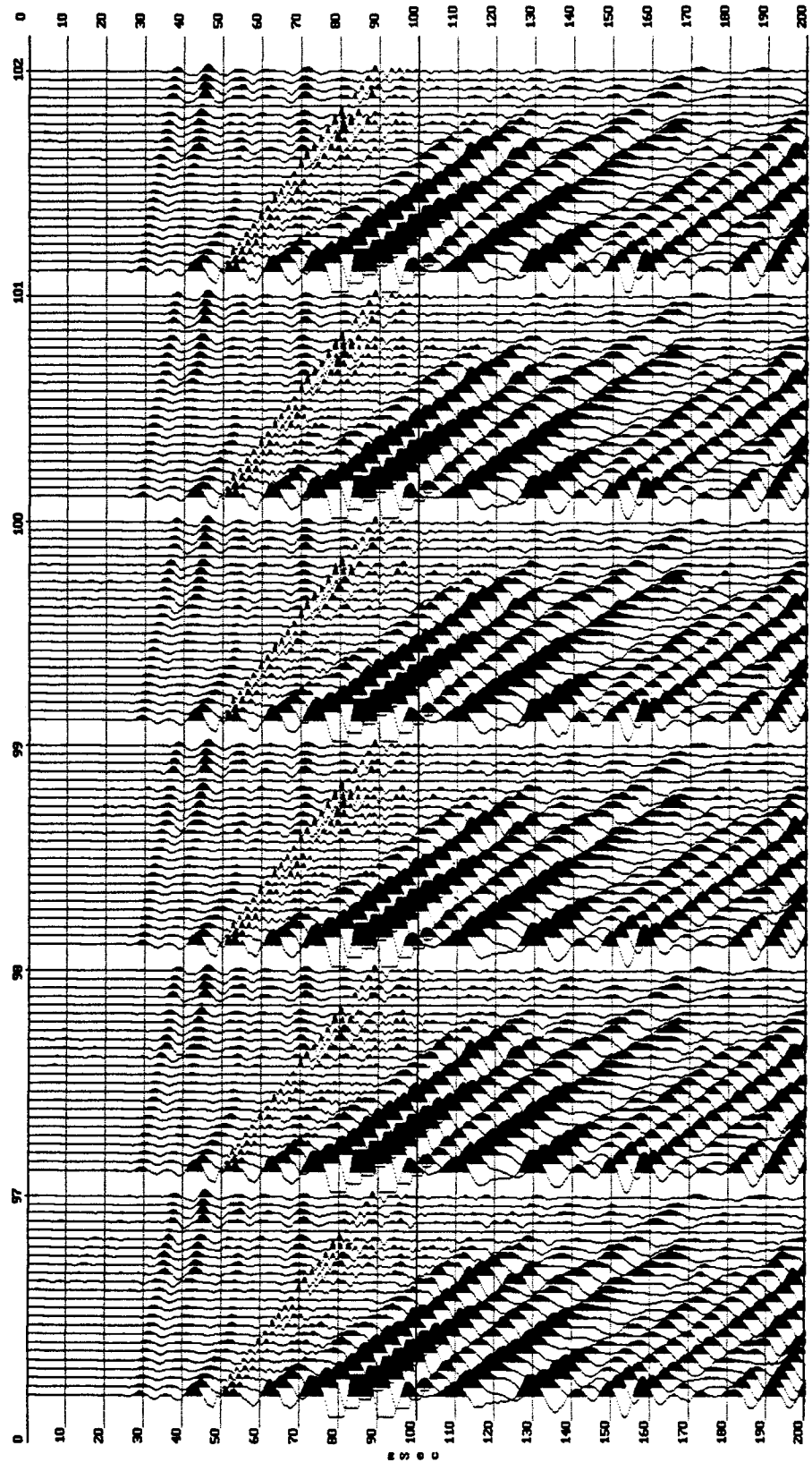
0
10
20
30
40
50
60
70
80
90
100
110
120
130
140
150
160
170
180
190
200
102
101
100
99
98
97
0
msec

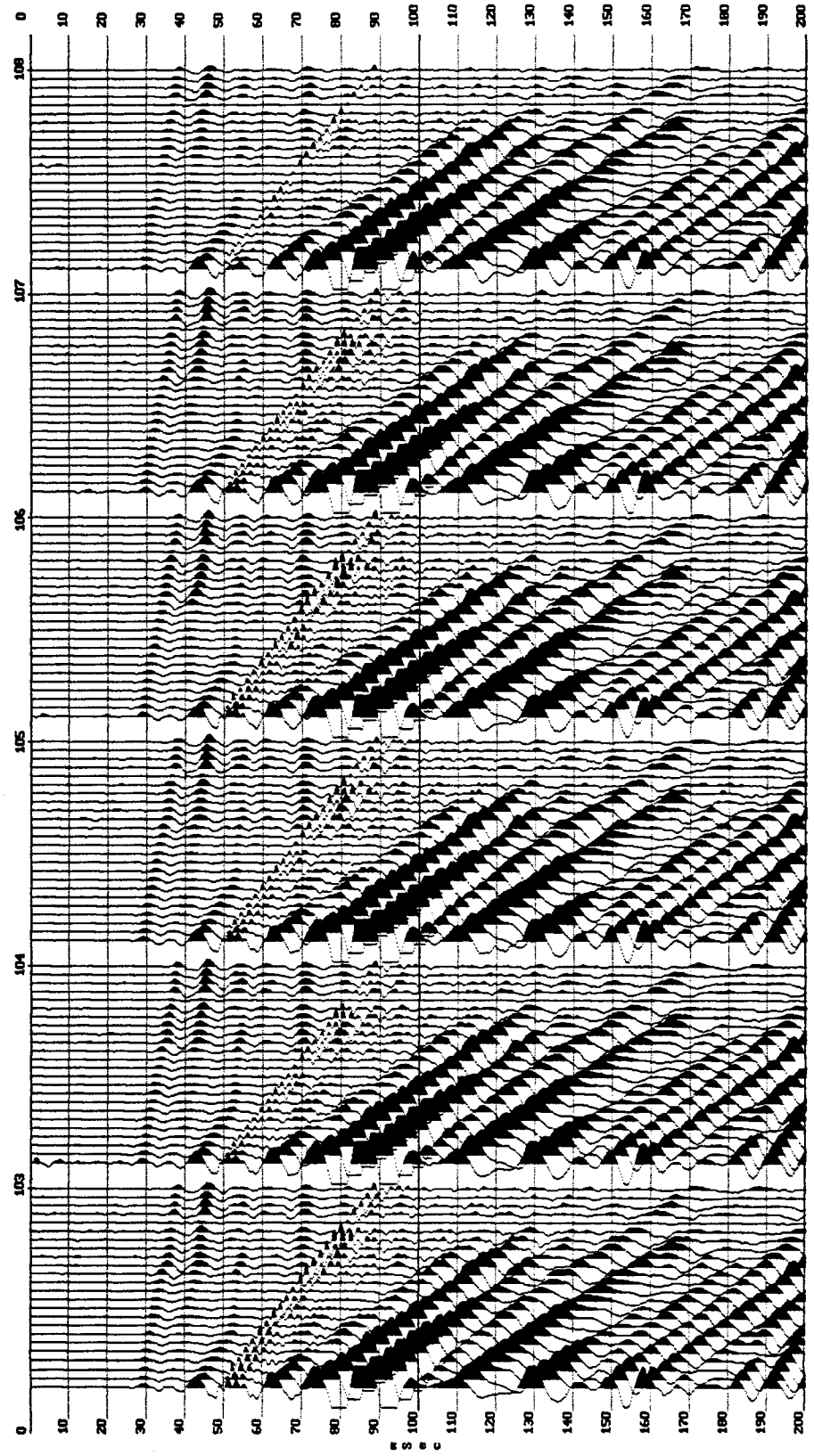
0
10
20
30
40
50
60
70
80
90
100
110
120
130
140
150
160
170
180
190
200
108
107
106
105
104
103
msec

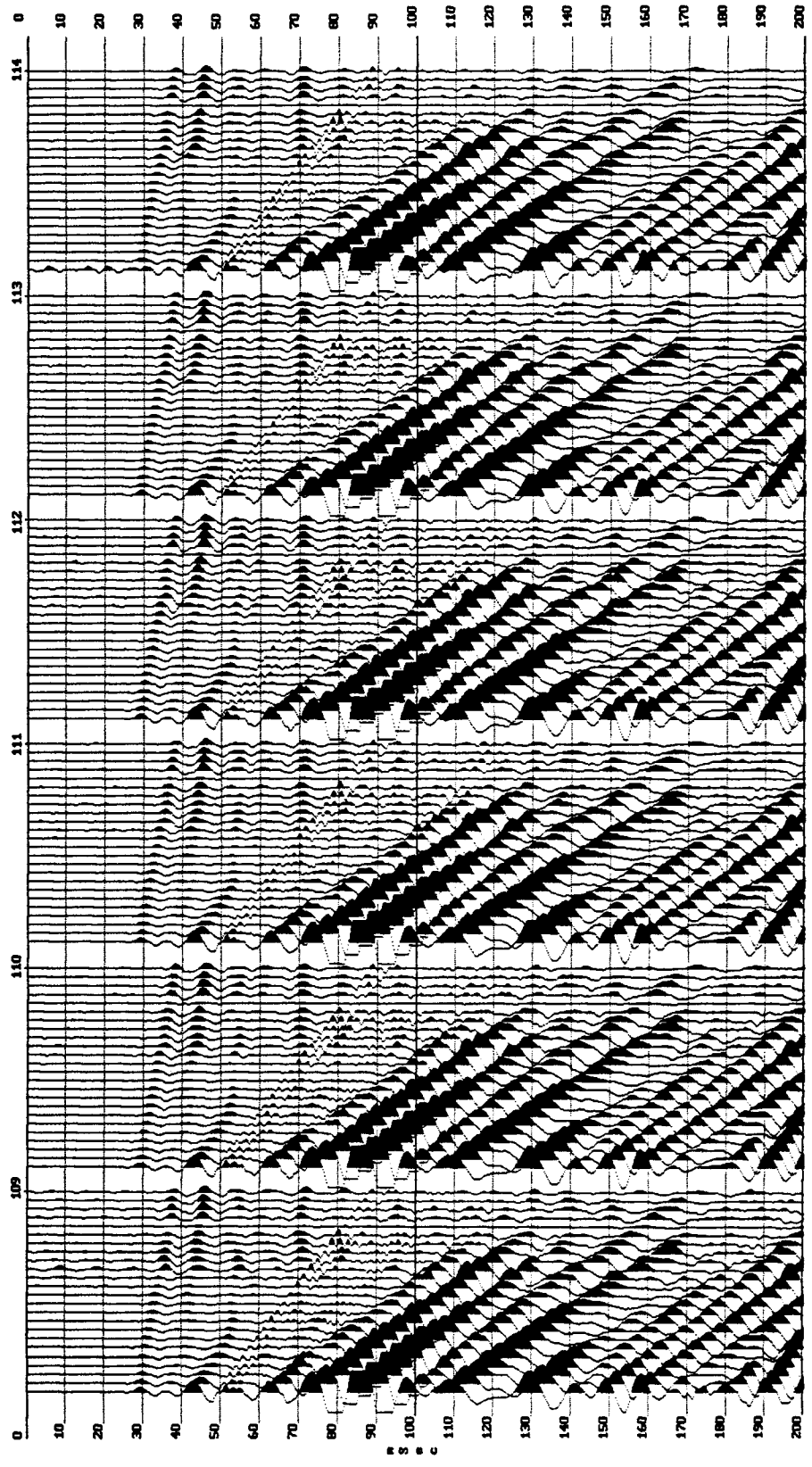
0
10
20
30
40
50
60
70
80
90
100
110
120
130
140
150
160
170
180
190
200
114
113
112
111
110
109
0
msec

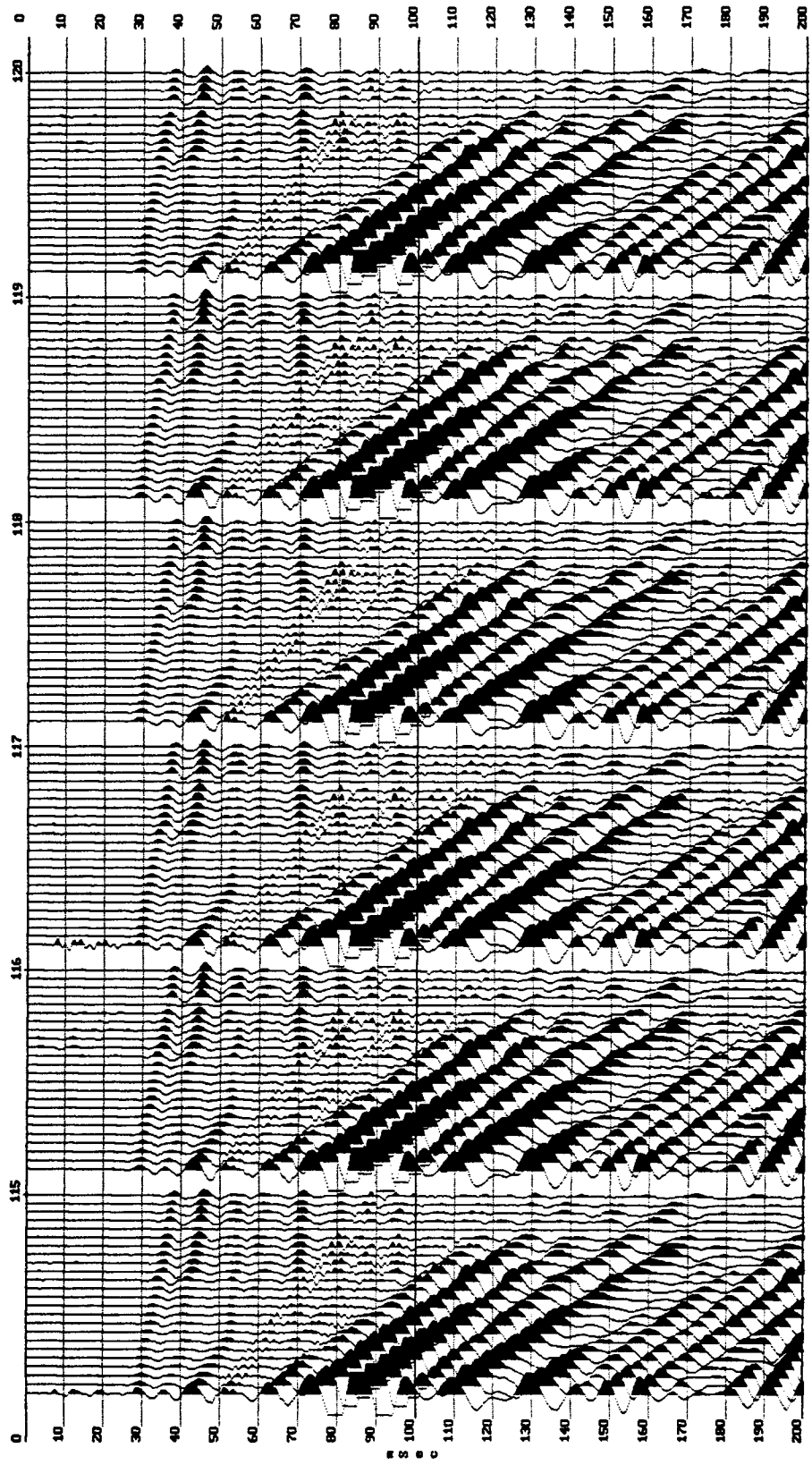
0
10
20
30
40
50
60
70
80
90
100
110
120
130
140
150
160
170
180
190
200
120
119
118
117
116
115
msec

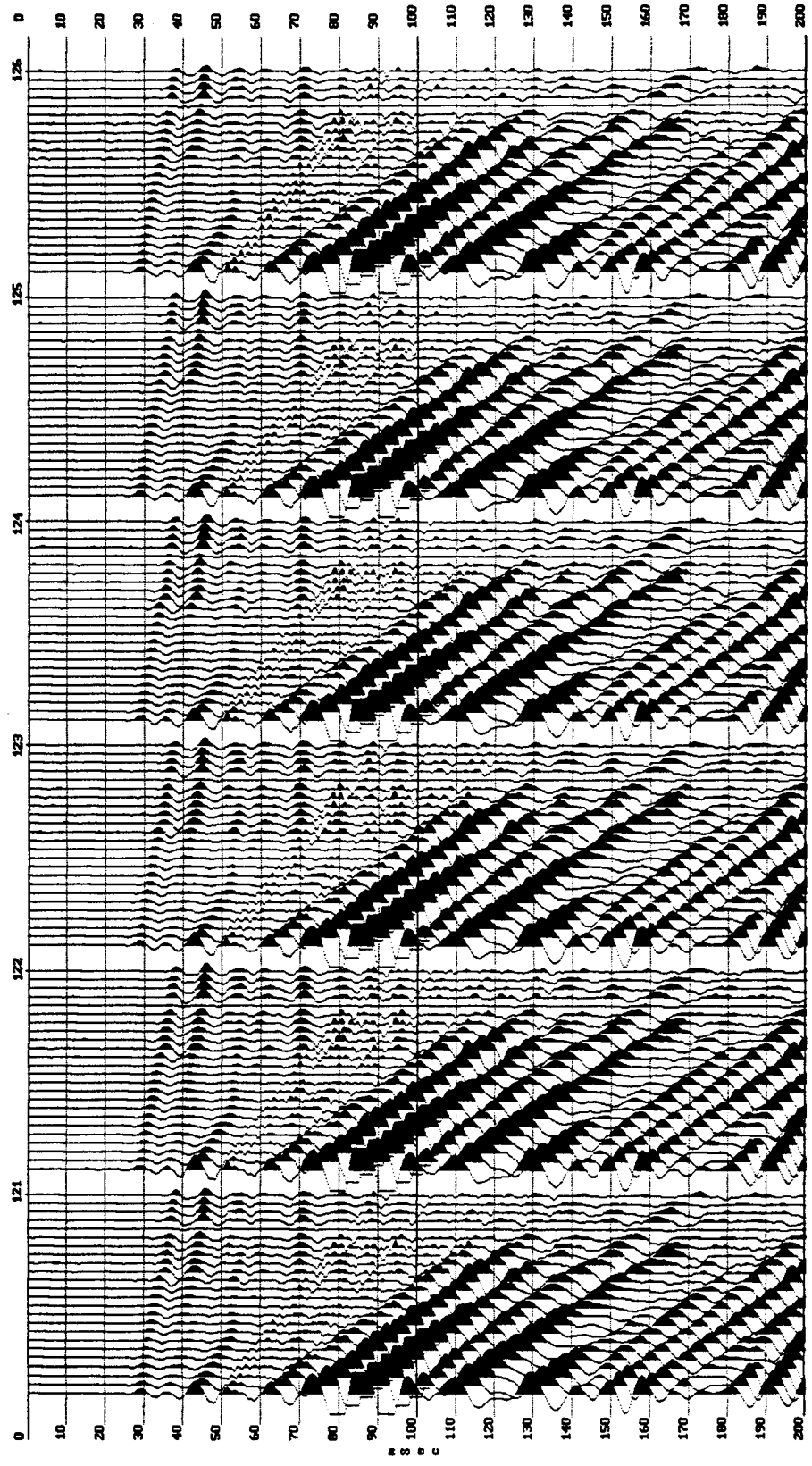
0
10
20
30
40
50
60
70
80
90
100
110
120
130
140
150
160
170
180
190
200
126
125
124
123
122
121
msec

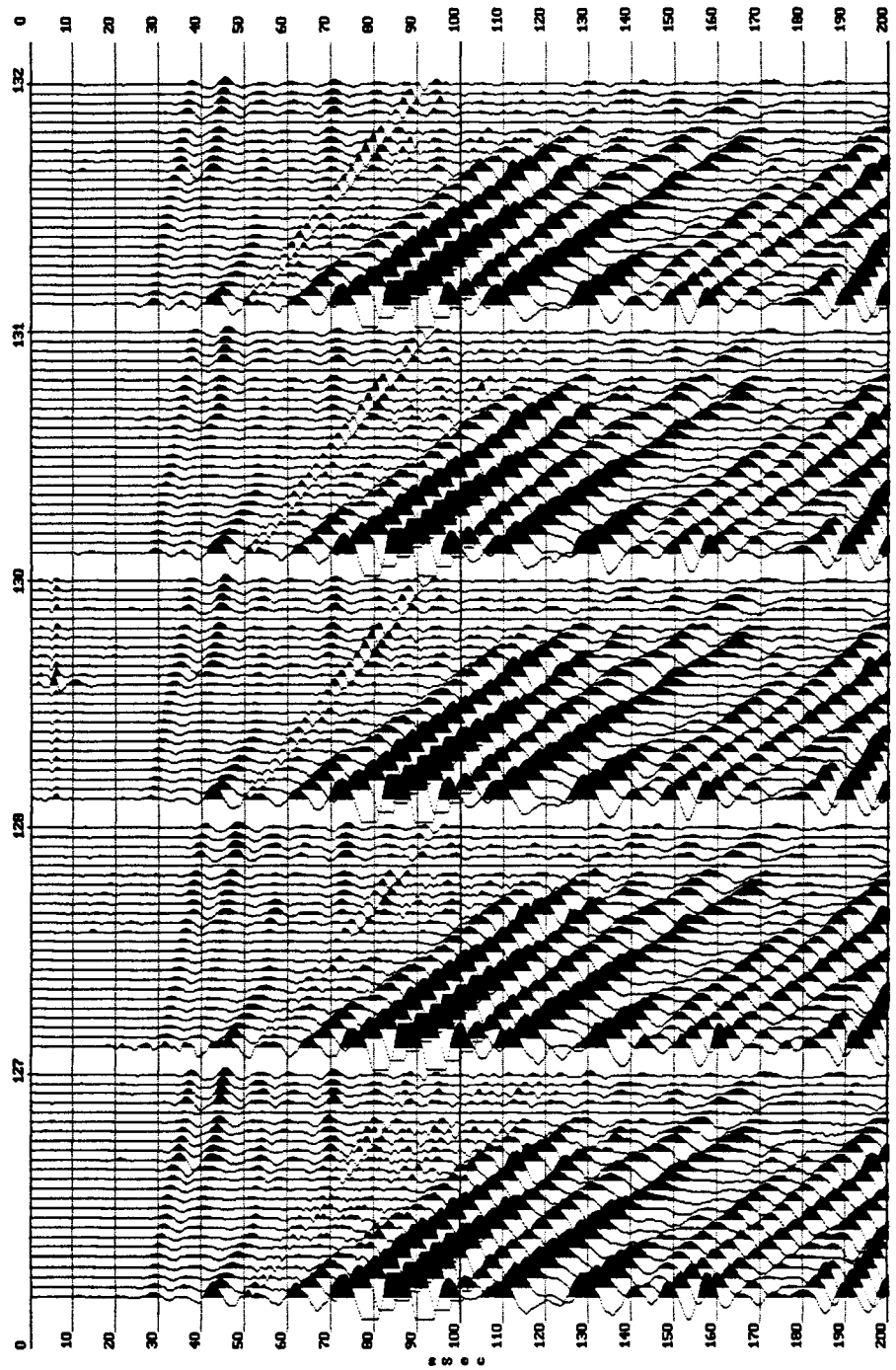
0
10
20
30
40
50
60
70
80
90
100
110
120
130
140
150
160
170
180
190
200
132
131
130
128
127
msec

141

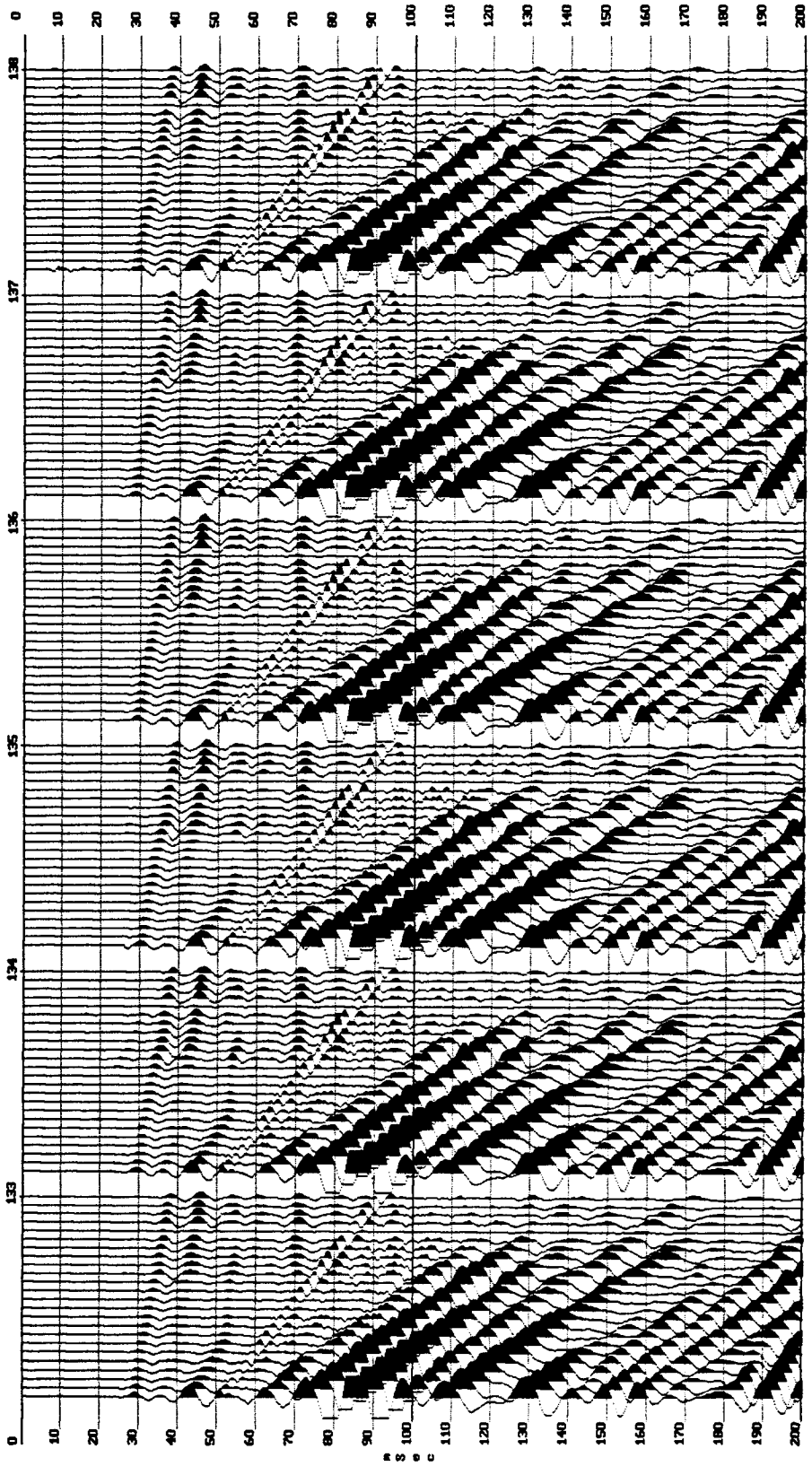
0
10
20
30
40
50
60
70
80
90
100
110
120
130
140
150
160
170
180
190
200
138
137
136
135
134
133
0
10
20
30
40
50
60
70
80
90
100
110
120
130
140
150
160
170
180
190
200

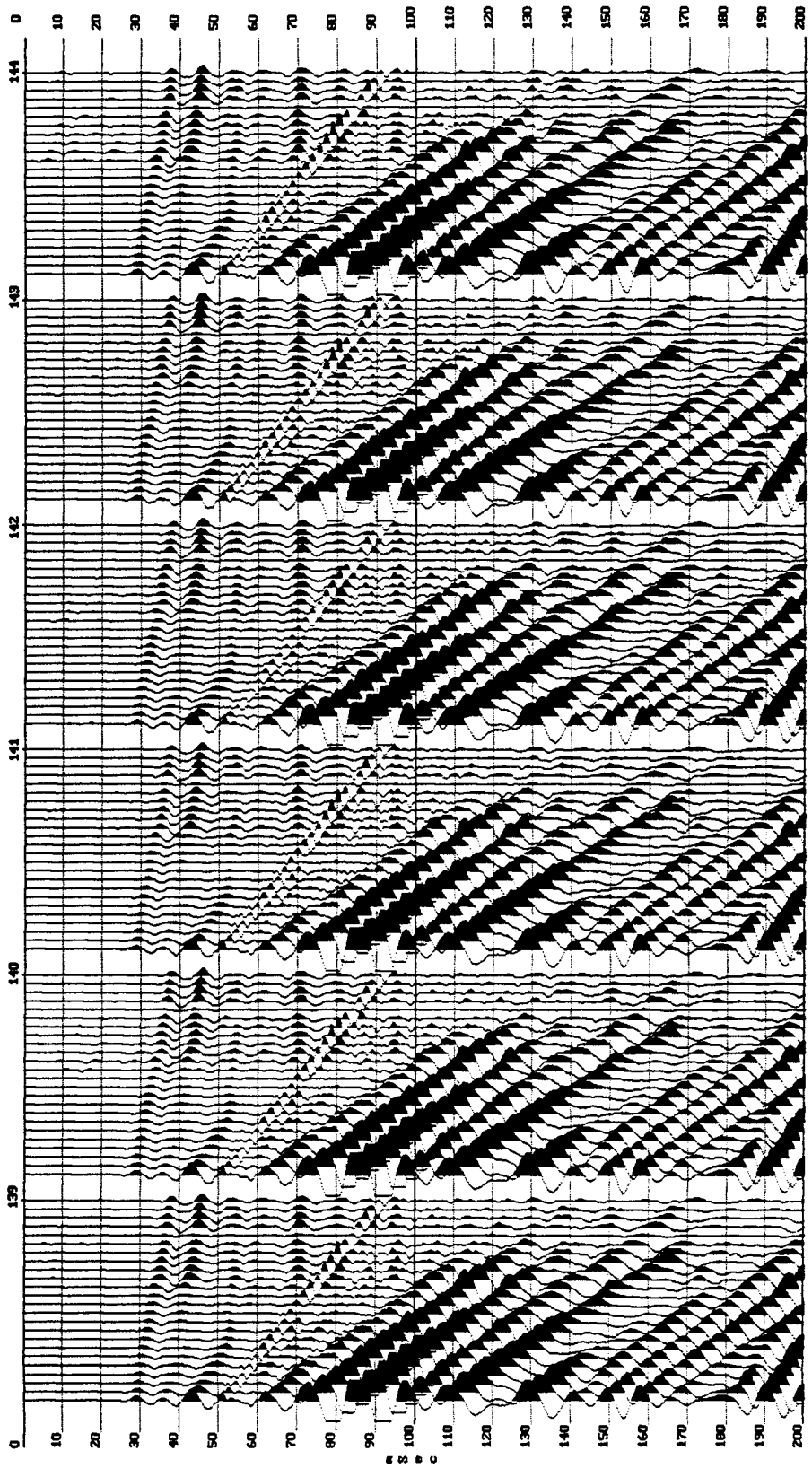
0
10
20
30
40
50
60
70
80
90
100
110
120
130
140
150
160
170
180
190
200
144
143
142
141
140
139
msec

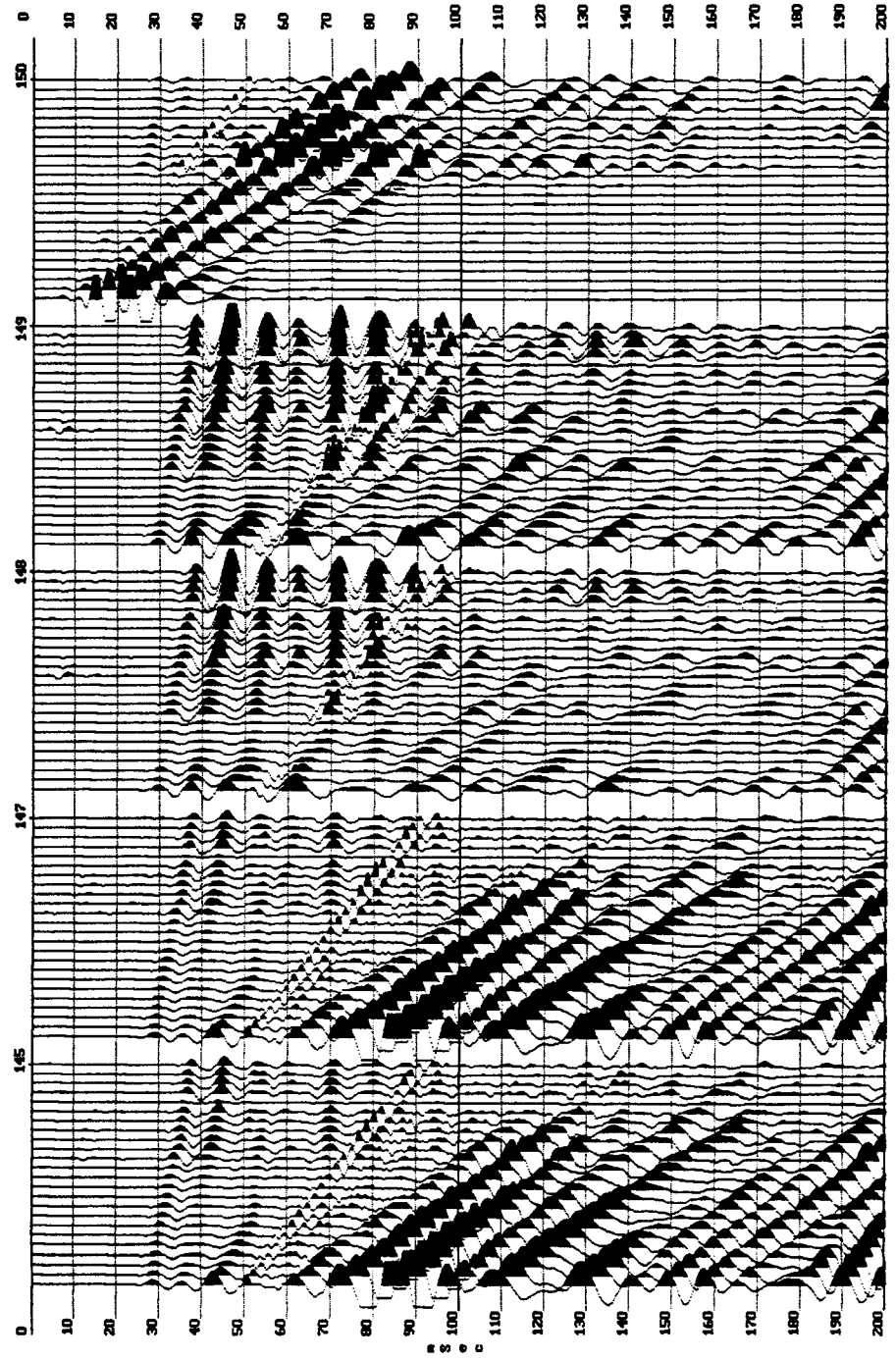
0
10
20
30
40
50
60
70
80
90
100
110
120
130
140
150
160
170
180
190
200
150
149
148
147
145

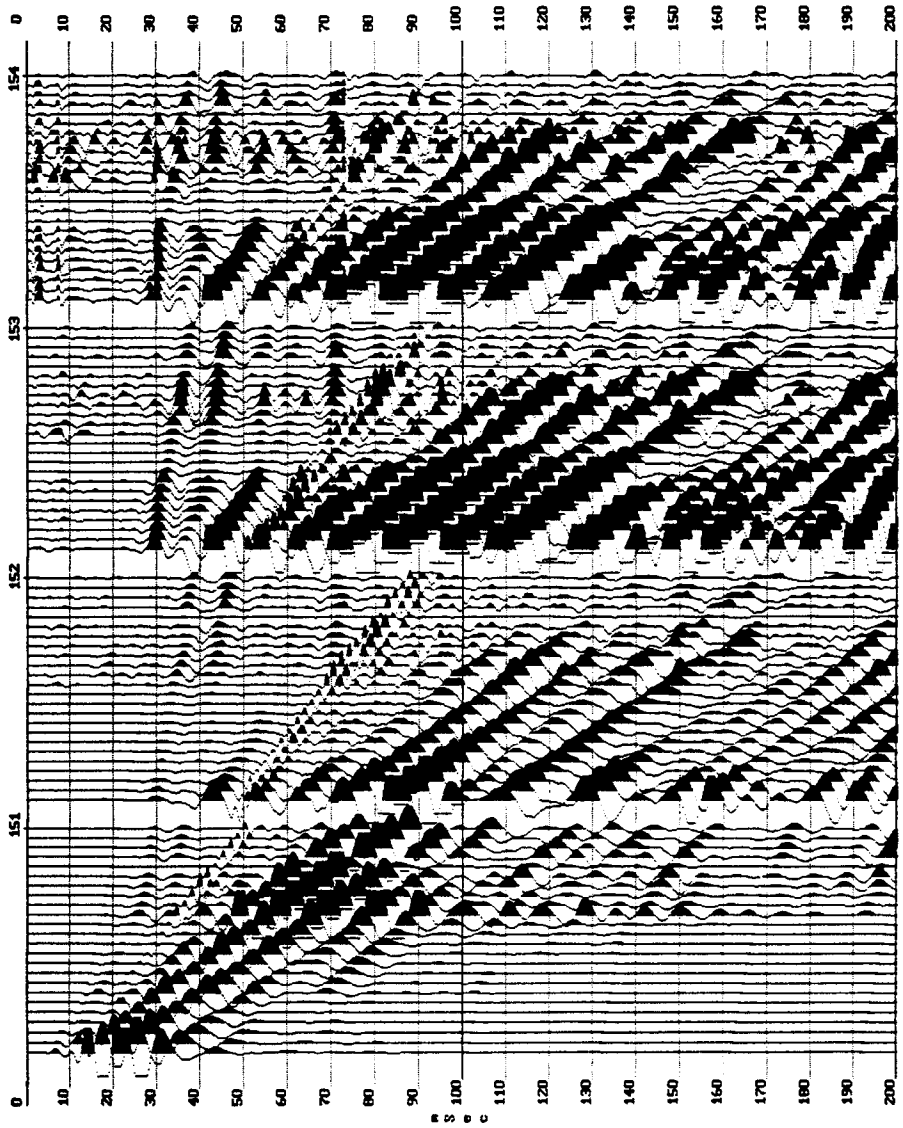
0
10
20
30
40
50
60
70
80
90
100
110
120
130
140
150
160
170
180
190
200
154
153
152
151
msec